CO_2CAPTURE FROM LIQUID FUEL BASED POWER PLANTS USING CLC: THERMODYNAMIC MODELING AND NICKEL-FERROUS OXYGEN CARRIER DEVELOPMENT

BY

AHMED AHEED ALI MOHAMMED

A Thesis Presented to the

DEANSHIP OF GRADUATE STUDIES

KING FAHD UNIVERSITY OF PETROLEUM & MINERALS

DHAHRAN, SAUDI ARABIA

In Partial Fulfillment of the

Requirements for the Degree of

MASTER OF SCIENCE

In

CHEMICAL ENGINEERING

OCTOBER 2015

KING FAHD UNIVERSITY OF PETROLEUM & MINERALS

DHAHRAN- 31261, SAUDI ARABIA

DEANSHIP OF GRADUATE STUDIES

This thesis, written by **AHMED AHEED ALI MOHAMMED** under the direction his thesis advisor and approved by his thesis committee, has been presented and accepted by the Dean of Graduate Studies, in partial fulfillment of the requirements for the degree of **MASTER OF SCIENCE IN CHEMICAL ENGINEERING**.

B.H.

Dr. Housam Binous
(Advisor)

Dr. Mohammed S. Ba-Shammakh
Department Chairman

Mozahar Hossain

Dr. M. Mozahar Hossain
(Co-Advisor)

Dr. Salam A. Zummo
Dean of Graduate Studies

عمادة الدراسات العليا
DEANSHIP OF GRADUATE STUDIES

Dr. Mamdouh Al-Harthi
(Member)

23/12/15

Date

Dr. Nadhir A. Al-Baghli
(Member)

Shaikh Abdur Razzak

Dr. Shaikh Abdur Razzak
(Member)

Dedicated to my Parents

ACKNOWLEDGMENTS

First of all, الحمد لله

Secondly, I would like to express my deep gratitude to KFUPM for providing me this nice full scholar ship to presume my graduate studies. Also, I am so thankful to my supervisor Dr. HousamBinous for helping and guiding me through all modeling practice, and my co-advisor Dr. Mohammad Mozahar Hossain who provide me all essential materials to carry out this interesting research. In addition, special thanks to KACST-TIC on CCS for funding this study.

Last but not the least, I am thankful to all persons who help me in this work and let it being done smoothly.

TABLE OF CONTENTS

LIST OF TABLES

LIST OF FIGURES

LIST OF ABBREVIATIONS

a_{ik} : Number of atoms of k^{th} element involved in i^{th} component

A_k : Total number of atomic masses of kth element in the system

$C_{p,i}$: i^{th} component constant pressure heat capacity (J/mol*K)

$G_{i_{298.15}}$: Gibbs free energy of i^{th} component at 298.15 K (J/mol)

G_i^o : Standard Gibbs free energy for i^{th} component (J/mol)

G_{mix}^{ig} : Ideal gas Gibbs free energy of the mixture (J/mol)

G_{mix}^{R} : Residual Gibbs free energy of the mixture (J/mol)

$\Delta {G_j}^o$: j^{th} chemical reaction Gibbs free energy (J/mol)

k_{ij} : Binary interaction parameter between i^{th} and j^{th} components

K_j : j^{th} chemical reaction equilibrium constant

n_T : Total number of moles in the system

n_i : Number of moles of i^{th} component

n_0 : Initial total number of moles

n_{i_0} : Initial number of moles of i^{th} component

P : Pressure (bar)

P_c : Critical pressure (bar)

P^o : Standard pressure (bar)

R : Universal gas constant (J/mol*K)

$S_{i_{298.15}}$: i^{th} component entropy at 298.15 K (J/mol*K)

T : Temperature (K)

T_c : Critical temperature (K)

V : Molar volume (cm^3/mol)

y_i : Mole fraction of component i

R_o : Oxygen transport capability of oxide

m_o : mass of fully oxidized form

m_r : mass of fully reduced form

R_{oc} : Oxygen transport capacity

x_{oc} : Fraction of active material for oxygen transport

$\dot{m}_{oc}$: Solid circulation flow rate

X_s : Solid conversion

τ : mean size of the ordered (crystalline) domains

κ : dimensionless shape factor

λ : X-ray wavelength;

β : Broadening at half the maximum intensity

θ : Bragg angle

λ_k : k^{th} Lagrange multiplier

$\hat{\phi}_i$: i^{th} component fugacity coefficient

ω : Acentric factor

x : Fuel conversion

Θ :CO_2 selectivity

ABSTRACT

Full Name : [Ahmed Aheed Ali Mohammed]

Thesis Title : [CO2 Capture From Liquid Fuel Based Power Plants Using CLC: Thermodynamic Modeling And Ni-Fe Oxygen Carrier Development]

Major Field : [Chemical Engineering]

Date of Degree : [October 2015]

The present study is focused on CO_2 capture from liquid fuel based power plants using chemical looping combustion (CLC). In this regard, (i) a thermodynamic equilibrium model has been developed to identify the reaction conditions for complete fuel combustions and (ii) NiO-Fe_2O_3/La-γAl_2O_3 have been synthesized and evaluated as a suitable oxygen carrier for the liquid fuel based CLC process.

The thermodynamic model is based on Gibbs free energy minimization approach. This technique allowed us to take into account of solid reactants (oxygen carrier, coke etc). The model prediction (equilibrium compositions) is compared with experimental values available in the literature. It is found that appropriate combustion temperature and an efficient oxygen carrier can achieve complete fuel conversion. For the oxygen carrier formulation, lanthanum is employed as a support modifier providing thermal stability of γAl_2O_3, while Ni/Fe are the main active components to carry oxygen for fuel combustion. XRD shows that higher nickel loadings (above 5 %) cause the formation of ferrous nickel aluminum (FeNi0.5AlO4) crystals, which is difficult to reduce (TPR). The presence of lanthanum helps improve the reducibility of the oxygen carrier by minimizing the metal support interaction. Finally, the prepared oxygen carriers were evaluated in a fluidized CREC Riser Simulator using hexane as liquid fuel. It is found that approximately 95 %

hexane can be converted into carbon dioxide 650 °C using the prepared Ni/Fe based oxygen carriers.

ملخص الرسالة

الاسم الكامل : أحمد أحيد علي محمد

عنوان الرسالة : احتجاز غاز ثاني أكسيد الكربون من محطات الطاقة المستخدمة للوقود السائل : النمذجة الثيرموديناميكية و تطوير حامل الأكسجين المركب من عنصري النيكل والحديد

التخصص : الهندسة الكيميائية

تاريخ الدرجة العلمية : أكتوبر 2015

تركز هذه الدراسة على حجز غاز ثاني أكسيد الكربون (CO_2) المنبعث من محطات توليد الطاقة التي تستخدم الوقود السائل وذلك عن طريق الاحتراق الكيميائي الحلقي. لهذا الصدد ، تم : (i) عمل نموذج الاتزان الثيرموديناميكي لتحديد الظروف المطلوبة للتفاعل للوصول للاحتراق الكلي التام و (ii)تركيب وتقييم $NiO\text{-}Fe_2O_3/La\text{-}\gamma Al_2O_3$كحامل أكسجين مناسب لعملية الاحتراق الكيميائي الحلقي المبنية على الوقود السائل.

تم إنشاء النموذج الثيرموديناميكي بناءً على أسلوب تقليل طاقة Gibbs الحرة للنظام(هذا الأسلوب يمكن من أخذ المتفاعلات الصلبة في الاعتبار (فحم , حامل أكسجين , الخ)) ، ومن ثم قورنت نتائج وتنبؤات النموذج مع القيم التجريبية المتاحة في الأدب. وجد أن درجة حرارة الاحتراق المناسبة وحامل الاكسجين الفعال يمكنا من تحويل الوقود بصورة كاملة.

بالنسبة لتركيب حامل الاكسجين ، تم إدخال عنصر اللانثانوم كمحسن للداعم وذلك بتوفير الاستقرار الحراري ل γAl_2O_3 ، في حين أنNi/Fe هما المكونان الرئيسيان النشطان لحمل الاكسجين لحرق الوقود.أوضحت نتائج تحليل XRD أن نسب تحميل عنصر النيكل المرتفعة (أعلى من 5%) تؤدي الى تكوين بلورات مادة FeNi0.5AlO4 والتي يصعب إختزالها (أخذ الاكسجين منها) كما أشارت نتائج تحليل TPR. وجود عنصر اللانثانوم يساعد إختزالية حامل الاكسجين وذلك بتقليل التفاعلات بين الفلز (المعدن) والداعم. أخيراً تم تقييم حاملات الاكسجين المعدة في مفاعل CRECالمميع والمحاكي للناهض باستخدام الهكسان كوقود سائل. وجد أنه يمكن تحويل ما يقارب 95% من الهكسان الى ثاني اكسيد الكربون عند درجة حرارة 650°C باستخدام حاملات الاكسجين المعدة والمبنية على معدني النيكل والحديد (Ni/Fe).

CHAPTER 1

INTRODUCTION

1.1. CO_2 emission and global warming

It has been reported that one of the major contributors to global warming is CO_2 which traps and reflects back some heat (comes from the sun) to the earth. This imbalances earth's net heat and causes rise in earth's surface temperature (global warming). For earth's thermal balance to be established, the net heat outflow has to equal the geothermal energy which is the only natural heat source on earth [1]. Normally, there are two main resources for heat inflow: geothermal energy and sun, but the heat emitted by the sun and reaches earth's surface is emitted back again by the earth at the same rate, and that balances the heat of earth. So, excessive use of nonrenewable energy sources (such as fossil fuels) increases the heat inflow. This added heat needs to be removed in order to maintain earth's thermal equilibrium. The only way to cool down earth is by emitting some of its heat to the space until it reaches equilibrium condition. However, gases resulting from using of nonrenewable resources act as obstacles to this process (Greenhouse Gases Effect). Figure 1.1 shows how greenhouse gases affect global warming.

Due to this, the need of treating greenhouse gases (or capturing in other words) has become very important. Generally, the major constituent of greenhouse gases isCO_2 as can be seen in Figure1.2. However, methane is much more harmful than carbon dioxide.It

can be burnt easily to form water vapor and carbon dioxide that is not easy to be converted to other less climate damageable substance. And thus the idea of CO_2capturing rose.

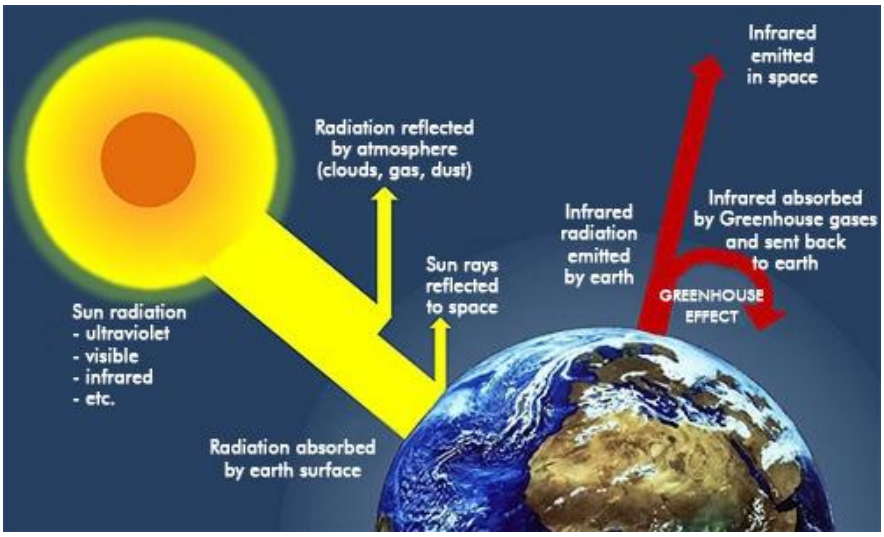

Figure 0.1: Greenhouse effect on global warming

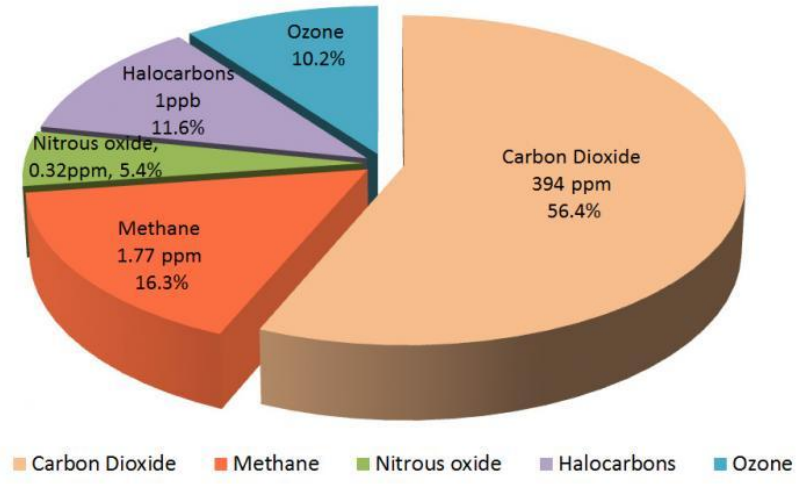

Figure 0.2: Greenhouse gases

CO_2 isformed and consumed generally by four processes: photosynthesis, respiration, organic decomposition and combustion of organic materials. The first three occur naturally. However, a major part of the last one can be considered anthropogenic (due to human activities). These natural processes generate little amount of CO_2in comparison with the combustion process, and so they have no remarkable effect on the atmosphere since the CO_2 emitted through some of them (respiration and organic decomposition) gets depleted through the other one (photosynthesis). This means that the huge effect on the atmosphere comes from combustion process. One of the main causes of human need to combust fuels is energy demand which is much higher than can be covered by other energy sources (renewable ones such as solar and wind energies) without any CO_2 emissions[2]. In fact, about one-third of anthropogenic CO_2 emissions is resulted from power generation using fossil fuels [3]. That led to the so called Kyoto protocol which has been signed by many industrial countries. Figure1.3 shows different CO_2 emission sources and their contribution.

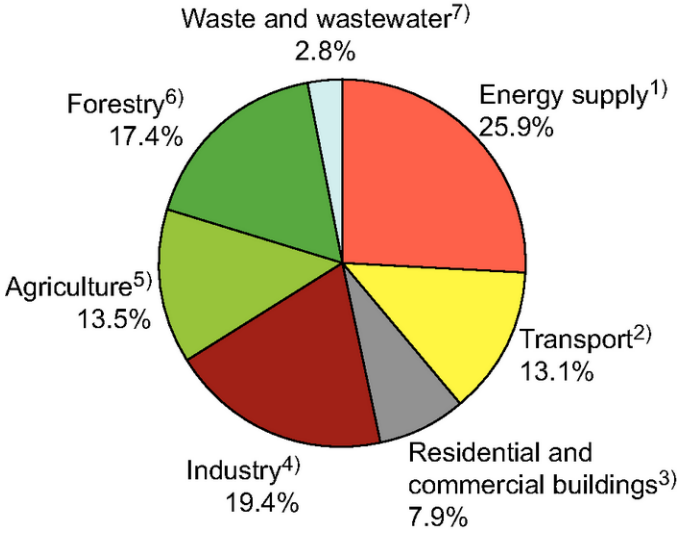

Figure 0.3: CO_2 emission sources

1.2. CO_2capturingtechnologies

Currently, there are three main categories of processes to capture CO_2[4]:

i. Pre-combustion (or de-carbonation) processes: These type of processes separate carbon from the fuel before combustion takes place. In other words, they use the hydrogen gas resulted from such separation process as the fuel.

ii. Oxy-fuel combustion processes: These processes provide pure oxygen (got from cryogenic nitrogen separation from the air) to the combustion to being held.

iii. Post-combustion separation processes: In these processes, the resulted CO_2(from combustion) is separated from the flue gas.

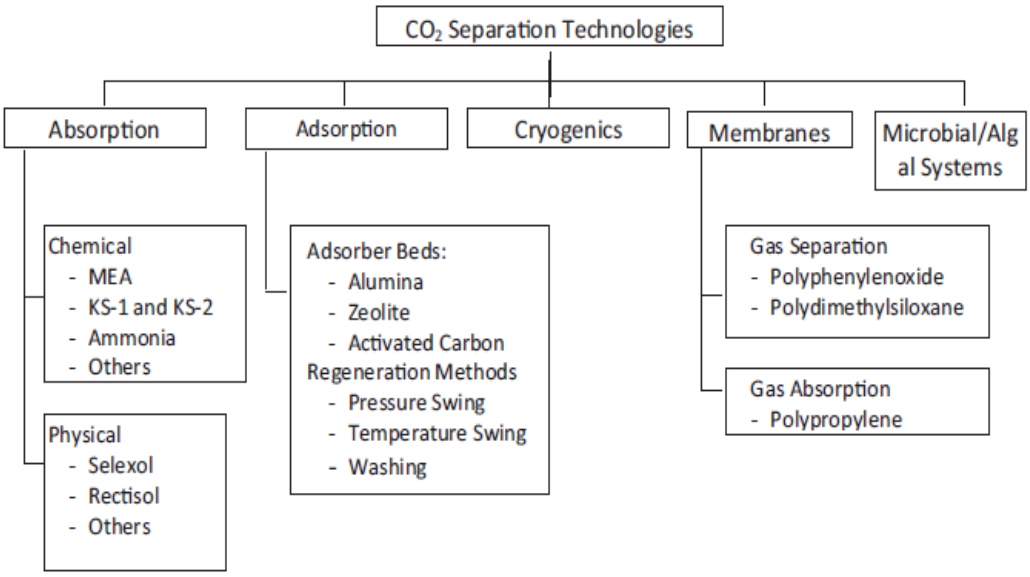

Figure 0.4: Different CO_2 separation processes

One should notice that all these separation techniques need huge amount of energy to be applied. Pre-combustion CO_2capturing processes, de-carbonation and hydrogen production processes require high temperature. When oxy-fuel combustion is performed, it means connection with cryogenic facility which is considered as an intensive energy consumer process. For post-combustion processes, generally the main separation process (CO_2capturing) does not require a lot of energy but the regeneration process does (for example: regeneration of absorbent, adsorbent, etc.). Figure1.4 shows some of the post-combustionCO_2capturing technologies. In this respect, chemical-looping combustion (CLC) process has been brought. The main advantage of CLC is efficient capturing of CO_2without any need of applying intensive additional energy.

1.3. Chemical-looping combustion (CLC)

As shown in Figure1.5, CLC consists of two main interconnected reactors, air reactor (AR) and fuel reactor (FR), and utilizes solid material (Oxygen Carrier or OC) to take the oxygen from air and provide it to the fuel to combust. OC is a metal oxide (or any material that can be oxidized and reduced easily). This OC is circulated between the two reactors in cyclic manner.

In details, at first, OC enters the air reactor as a reduced metal oxide (MeO_{x-1})in order to get the oxygen from air according to [4]:

$$Me_yO_{x-1} + \frac{1}{2}O_2(\text{air}) \rightarrow Me_yO_x + (\text{air}: N_2 + \text{unreacted } O_2) \qquad (1.1)$$

After it gets oxidized, it is sent to the fuel reactor where it reacts with the fuel (provides oxygen needed for combustion) according to:

$$(2n+m)Me_yO_x + C_nH_{2m} \rightarrow (2n+m)Me_yO_{x-1} + mH_2O + nCO_2 \qquad (1.2)$$

When it reacts with the fuel and gets reduced, it flows back to the AR to get re-oxidized again and by this, completes one cycle and begins a new one. It is clear that (from chemical reaction 2) combustion process products are oxygen depleted solid material (reduced OC), water vapor and carbon dioxide only (if enough oxygen is provided for complete combustion). So, by applying cooling to the flue gas that results from combustion of fuel with OC, water vapor can be separated due to condensation which will leave behind almost pure CO_2 stream ready for sequestration and other chemical operations. In addition, there is no chance of nitrogen oxides to form since there is no contact between oxygen and nitrogen in the fuel reactor [2][4].

Till date, the commercialization of CLC has not been done yet because it depends on the availability of suitable OC [3]. For OC to be considered as suitable, there are some important factors and qualifications (physical and chemical properties) it has to meet, such as: (i) availability, (ii) ability to operate under CLC conditions and stability, (iii) high reactivity, (iv) suitable oxygen carrying capacity, (v) reasonable cost and (vi) safety (in using and disposal).

A lot of researches were undertaken for finding this suitable material (OC) and they showed that it is better to use supported active agents (metals/metals oxides) rather than

pure ones to enhance the mechanical strength of the OC [5] and to avoid some problems made by severe CLC conditions such as attrition and agglomeration which decreases the active surface area and may affect the fluidization of the particles.

Currently, the applications of CLC go further than just CO_2 capturing.For example, there are new branches of CLC that deal with reforming processes like Chemical Looping Reforming (CLR) and Steam Reforming with Chemical Looping Combustion (SR-CLC), and some other concerns like hydrogen production (Chemical Looping Hydrogen Generation (CLH)) and gasification process (Integrated Gasification Chemical Looping Combustion (IG-CLC)) [3]. According to this, the present study belongs to SR-CLC.

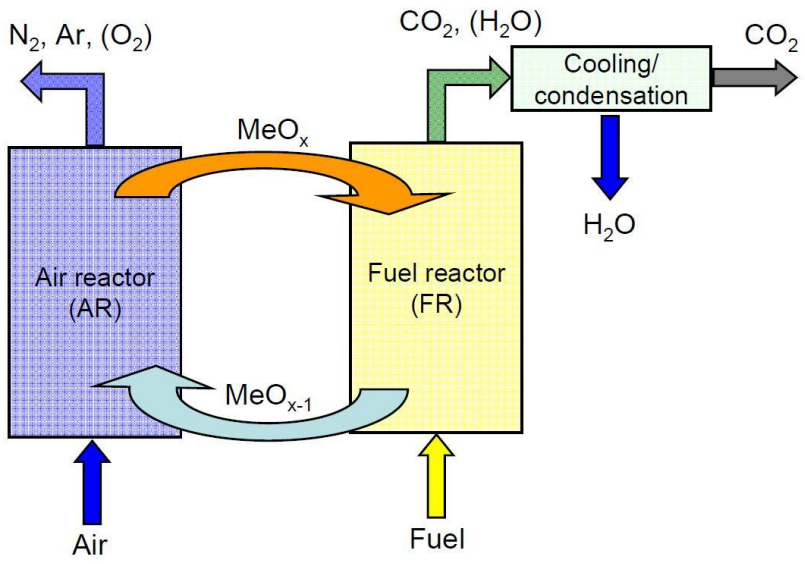

Figure 0.5: Schematic diagram of CLC

Up to now, most of the established CLC units (and studies) deal with gaseous and solid fuels respectively (because of the use of them in running power plants). But due to

increasing amounts of heavy fuels (resulting from distillation processes that can be considered as interesting feedstock) and the fact that 10-15% of existing power plants are using liquid fuels, investigating the feasibility of using such fuels in CLC have become very important [6].

In liquid-fuel based CLC, fuel evaporation is taking place at first by applying superheated steam to be in contact with the fuel directly, this steam accelerates fuel evaporation by means of efficient heat distribution as well as gasification/reforming process. When gasification/reforming takes place, the resultant gas mixture has higher heating value than the original fuel. Also, the presence of steam inhibits coke formation. Moreover, if Ni-based oxygen carriers are used, active free nickel in OC also acts as catalyst for fuel reforming [7]. So, the bifunctionality of Ni opens the door toward studying the behavior of Ni-based OC in liquid-fuel based CLC. But due to high cost and toxicity of Ni, researchers made a lot of trials so as to minimize Ni loading as much as possible without losing or affecting its catalytic activity. This goal can be achieved by using mixed metallic Ni-based OC. For example, some studies investigated promoter addition [7] and others dealt with options of bi and mixed metallic Ni-based OCs [3]. In this respect, the use of bimetallic Fe-Ni OCs in methane fueled CLC showed excellent and promising features [8]. The reasons for choosing Fe are its abundance, cheapness, mechanical strength, acceptable moderate oxygen carrying capacity and non-toxicity. On the other hand, the main drawback of this combination is the Ni-Fe chemical interactions which result in (Ni_xFe_{1-x}) formation and thus reduces the Ni catalytic effect.

1.4. Contribution of the present research

The present study deals with application of Lanthanum modified Ni-Fe bimetallic oxygen carrier in liquid-fuel based CLC. The presence of lanthanum oxide plays many main roles simultaneously; it 1) increases thermal stability of support [7], 2) reduces Lewis acidity and increases basicity of the support which is important to carbon deposition [7], 3) increases Ni active side dispersion, 4) minimizes Nickel Aluminates formation and reduces Ni-Fe interactions.

Following are the major contributions of this research:

i. Developed highly active Ni-Fe bimetallic based oxygen carriers,

ii. Investigated the effects of La_2O_3 on the prepared OC,

iii. Investigated the effects of different Ni/Fe ratios,

iv. Evaluated the reactivity and stability of the synthesized fluidizable OC in a CREC Riser Simulator under the real CLC conditions,

v. Investigated the effects of reaction conditions on the combustion product yields using thermodynamic modeling approach by Gibbs free energy minimization.

CHAPTER 2

LITERATURE REVIEW

2.1. Background

The idea of CLC originated first in 1951 by Lewis and Gilliland to produce pure carbon dioxide [3].However, the first researchers have generalized such idea for CO_2 capturing and called it chemical looping combustion are Ishida, Zheng and Akehata [9] when they were working on thermodynamic study of energy loss associated with conversion of fuel energy to thermal energy in natural gas fueled conventional power plants. Since that time, researchers dealt with CLC as CO_2 capturing technology that can cooperate with running power plants without the need of intensive energy such as the one needed in conventional CO_2 separation processes. They studied gaseous-fuel (natural gas) based and solid-fuel (coke) based CLC processes extensively. However, the difference between the two of them is not much because, in reality, the fuel that will be in contact with the OC first, is syngas resulted from steam or air coal gasification process (except in CLOU) which has been reported as a controlling step in the solid-fuel based CLC all-over . The name of solid fuel-based comes from the initial form or type of fuel being applied to the operation. To get an idea about solid fuel-based CLC, consider coal as fuel for example. There are two approaches to work coal fueled CLC; either by carrying out coal gasification in different steps (or separated reactor), then feeding the fuel reactor by the syngas resulted from it, or by direct feeding of coal to the fuel reactor [2]. The second approach depends on two mechanisms (since chemical reaction between two solid materials is not

applicable).The first one is gasification also. But this time, gasification takes place in the fuel reactor when steam or carbon dioxide is supplied as fluidizing agent. The second one is the reaction of solid fuel with gaseous oxygen released by OC in the fuel reactor which is called CLOU [10]. Figures 2.1 and 2.2 show these types of CLC processes and mechanisms involved in them [2].

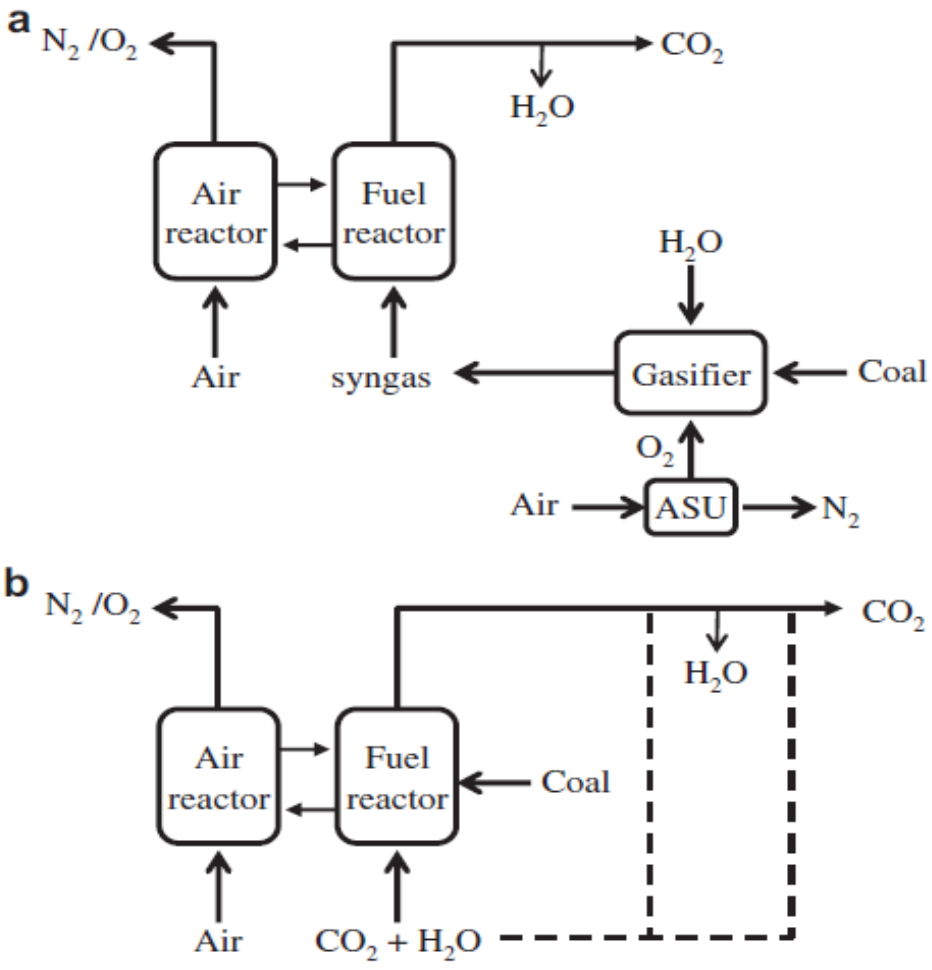

Figure 0.1: Layout of two alternatives of solid fuel-based CLC: (a) syngas-CLC and (b) solid fueled-CLC

Usually, the syngas production by means of coal gasification is an endothermic process. So, the energy needed for this step can be provided by power gained from air reactor during OC oxidation [2].

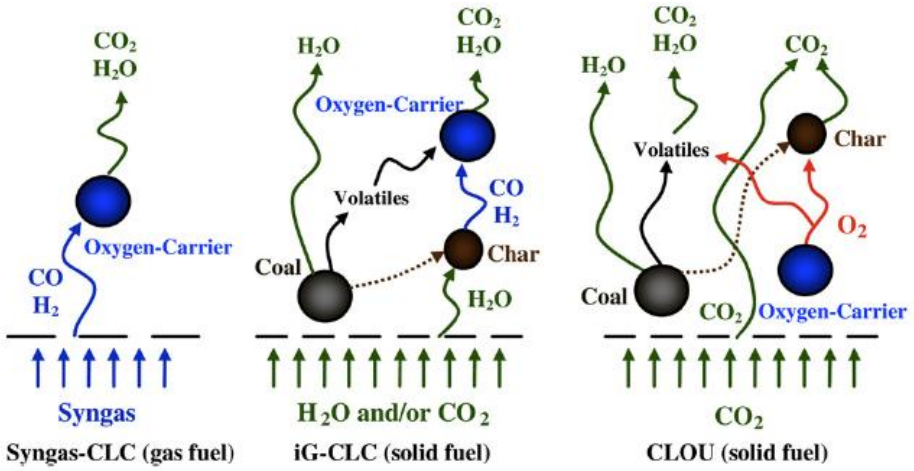

Figure 0.2: Combustion mechanism for different solid fuel-based CLC alternatives

2.2. Development of CLC

A lot of studies have been carried out to investigate gaseous and solid fuelled CLC in order to establish an efficient carbon dioxide capturing technology that can be connected to the running power plants that use those types of fuels. As a result of their abundance and ease of their reaction with OC, gaseous fuels experienced the largest amount of experiments with different OCs and conditions till now. The most commonly used fuels are methane and hydrogen in lab scale equipments (TGA and CREC Riser), and natural gas and syngas in pilot plants built to study the behavior and efficiency of the proposed CLC process. In this respect, many designs and configurations for the two interconnected chemical reactors (A and FR) have been proposed, which are [2]: (a) moving or

fluidized-bed reactors, (b) alternated packed (fixed) bed reactors and (c) rotating reactor. Figure 2.3 shows these configurations [2][11].

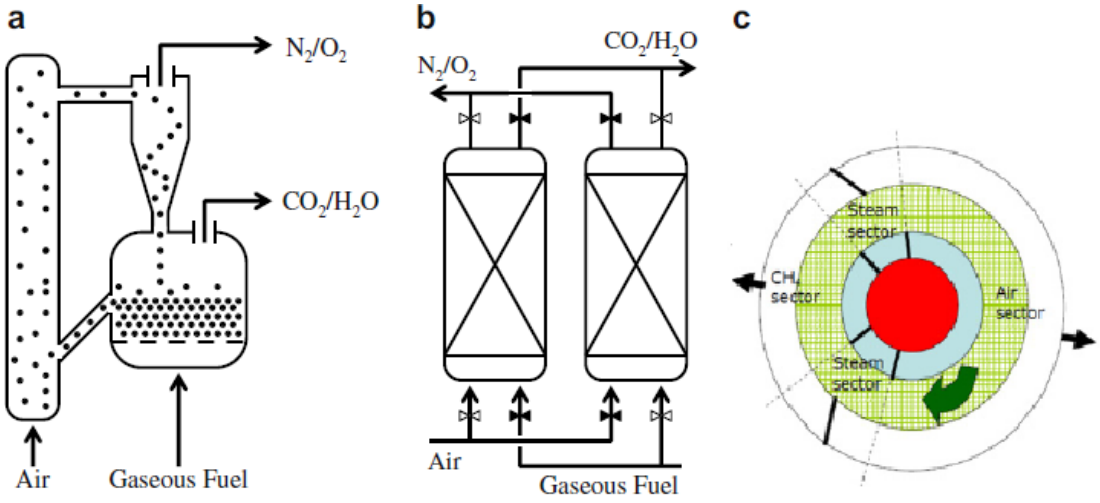

Figure 0.3: a) Fluidized-bed reactors, b) Alternating fixed bed reactors, c) Rotating reactor

However, due to the mixing effect on enhancing reaction process, the most common reactor configuration of existing CLC plants is fluidized-bed. In this type, there is a need of using two loop-seals to avoid gas leakage between the reactors which minimizes the overall efficiency of the process. Such configuration was first used for combustion of gaseous fuels under atmospheric pressure. In 2001, Lyngfelt et al. [12] introduced the idea of circulating fluidized bed (CFB) which has many advantages over the other alternatives; taking into account the need for a good contact between gas and solid materials within the reactors and solid material circulating between two of them [2]. Other works stated the feasibility of carrying out CLC process in different configurations if and only if they consist of a high velocity riser as an air reactor and low velocity

bubbling fluidized bed one as a fuel reactor [13][14][15][16]. The goodness of this type mainly lies in matching with OCs reactivity (oxidation is much faster than reduction that need notable residence time) [17][18]. Another advantage is that in this configuration riser plays two roles at the same time, it has: 1) to offer the oxygen needed for complete or desired fuel conversion, 2) to supply the driving force to the solid material throughout the process. But for other concerns, other works considered both reactors to be bubbling fluidized ones [19][20]. The most recent pilot plants and studies dealt with dual circulating fluidized bed reactors (DCFB) directly connected by fluidization [15]. This configuration forces both reactors to work in turbulent regime which is favorable for gas-solid contact and has positive features over the bubbling one. In addition, the solid holdup is stabilized by direct hydraulic link between the reactors and solid circulation controlled by air flow completely. Studies showed that this configuration needs low solid inventory (as compared to other configurations) and is suitable for high solid circulation processes [2]. Figure 2.4 shows the different types of fluidized beds [3].

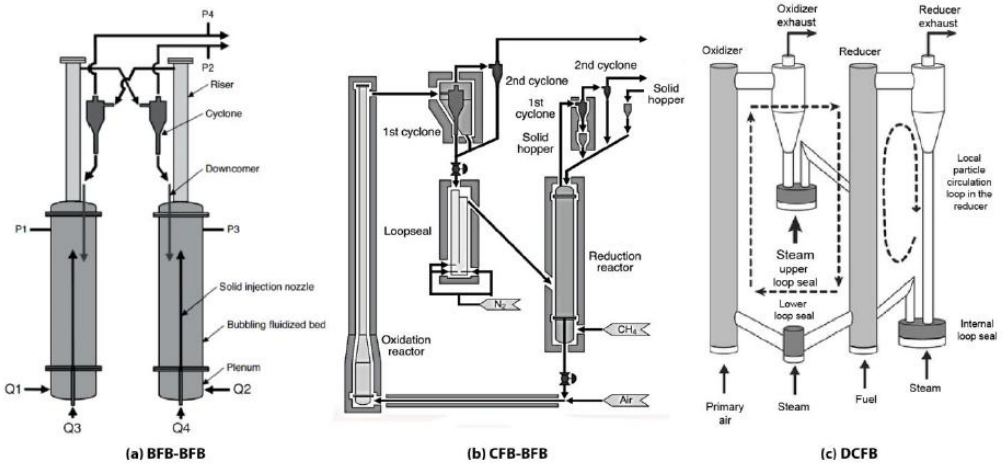

Figure 0.4: Different CLC reactor configurations

In 2006, Son and Kim [21] made another design or modification to CLC reactor system. They fabricated an annular shape bubbling fluidized bed reactor (1 kW_{th}) connected with double circulating fluidized bed loops. The OC circulates between the two fluidized sections through the annular reactor, it gets oxidized in the inner one (air reactor) and reduced in the other one (fuel reactor). The aim was to optimize the heat transfer from oxidation reactor to the reduction one by applying this annular shape.

Regarding solid fuel based CLC, first, in 2009, Shen and his group [22] studied a biomass and coal fueled CLC with a spout fluid bed being used as fuel reactor with aim of offering strong mixing and long residence time of fuel particles, and fast riser as an air one. The spout bed is composed of two main parts: reaction chamber and inner seal.

2.3. Oxygen carrier

As mentioned before, oxygen carrier is a solid material used to transfer the oxygen from the air to the fuel to combust partially or fully in an air free medium. To facilitate the combustion process, OC is provided in a powder form so as to be easily fluidized as well as offering required active surface area for combustion reaction. Due to CLC conditions and requirements, it has been reported that the suitable materials that can cope with such process are metals and metals oxides [3]. Metals and their oxides showed high reactivity (especially in oxidation and reduction) and strong mechanical strength when used as OCs as well as stability and chemical selectivity.

A lot of metals have been considered as proper oxygen carriers. There are more than 700 different materials based on Ni, Fe, Cu, Mn, Co beside the mixed oxides. Low cost

materials have been dealt with as OCs in different CLC configurations with different fuels [2]. Up to 2010, the total time of experimental work is about 3500 h [2]. However, a huge work is done and long time is spent in CLC development, it's commercialization is still contingent upon coming up with suitable oxygen carrier that meets all required or important qualifications.

2.3.1. Oxygen carrier selection criteria

To be considered as a suitable and feasible choice, an oxygen carrier has to meet these requirements:

i. High oxygen carrying capacity
ii. High reactivity in both oxidation and reduction reactions
iii. Availability and low cost
iv. Stability and mechanical strength
v. Favorable thermodynamic limitations (to achieve the desired fuel conversion)
vi. Resistance to agglomeration and fluidizability
vii. Safety and environment considerations.

In fact, pure metals/ metals oxides do not satisfy all mentioned characteristics which creates the need of using porous material as a support [23][24]. However, support presence has advantages as well as disadvantages. Its advantages are offering high surface area for reaction, increasing ionic conductivity [25] which enhances reactivity, inhibiting particles attrition and improving mechanical strength by means of binding behavior and decreases toxicity if the active agent being used is harmful. But on the other

hand, the oxygen transporting capacity will decrease (per unit weight of catalyst). In addition, when supported carriers were used, reactants faced another type of resistance to react. That is, diffusion within particle pores in order to reach the active site to react. This process depends intrinsically on both physical and chemical properties of the particles. Physically, it depends on pore size, pore diameter and surface morphology, and chemically it depends on affinity of reactants to permeate particles. This affinity is normally measured by acidity or basicity of the particles. Furthermore, support material can interact with the active agent and form other less or even non reducible compounds and then the particle becomes useless. The presence of support material adds another factor to selection criteria. That is, the active sites must be well dispersed on the support material surface and inside the pores. So, to meet these two additional qualifications (good dispersion and support-active agent interaction minimization), promoter or modifier may be added. Supported oxygen carriers showed better overall performance than unsupported ones when they were tested in CLC prototypes under same CLC field conditions. Despite their good characteristics, mono metallic supported OCs suffer from critical problems such as agglomeration, sintering, support-active agent interaction and weak mechanical strength. This led to the idea of using mixed metallic supported OCs instead of mono metallic ones.

2.3.2. Oxygen carrying capacity

Oxygen carrying or transferring capability is a very important characteristic of the OC since it determines the amount of particles needed to achieve certain fuel conversion as well as the quantity of power that is generated. It measures the amount of oxygen taken by the solid OC and provided to fuel to combust with. To measure the oxygen carrying

capacity of OCs, fully oxidized and reduced forms have to be known. In fact, these two forms directly show the oxygen portion that can be transferred.

Active agent oxygen carrying capacity defined as the fraction of transferable oxygen in fully oxidized form of OC as shown by equation (2.1) as:

$$R_o = \frac{m_o - m_r}{m_o} \tag{2.1}$$

However, this quantity has to be modified for the entire OC amount by taking the support material into account since it acts as an inert which means no oxygen will be offered by it. This can be done by multiplying the pure active agent's oxygen carrying capacity by its fraction in the OC as equation (2.2).

$$R_{oc} = x_{oc} R_o \tag{2.2}$$

Figure 2.5 shows some metal oxides/ metals systems and their corresponding oxygen carrying capacity [3].

Based on that, the required particles circulation rate to generate specific power is determined by equation (2.3) as follows[26]:

$$\dot{m}_{oc} = \frac{P_{wr}}{R_{oc} \Delta X_s} \frac{2dM_o}{\Delta H_c^o} \tag{2.3}$$

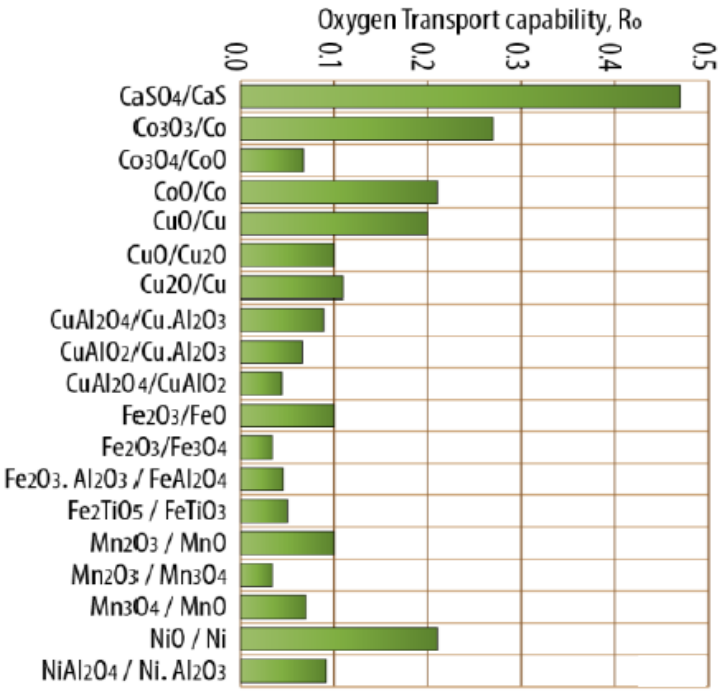

Figure 0.5: Oxygen transport capability of different oxide form/ reduced form systems

Where ΔX_s represents the change in solid conversion between reactor (air or fuel) inlet and outlet, whereas the solid conversion is calculated by:

$$X_s = \frac{m_{oc} - m_{r,oc}}{m_{o,oc} - m_{r,oc}} = \frac{m_{oc} - m_{r,oc}}{R_{oc} m_{o,oc}} \qquad (2.4)$$

It is clear from Figure 2.5 that the largest oxygen carrying capacity is that of calcium sulfate (about 0.47).In addition, it is of natural origin which reduces preparation cost (as compared to others). So, it seems to be good choice at first glance. However, it is not. Calcium sulfate showed instable behavior in terms of mechanical strength as well as reactivity when it is tested in CLC as stated by Ning Ding et al [27]. In addition, the release of undesired gases (SO_2, H_2S) with flue gas stream becomes massive if higher

temperatures are experienced (like those in CLC)[28]. Hence, the good choice is not an OC that has high oxygen carrying capacity or good in certain other point, but the OC which appreciated and favored overall performance in CLC. But on the other hand, there is a lower limit of oxygen carrying capacity for an OC to have. In fact, an oxygen carrier with carrying capacity equal or less than 0.004 is not suitable for CLC [26] based on maximum particles circulation rate of 16 kg/s MW. According to this, 2 wt% of NiO or CuO in OC is sufficient. However, higher percentages are needed when other metal oxides are being used (> 6 wt% and > 12 wt% for Mn_3O_4 and Fe_2O_3 respectively). Actually, those numbers are calculated based on the ideal behavior of OC (no active agent-support interactions or no losses in oxygen carrying capacity made by other reasons; in other words, working with the full capacity) which is not the case in most applications. It has been noticed that one of the main reasons of this undesired active agent-support interactions is the high working temperatures of CLC process which enhance the solid-solution formation. But in contradiction with this, high temperatures are required for those formed solid-solutions to behave like OCs (generally, they are in oxidized state, and they need high temperature to be reduced) as well as free active agents themselves. Thus, OC's nature and behavior determine the optimum conditions which are very important for plant design.

2.3.3. Reactivity and thermodynamic limitations

Oxidation reactivity can be determined by studying the kinetics of OC's reaction with air directly. However, the reduction step depends on the type of fuel being used. Since all

naturally found or produced fuels are cuts or complex compounds, most of the reduction reactivity studies were carried out using CH_4, H_2 and CO as model fuels for gaseous fueled CLC, and C for solid fueled CLC. These types of materials were chosen for reactivity studies because of: 1) their known properties, 2) simple chemical reaction networks, and 3) existence in some step in the CLC process. The simple chemical reaction network helps in calculating equilibrium curve (thermodynamic limit) of the process, how fast reactions are and by what mechanism (kinetics) they occur. Thermodynamic analysis sets the maximum fuel conversion that can be achieved under certain conditions. Moreover, the heat released or needed for both oxidation and reduction reactions is also determined by thermodynamic analysis of the operation. Table (2.1) [3] shows the heats of reactions for some OCs with those fuels. The equilibrium reaction constant of reduction step were calculated under assumption of complete combustion as follows:

$$Me_yO_x + \frac{1}{4}CH_4 \rightarrow Me_yO_{x-1} + \frac{1}{4}CO_2 + \frac{1}{2}H_2O \qquad (2.5)$$

Based on this reaction, one can determine the conversion. Figure 2.6[29] shows the equilibrium constants for different OCs' reduction with CH_4. Represented K values in Figure 2.6are calculated as if the process or combustion is taking place under atmospheric pressure. Besides showing the nature of equilibrium of the combustion reaction with different OCs, this study also stated that the optimal operating temperature for variety of choices should be in range (600-1200 ^oC). Accordingly, the conversion of methane to carbon dioxide is explained in Figure2.7.

But as known, thermodynamic analysis does not demonstrate the real reaction mechanism and its quickness. That means, it is not sufficient so as to fully describe the process. In this respect, kinetic analysis carried out (for different OCs with those model simple fuels) and reduction and oxidation reaction rate's constants are shown in Table(2.2) (in terms of activation energy). Since OC-fuel interaction in general is a solid-gas reaction, a lot of hypothesis and models are used to describe its mechanism as can be seen in Table(2.2). In names, they are Changing Grain Size Model(CGSM), Nucleation and Nuclei Growth Model (NNGM), Power Low Model (PLM) and Shrinking Core Model (SCM). A suitable model depends on type of the OC as well as the fuel being used. However, most OCs show that NNGM is the most agreeable model for its best experimental data [4]. Figure 2.8 show general description of these kinetic models [30].

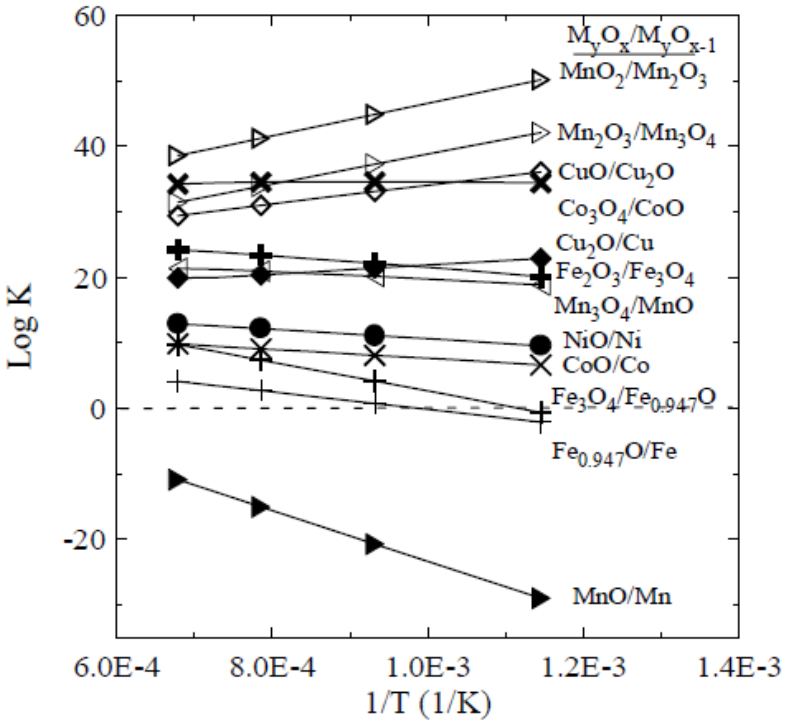

Figure 0.6: Log K as function of temperature for some OCs

All of these models deal with pure active agents (solid reactants) without any consideration of the support material. Ignorance of the support material leads to exclusion of active agent-support martial interaction automatically which can affect the reaction mechanism severely. So, application of any one of these models is contingent on OC structure and nature. In fact, their application is still meaningful for mono metallic (single active agent) OCs because the support material is chosen with certain characteristics to behave as inert as much as possible which reduces the possibility or the extent of active agent-support interaction. Moreover, the model is close to the reality in representing the overall mechanism. Actually, most experimental data found agree with the NNGM model.

However, in case of using mixed active agents, all previously mentioned models need modification to take relative dispersion besides all interactions among various used active agents into account. Relative dispersion affects the reaction mechanism. For example, by considering nickel and iron as active agents (which is the case in this study), if the fuel (hydrocarbon)reaches NiO first, it will combust with it and produce metallic Ni which acts as the catalyst for cracking and reforming the rest of the fuel. Cracking and reforming processes produce lighter hydrocarbons as well as hydrogen and CO. This increases the heating value and combustion rate at the same time. Moreover, heat is also needed and preferred for the cracking process, which means that the process will be autocatalytic. Furthermore, Hydrogen and carbon monoxide reacts much faster with iron oxide than any other hydrocarbon's combustion with iron oxide. On the opposite side, if the fuel reaches iron oxide at first, that sequence will never occur. In addition, nickel's reactivity with hydrogen is lower than that with lighter hydrocarbons. So, the whole

process is affected by the relative dispersion and ordering of these two active agents. Accordingly, to create a model that can describe the real kinetic behavior of multi active agent supported OC, dispersion and ordering must be included in it.

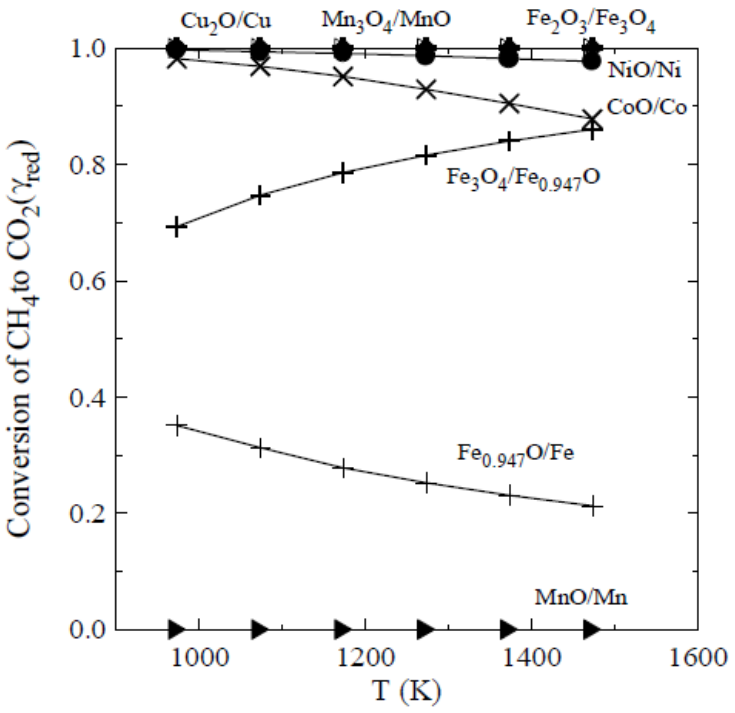

Figure 0.7: Conversion of CH4 to CO2 Vs temperature when reacts with some OCs

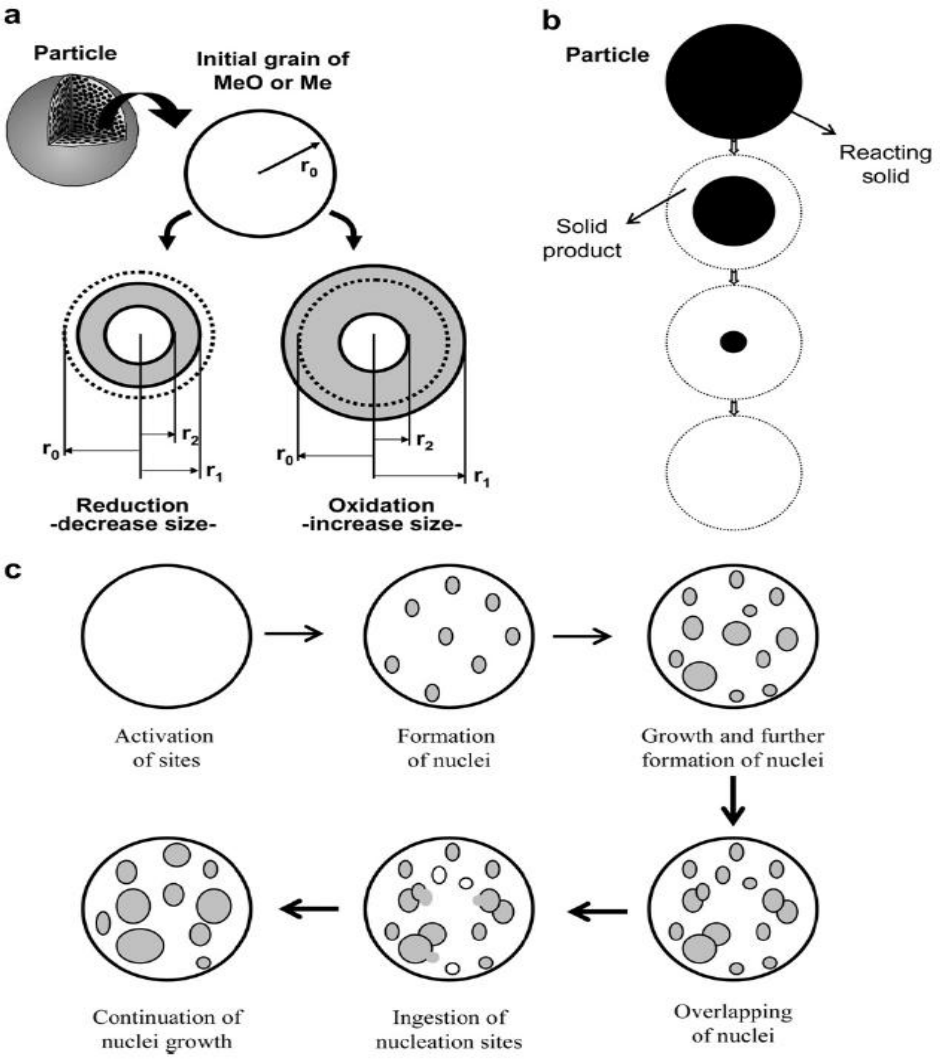

Figure 0.8: Solid material reaction kinetics:(a) Changing grain size model {CGSM}, (b) Shrinking core model {SCM} [31] and (c) Nucleation and nuclei growth model {NNGM}.

Table2.1: Standard heat of reactions for some OCs with CH4, H2, CO, C and O2

Redox System	$\Delta H_R^0\ (kJ/mol)$				
	CH_4	H_2	CO	C	O_2
$CaSO_4/CaS$	158.6	−1.6	−42.7	86.9	−480.5
Co_3O_4/Co	107.9	−14.3	−55.4	61.6	−455.1
Co_3O4/CoO	−16.8	−45.5	−86.6	−0.8	−392.7
CoO/Co	149.5	−3.9	−45.0	82.4	−475.9
CuO/Cu	−178.0	−85.8	−126.9	−81.4	−312.1
CuO/Cu_2O	−236.6	−100.4	−141.6	−110.7	−282.8
Cu_2O/Cu	−119.5	−71.1	−112.3	−52.1	−341.4
$CuAl_2O4/Cu.Al_2O_3$	282.2	29.3	−11.8	148.7	−542.2
$CuAlO_2/Cu.Al_2O_3$	−24.1	−47.3	−88.4	−4.4	−389.1
$CuAl_2O_4/CuAlO_2$	588.5	105.9	64.7	301.9	−695.4
Fe_2O_3/Fe_3O_4	141.6	−5.8	−47.0	78.4	−472.0
Fe_2O_3/FeO	318.4	38.3	−2.8	166.8	−560.3
$Fe_2O_3.Al_2O_3/FeAl_2O_4$	−62.3	−56.8	−98.0	−23.5	−370.0
$Fe_2TiO_5/FeTiO_3$	106.5	−14.6	−55.8	60.9	−454.4
Mn_2O_3/MnO	−48.0	−53.3	−94.4	−16.4	−377.1
Mn_2O_3/Mn_3O_4	−396.6	−140.4	−181.6	−190.7	−202.8
Mn_3O_4/MnO	126.3	−9.7	−50.8	70.8	−464.3
NiO/Ni	156.5	−2.1	−43.3	85.9	−479.4
$NiAl_2O_4/Ni.Al_2O_3$	158.6	−1.6	−42.8	86.9	−480.4

Table2.2: Kinetic parameter for reduction and oxidation for some OCs

Oxygen Carrier (wt%)/Support	Experimental Conditions	Kinetic Model	Activation Energy (kJ/mol)	Reference
NiO(60)/YSZ	TGA (800-1000 ^oC)	SCM	$E_{H_2} = 82$ $E_{O_2} = 17$	[24]
NiO(58)/Bentonite	TGA (600-750 ^oC)	SCM	$E_{CH_4} = 37$	[32]
NiO(78)/Bentonite	TGA (600-750 ^oC)	SCM	$E_{O_2} = 131$	[32]

NiO(60)/Bentonite	TGA (700-1000 ^{o}C)	SCM, MVM	$E_{CH_4} = 57$ $E_{H_2} = 2.4$	[21]
NiO(60)/$NiAl_2O_4$	TGA (750 ^{o}C)	SCM	-	[33]
NiO(60)/Al_2O_3	TGA (600-950 ^{o}C)	SCM	$E_{CH_4} = 78$ $E_{H_2} = 26$ $E_{CO} = 25$ $E_{O_2} = 7$	[26], [34]
NiO(60)/Mg	TGA (800-1000 ^{o}C)	SCM	$E_{CH_4} = 114$ $E_{O_2} = 40$	[35]
NiO(20)/Al_2O_3	TPR-TPO (200-750 ^{o}C)	NNGM	$E_{H_2} = 53$ $E_{O_2} = 45$	[36]
NiO(20)-Co/Al_2O_3	TPR-TPO (200-750 ^{o}C) CREC Riser (650 ^{o}C)	NNGM	$E_{CH_4} = 49$ $E_{H_2} = 45$ $E_{O_2} = 44$	[30]
NiO(20)/Al_2O_3	CREC Riser (680 ^{o}C)	SCM, NNGM, PLM	$E_{CH_4} = 51$, $E_{CH_4} = 44$, $E_{CH_4} = 39$	[37]
NiO(20)/La-Al_2O_3	TPR-TPO (200-750 ^{o}C) CREC Riser (650 ^{o}C)	NNGM	$E_{H_2} = 73$ $E_{CH_4} = 70$	[38]
NiO(40)/$NiAl_2O_4$	TPR (300-600 ^{o}C)	SCM	$E_{H_2} = 96$	[39]
NiO(65)/Al_2O_3	TGA (800-950 ^{o}C)	SCM	$E_{CH_4} = 55$ $E_{H_2} = 28$ $E_{CO} = 28$	[40]
NiO(15)/Al_2O_3	Fixed Bed (600-900 ^{o}C)	CGSM	$E_{CH_4} = 77$ $E_{H_2} = 26$ $E_{CO} = 27$	[41]

$NiO(40)/NiAl_2O_4$	TGA (750-1000 ^oC)	SCM	$E_{CH_4} = 70$ $E_{H_2} = 35$ $E_{CO} = 34$	[42]
$NiO(18)/Al_2O_3$	TGA (700-950 ^oC)	SCM	$E_{CH_4} = 137$ $E_{H_2} = 20$ $E_{CO} = 18$ $E_{O_2} = 24$	[3]
$CuO(60)/SiO_2$	TGA (700-850 ^oC)	SCM	$E_{CH_4} = 41$	[2]
$CuO(10)/Al_2O_3$	TGA (600-800 ^oC)	SCM	$E_{CH_4} = 60$ $E_{H_2} = 33$ $E_{CO} = 14$ $E_{O_2} = 15$	[43]
$CuO(82)/Al_2O_3$	Fluidized Bed (250-900 ^oC)	DRM	$(CuO \rightarrow Cu_2O) \Rightarrow E_{H_2} = 58$ $(Cu_2O \rightarrow Cu) \Rightarrow E_{H_2} = 44$ $E_{CO} = 52$ $(Cu \rightarrow Cu_2O) \Rightarrow E_{O_2} = 40$ $(Cu_2O \rightarrow CuO) \Rightarrow E_{O_2} = 60$	[44], [45], [46]
$CuO(62)/Al_2O_3$	TGA (600-800 ^oC)	SCM	$E_{H_2} = 30$ $E_{CO} = 16$	[40]
$CuO(14)/Al_2O_3$	TGA (600-800 ^oC)	SCM	$E_{CH_4} = 106$ $E_{H_2} = 20$ $E_{CO} = 11$	[47]
$Fe_2O_3(60)/Bentonite$	TGA (700-1000 ^oC)	MVM	$E_{CH_4} = 29$ $E_{O_2} = 6$	[21]
$Fe_2O_3(60)/Al_2O_3$	TGA (600-950 ^oC)	SCM	$E_{CH_4} = 49$ $E_{H_2} = 24$ $E_{CO} = 20$ $E_{O_2} = 14$	[26], [34]

$Fe_2O_3(58)/Al_2O_3$	TGA (800-850 ^oC)	SCM	$E_{CH_4} = 25$ $E_{H_2} = 22$ $E_{CO} = 19$	[40]
Fe_2O_3	Fluidized Bed (250-900 ^oC)	DRM	$E_{CO} = 75$	[48]
$Mn_3O_4(40)/Mg\text{-}ZrO_2$	TGA (800-1000 ^oC)	ChRSM	$E_{CH_4} = 119$ $E_{O_2} = 20$	[35]
Calcined Fe_2TiO_5	TGA (800-850 ^oC)	SCM	$E_{CH_4} = 165$ $E_{H_2} = 109$ $E_{CO} = 113$ $E_{O_2} = 12$	[49]
Activated Fe_2TiO_5	TGA (800-850 ^oC)	SCM	$E_{CH_4} = 136$ $E_{H_2} = 65$ $E_{CO} = 80$ $E_{O_2} = 25$	[49]
$CaSO_4$	TPR (850-1200 ^oC)	AEM	$E_{CO} = 280$	[50]
$CaSO_4$	Fixed Bed (880-950 ^oC)	SCM	$E_{CO} = 145$	[51]

2.3.4. Material cost

Material or active agent cost mainly depends on its application, availability, accessibility and the form and source it is found in. In reality, the cheaper the source, the more contaminated the active (or desired) agent is. Figure 2.9[52] shows the cost variation of some materials with time. However, this Figure does not show the cost of those materials nowadays (2015), it represents the cost variation for some materials regarded as suitable

raw ones for certain promising active agents. Table (2.3)[53] is an extension for this Figure.

Table2.3: Average annual cost of some active agents raw materials suitable for CLC applications in period (2010-2014)

Material	Average Cost ($/kg) in **2010**	Average Cost ($/kg) in **2011**	Average Cost ($/kg) in **2012**	Average Cost ($/kg) in **2013**	Average Cost ($/kg) in **2014**
Co (SfC)	45.966	39.6612	13.02	28.4176	31.7466
Ni (LME)	21.804	22.89	17.533	15.018	16.863
Cu (LME)	7.678	8.9486	8.0976	7.4935	7.09889
Fe (Iron ore)	0.09879	0.09945	0.09816	0.1049	0.101
Fe (Iron & steel scrap)	0.319	0.392	0.36	0.341	0.352
Mn (Metallurgical ore)	0.00845	0.00667	0.00497	0.00461	0.0043

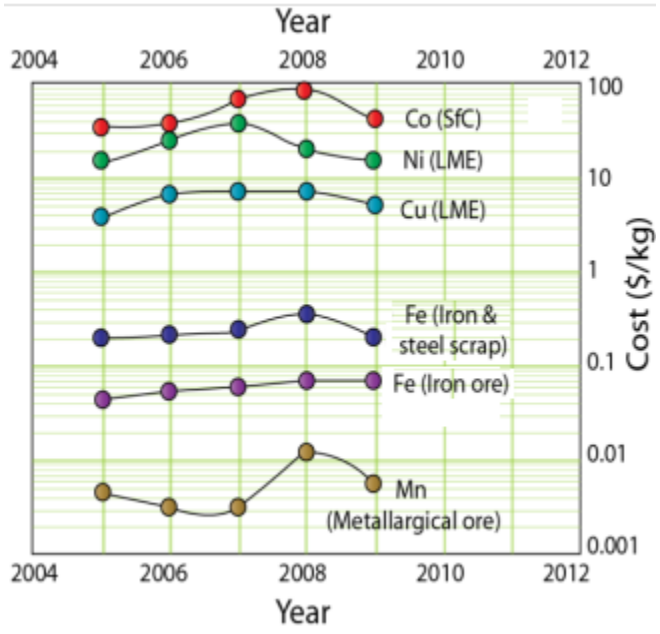

Figure 0.9: Average annual cost of materials used for OC preparation in (2005-2009)

2.3.5. Mechanical strength

Oxygen carrier has to withstand CLC conditions, such as high temperatures. Thus, its melting point should be far enough from operating CLC temperature to avoid or minimize the particles' structural damages. This margin (gap between working and melting temperatures) ensures the low attrition rate of particles to some extent, which means a longer lifetime. In addition, when the operating temperature is near the OC melting point, the chemical and physical bonds (between active agent and support) and behavior of the OC changes and its efficiency falls down. Moreover, agglomeration is most likely to take place when the crystals or particles lose their stiffness and start to melt. Furthermore, some OCs will decompose if they are exposed to temperatures close to or higher than their melting points. Practically, if the particles crumble into smaller fragments, their separation and capturing from gas stream becomes difficult and, thus, they will be lost from exhaust of air and fuel reactors which means a needof larger make-up.In addition, losing the particles from air reactor exhaust leads to incomplete fuel combustion, or even just cracking due to the lack of sufficient oxygen. Table(2.4)[4] represents melting points of some metals and their oxides that are suitable for CLC.

Table2.4: Melting points of metals/metals oxides suitable for CLC

Active Agent	**Melting Point (^{o}C)**	**Active Agent**	**Melting Point (^{o}C)**
Fe	1536	FeO	1378
Fe_3O_4	1597	Fe_2O_3	1594
Ni	1453	NiO	1955
Co	1495	CoO	1805
Cu	1083	Cu_2O	1236
Mn	1244	MnO	1875
Mn_3O_4	1565	W	3410
WO_2	1724	WO_3	1472

Mo	2620	MoO_3	800
Cr	1875	Cr_2O_3	2400
CrO_3	185	Nb	2468
NbO	1935	NbO_2	1902
Nb_2O_5	1510	V	1902
VO	1790	V_2O_3	2070
VO_2	1545	V_2O_5	670
Ce	798	In	157
In_2O_3	1910	Sn	232
SnO_2	2000		

Table2.5: Attrition rate and lifetime of some OCs

Oxygen Carrier	CLC (kW_{th})	Operation time (h)	FR T(^oC)	AR T(^oC)	Attrition rate (%/h)	Lifeti me (h)	Ref.
NiO/Al_2O_3	10	100	900	1000	0.0023	40000	[17]
$NiO/NiAl_2O_4+MgAl_2O_3$	10	1016	940	1000	0.003	33000	[54], [55]
$NiO/ NiAl_2O_4$	10	160	940	1000	0.022	4500	[56]
$NiO/\alpha\text{-}Al_2O_3$	500	70	880	950	0.01	10000	[57]
$CuO/\gamma\text{-}Al_2O_3$	10	100	800	800	0.04	2400	[58]
$CuO/\gamma\text{-}Al_2O_3$	500	60	800	900	0.09	1100	[59]
$CuO/NiO/Al_2O_3$	500	67	900	950	0.04	2700	[60]
Iron Ore	1	10	950	1010	0.0625	1600	[61]

2.3.6. Nickel based oxygen carriers

As can be noticed from the name, these carriers have nickel or nickel oxide as an active agent. However, they have different support materials. Many feasibility studies are carried out using unsupported Ni and NiO showed that those materials have low re-oxidation rate under repeated oxidation-reduction cycles. This is mainly due to the tendency of Nickel to agglomerate at CLC temperature range. So, supported Ni-based OCs are being considered as another choice.

There are many materials that have been considered as supports for those OCs, among which are Al_2O_3, $MgAl_2O_4$, YSZ, Bentonite, TiO_2, SiO_2, and ZrO_2

i. Al_2O_3: It has good fluidization properties, acceptable thermal stability and offers high dispersion of nickel oxide which prevents it from agglomeration. But the main drawback is that Ni/Al_2O_3 is most likely to form $NiAl_2O_4$ which has no contribution in CLC cycle (behaves as inert) which means the loss of a remarkable amount of nickel. Due to this, Cho et al. and Matisson et al. (2005) proposed increasing the nickel loading to compensate that portion which was consumed in the formation of nickel aluminate. Results showed that stable Ni/Al_2O_3 can be obtained after few oxidation/reduction cycles. Another suggestion having the same idea is to use $NiAl_2O_4$as a support instead of Al_2O_3which provides high stability and reactivity and also prevents the oxygen carrier from agglomeration. But, of course, needs additional amount of nickel.

ii. $MgAl_2O_4$: It has been noticed that the Mg minimizes the sintering of NiO and allows the OC to be stable under repeated oxidation/reduction cycles' nature; even above 1300℃.

iii. YSZ: Ni/YSZ has high reactivity and regeneration ability because of high exposure of Ni and NiO in the oxidation and reduction reactions respectively, which means YSZ offers high solid diffusivity. In addition, when YSZ is used, no remarkable Ni support interaction is detected.

iv. Bentonite: Bentonite displays excellent reactivity and stability. However, its performance decreases when temperature increases, as a result of its limited thermal stability.

v. TiO_2: Like Al_2O_3,when $TiO_2$is used as a support, high amount of nickel react with TiO_2 and form NiTiO3 and this is the reason why it shows lower reactivity when it is compared with Al_2O_3. In addition, coke formation is detected, which means the portion of carbon associated with reduced particles will enter the air reactor and result in carbon dioxide stream in the effluent of the air reactor (or reduced air stream).This decreases the overall carbon dioxide capture efficiency of the process.

vi. SiO_2 and ZrO_2: Both those materials have the same behavior qualitatively. They have strong interactions with nickel at temperatures above 900℃.

2.3.7. Iron based oxygen carriers

Iron received a lot of attention because of its suitability for commercial use. Indeed it is cheap and readily available in the nature. In general, iron is found in nature in many forms; among them hematite is one (i.e., an iron oxide). When iron is used without any support material, agglomeration at high temperature is observed similar to what is seen with nickel. To overcome this problem, a number of support materials have been proposed:

i. Al_2O_3: It is noticed that when hematite is added as an active agent, the sequence of reduction of hematite to magnetite, magnetite to ferrous oxide and ferrous oxide to iron takes place. On the other hand, the reactivity of iron on Al_2O_3 decreases further and further under repeated oxidation/reduction cycles nature due to observable solid-state interactions between iron and Al_2O_3. Some studies state that the interaction of Fe_2O_3 with Al_2O_3 leads to $FeAl_2O_4$.

ii. $MgAl_2O_4$: This is an alternative support for Fe_2O_3 to avoid formation of $FeAl_2O_4$. The main advantage of this support when it is used with Fe_2O_3 is the high reactivity and stability up to 1100℃, but its disadvantage is the agglomeration occurrence at high temperature and repeated oxidation/reduction cycles.

iii. YSZ: Fe_2O_3/YSZ displayed stable activity and no metal support interactions during oxidation/reduction cycles. However, it has been observed that the reduction rates of Fe_2O_3/YSZ is much lower than Fe_2O_3/Al_2O_3.

iv. TiO_2: This material has very strong interaction with Fe_2O_3 (which forms $FeTiO_3$).

v. SiO_2:When$SiO_2$is being a support forFe_2O_3, the resulting material shows high reactivity in first oxidation/reduction cycles. Then, a decrease in reactivity is observed. This is due to a strong interaction of SiO_2 with Fe_2O_3 that results in the formation of unreactive materials; specifically iron silicate.

2.3.8. Copper based oxygen carriers

In reality, copper has more attractive properties than the mentioned OCs such as:

i. High reactivity in oxidation/reduction processes (among stated OCs).

ii. High oxygen carrying capacity.

iii. Ease of complete fuel combustion (in case of using gaseous hydrocarbons as fuels, and this can be expressed by the thermodynamic analysis of the reduction of CuO).

iv. The oxidation and reduction reactions are both exothermic if Cu-based OCs are used.

v. Cheapness (commercial feasibility).

But applicably, Cu-based OCs are considered to be extremely unsuitable for CLC due to the decomposition of CuO to CuO_2at relatively low temperatures. Moreover, there is a possibility of agglomeration taking place as a result of low melting point of Cu (in comparison with CLC conditions). And this is why CuO/Cu shows high reactivity in the first cycles of reduction/oxidation (up to 950℃), then this reactivity sharply decreases.

Cho et al. and Diego et al. found that the main cause of decomposition of CuO to Cu_2O is the low oxygen concentrations. So, excess air is required to overcome or at least minimize this problem.

On the other hand, the normal and common alternative to stabilize this type of OCs is also studied. That is to support this active agent by another material or metal specifically.

Suggested and studied supporters:

i. Al_2O_3: The resultant catalyst Cu/Al_2O_3 has a lot of problems, the most important one is particle agglomeration which causes sharp decrease in the catalyst's reactivity and resist the fluidization process of the particles strongly at high temperatures. In addition to that, Formation of $CuAl_2O_4$which also reduces the reactivity is most likely to occur.

ii. SiO_2: Cu/SiO_2 provides good quality as an OC. It shows accepted reactivity and stability over frequent oxidation/reduction cycles. In addition, no Cu – SiO_2 interaction is detected. But the main drawback in this catalyst is the decomposition of CuO to Cu_2O.

iii. TiO_2: The option of using this support is rejected because of strong formation of $CuTiO_4$.

2.3.9. Mixed metallic oxygen carriers

The idea of using mixed oxygen carriers is originated in order to let each of the metallic (active agent or support) to share its own advantages with others and to limit the overall drawbacks and disadvantages of the mixture. Fortunately, Sinfelt(1983) found that the overall reactivity is enhanced when he used some mixed metallic OCs. In 1998, Jin et al. reported the cooperation behavior of NiO with CoO on YSZ support material. The mixed OC displayed good regeneration ability, but it has low thermal stability. There is no many studies are taken in this OC because of the reason mentioned previously and the expense of YSZ. Another study carried out by Adanez (2006) showed that Cu and Ni can provide stable bimetallic mixture when they are added to Al_2O_3 (support). In addition, the resultant catalyst showed high oxygen carrying capacity. Same findings were achieved by Johansson et al. (2006) when he studied and analyzed the behavior of mixed iron –nickel oxygen carriers. Readman et al. (2005) ran other experiment on $La_{0.8}Sr_{0.2}Co_{0.2}Fe_{0.8}O_{3-\delta}$ where δ shows oxygen content. The results obtained from this work stated high stability and reactivity in continuous oxidation/reduction cycles despite the low oxygen carrying capacity of that catalyst. Hossain and de Lasa (2007) studied Co with Ni over $Al_2O_3$and claimed high reactivity and stability of that material. Many advantages (i.e., absence of sintering and agglomeration)were detected. But it should be noticed that in this study, Co played two roles, 1) the first role is as a promoter, and 2) the other one is as an OC. This

promotion role has more than one activity or action. For example, the addition of Co promotes the dispersion of Ni over Al_2O_3 and limits the interaction between them. Furthermore, an average of conversion of 86% is achieved while the highest conversion obtained in case of nickel-based OC only is about 78%. This can be accounted for by the higher surface area offered by Co-Ni/Al_2O_3 (roughly 15% greater than that offered by Ni/Al_2O_3).

CHAPTER3

OBJECTIVES

Following are the major objectives of this study:

- To develop a thermodynamic equilibrium model for the liquid fuel based CLC reaction systems to determine the product gas compositions and to identify the reaction conditions for complete fuel combustion. In this regard, Gibbs free energy minimization approach has been considered.
- To develop NiO-Fe_2O_3/La-γAl_2O_3 as an oxygen carrier(s) suitable for liquid fuel based chemical-looping combustion process. In oxygen carrier formulation, La is employed as a support modifier providing thermal stability of γAl_2O_3, while Ni/Fe is the main active component to carry oxygen for fuel combustion.

In order to achieve the main objectives, the following specific objectives are considered:

i. To formulate a thermodynamic model based on the possible reaction schemes during the combustion of liquid fuel using a solid phase oxygen carrier.
ii. To validate this model by using data from literature. Apply the model to the system under focus in order to evaluate OC's maximum.
iii. To prepare La modified NiO-Fe_2O_3/La-γAl_2O_3 oxygen carriers using different Ni/Fe ratios.
iv. To study the effects of La modification on the metal support interaction, and on Ni/Fe interaction.

v. To demonstrate the effect of Ni content in reforming/cracking of the fuel.

vi. To identify optimum practical conditions (in terms of temperature, steam fuel ratio, oxygen carrier to fuel ratio and oxygen carrier to steam ratio) for converting fuel carbon to carbon dioxide.

vii. To determine the conditions under which carbon (coke) deposition can be avoided (theoretically and practically).

CHAPTER 4

EXPERIMENTALS

4.1. Introduction

Experimental work is divided into three main parts: i) Oxygen carrier preparation (Synthesis part), ii) Oxygen carrier characterization (physical, chemical and physiochemical properties investigation part), and iii) Practical Evaluation. The upcoming section will be treating the first part when the other two parts will be treated in different chapters.

4.2. Oxygen Carrier Synthesis

As stated before, one of the goals of this study is to develop nickel and iron bimetallic oxygen carrier. The advantages of introducing iron are to minimize the toxicity and cost of prepared oxygen carrier. However, nickel cannot be totally removed from OC due to the need of its catalytic effect in reforming/cracking of heavy hydrocarbons. In fact, the previous studies on this mixed metallic OC [62]showed that nickel will interact with iron when both of them are mixed chemically (nickel and iron crystals on the same support). This has led to the idea of making a Lanthanum sandwich between nickel and iron to minimize this interaction.

The support used in this study is gamma alumina (γ-Al_2O_3) because of its excellent working behavior with nickel and iron as can be noticed from the literature review.

Oxygen carrier preparation methods are much (in literature) like impregnation, spray drying, ion exchange, precipitation, sol-gel etc. Detailed explanation for each of them can be found elsewhere[63]. Actually, impregnation by means of incipient wetness technique is reported as the most suitable method for nickel based oxygen carriers synthesization [3].This method allows quick and large loading of active agent over the support via simple and easily controllable steps. This is what makes it a promising tool for manufacturing of huge quantities of OCs and their commercialization. Practically, the advantage of this technique over its rivals is the ability to disperse the active agent over the support surface as well as through the pores of the support; something unlikely to occur with other methods. However, the main drawback of this method is the random (to some extent) dispersion of the active agent (possible non uniform deposition).

The main steps of incipient wetness technique are:

a) Support calcinations
b) Active agent (precursor) loading (impregnation of support)
c) Loaded support drying
d) Loaded support reduction (precursor reduction)
e) Oxidation of active agent-support combination.

It has been reported that the sequence followed and conditions used to prepare the oxygen carrier affect its characteristics extremely [64].

Four different active agent (nickel mainly) content samples were prepared by using this technique. The content of iron is kept constant in order to study the nickel-iron ratio effect. The four loadings obeyed the systematic ratios1/6, 2/6, 3/6 and 4/6. The targeted

samples consist of (2.5% Ni - 15% Fe – 2% La_2O_3)/γ-Al_2O_3, (5% Ni - 15% Fe – 2% La_2O_3)/γ-Al_2O_3, (7.5% Ni - 15% Fe – 2% La_2O_3)/γ-Al_2O_3, (10% Ni - 15% Fe – 2% La_2O_3)/γ-Al_2O_3.

First, 15g of carrier particles or powder (Al_2O_3 from Advanced Materials company with purity of 99.99% by weight: Ultra Pure Grade, lot AC07120UPG) was calcined at 750^{o}C for 8 hours in order to ensure gamma phase stability, prepare pores as well as break any bond with moisture. After that, the calcined powder is transferred to a conical flask with lateral outlet(filter flask) which was connected to a vacuum pump. Meanwhile, the first loading of lanthanum (1% La) was prepared using $LaN_3O_9.6H_2O$ (99.9% particles purity, 100587-948) as precursor. It is to be noted that, all these percentages are based on the support, not on the overall OC weight. Thus, in order to attain the needed amount of lanthanum, the precursor quantity is:

$$\text{Needed precursor} = \frac{\text{amount of needed metal} \times Mw \text{ of precursor}}{\text{metal } Mw \times \text{metal moles included in one mole of precursor}} \qquad (4.1)$$

The needed amount of precursor was dissolved in ethanol (C_2H_5OH more than 99.9% purity, 603-002-00-5, Merck-Chemicals) corresponds to the volume of the pores of support (0.8 cm^3 per gm [64]). Thus, for each gm of support, 0.8 cm^3 of ethanol was used to dissolve the required precursor amount. Ethanol is used instead of water for its higher volatility under atmospheric conditions (pressure and temperature) and relatively low boiling point; in addition to its strong ability to dissolve precursor materials (Nitrate-x hydrate crystals). Moreover, ethanol presence enhances water (which comes from precursor crystals) evaporation by means of azeotropic behavior of ethanol-water solution. So, all these features assure complete solvent evaporation after impregnation

step (if the loaded carrier is kept at atmospheric or under any other conditions to facilitate solvent evaporation). The conical flask was connected to a vacuum pump with its lateral outlet and a stirrer inserted inside it to perform mixing in order to achieve or to increase the possibility of uniform dispersion of the precursor, then the aimed material itself. Vacuum conditions facilitate and assure (to some extent) the evacuation of all trapped gases and moisture from the pores, and, in opposite direction, enable precursor solution to permeate inside the pores which, then, allows active site to be deposited all over the pores that provides high area of contact between gaseous reactants and active sites. The main flask open (outlet) was sealed with a rubber septum to satisfy and preserve vacuum condition. Precursor solution was added or loaded (introduced) drop by drop by using a syringe while powder mixing is taking place to distribute the solution over the powder uniformly (eye bases).Actually, lanthanum was added in two different stages of preparation. Immediately after support (γ-Al_2O_3) calcinations, to increase the support thermal stability (hamper alumina phase change), minimize iron-support and nickel-support interactions, increase iron and nickel dispersion, reduce thermal sintering, enhance reducibility of nickel oxide and reduce Lewis acidity with remarkable enhancement of support basicity which are favorable for inhibiting carbon deposition. The second stage was done after iron loading, in order to prevent nickel-iron interactions. First addition of lanthanum (at first stage) effect were studied elsewhere [7].So, the concern (or one of the concerns) of this research was to see how much nickel would interact with iron in presence the of lanthanum sandwich between the two of them. Lanthanum was distributed equally between those two stages (1% $La_2O_3$$\gamma$-$Al_2O_3$ added or

loaded in each stage).This means that the distribution of lanthanum itself can be enhanced as well as its crystal size.

After precursor loading, the loaded powder was kept inside an oven at 90^{o}C for 8 hours (with temperature ramp about 0.35^{o}C/min) (drying step) to ensure complete evaporation of the solvent (ethanol). This temperature (90^{0}C) was chosen because it approximately lies in the middle of the range or interval bound by ethanol (solvent) boiling point (78.37^{o}C) and the minimum precursor decomposition temperature (100^{o}C for $FeN_3O_9.9H_2O$). By this way, the evaporation will take place without any decomposition in this step (drying one). If precursor decomposition occurred in the drying step, this would have had a negative effect on prepared oxygen carrier characteristics as well as its reactivity and effectiveness[64]. Table(4.1) states decomposition temperature of different precursors used:

Table4.1: Decomposition Temperatures of Precursor Materials

Precursor	Decomposition Temperature (^{o}C)
$FeN_3O_9.9H_2O$	100
$N_2NiO_6.6H_2O$	200
$LaN_3O_9.6H_2O$	>126

Instead of changing drying temperature for each precursor used, 90^{o}C was kept fixed (drying temperature) throughout the drying processes for different precursors loaded carrier to minimize effort and avoiding multi tuning of the oven.

Dried powder (Al_2O_3 and LaN_3O_9) was then transferred to a vertical quartz reduction tube with 100 μm ceramic mesh that plays two roles :1) allows the gas to pass through and, 2) carry and holds the powder. The reduction tube was then placed inside a specially designed furnace (to handle the tube vertically) and connected to a Hydrogen (10% Hydrogen and Argon as balance)cylinder with its lower narrow neck (open). The lower and upper tube outlets are kept outside the furnace. The hydrogen cylinder was then opened and fluidization of the bed started. Meanwhile, the furnace was tuned on and it started heating with temperature ramp 3^oC/min until it reached 750^oC (in a 4 hour period). Oven temperature stayed at 750°Cfor a complete 8 hour period. Precursor reduction obeys the following reaction:

$$2LaN_3O_9 + 3H_2 \xrightarrow{heat} 3H_2O + La_2O_3 + 6NO_2 \qquad (4.2)$$

After spending 8 hours in furnace at 750^oC, the furnace automatically turned the heating off and the sample started cooling down until it reached the ambient temperature. Then the hydrogen cylinder was closed (hydrogen gas stopped).

Then, the OC was turned back to the conical flask with the rubber septum and lateral outlet. But this time, 5% Fe/γ-Al_2O_3wasloaded. However, the targeted amount of iron was fixed in all samples (15% Fe/γ-Al_2O_3); iron was loaded in three successive steps (5% Fe loaded in each step by means of successive incipient wetness impregnation). The reason behind this is, besides assuring high surface area as a result of fine crystal size deposited on the support and good dispersion, the total amount of iron cannot be dissolved totally in ethanol quantity which equals to pores volume of the support as one shot (this was what was seen practically in this study). After that, the drying took place as

it was performed previously for the 1% lanthanum loaded support. Thereafter, it was placed inside the furnace again to get the precursor reduced according to the reaction:

$$FeN_3O_9 + 3H_2 \xrightarrow{heat} Fe + 3H_2O + 3NO_2 \quad (4.3)$$

Iron precursor loaded support drying and reduction were performed until the target was achieved. After that, the remaining amount of lanthanum (another 1%) was loaded and the same sequence of drying and reduction was followed.

Then, nickel loading was started (in form of $N_2NiO_6.6H_2O$) with 2.5% in each addition step for 4 successive loading, drying and reduction cycles. This time, after each cycle, a sample was taken. Nickel precursor reduction follows the reaction below:

$$N_2NiO_6 + 2H_2 \xrightarrow{heat} Ni + 2H_2O + 2NO_2 \quad (4.4)$$

Hydrogen stream was kept flowing until the sample reached the ambient temperature during precursor reduction in order to avoid any contact with oxygen (present in ambient air) and to assure pure metal (complete reduction) at the end of the reduction process. If the oxygen enters in contact with the sample at that high temperature, the sample will get oxidized and then the calculation procedure, which is based on the reduced form, becomes useless. Moreover, oxidized form offers less surface area to new loadings to be carried inside pores and can cause pore blockage. Furthermore, successive oxidation and reduction cycles during preparation steps reduce the OC lifetime.

CHAPTER 5

THERMODYNAMIC MODELLING

Thermodynamic analysis calculates the equilibrium distribution (conversions) of different chemical species involved in specific system under certain conditions. Such system may contain chemical reactions occurring among involved compounds.

The main goal is to know the extremum conversions (or fractions) that can be achieved, which helps in evaluating the catalyst efficiency and overall performance.

To perform equilibrium conversions' calculations in reactive systems, the general idea is that the system attains the equilibrium when its total Gibbs free energy is at its global minimum value. To get the point at which the total Gibbs free energy of the system reaches the global minimum, there are two common methods:

i. Equilibrium constant-Reaction coordinate method: This method uses the fact that at equilibrium, (minimum Gibbs free energy point) the differential (or change) of total Gibbs free energy with respect to the number of moles (of each chemical species involved in the system) is zero. However, this is true only for constant temperature and pressure systems; it can also be applied for flow systems since each point (specific temperature and pressure) can be dealt with as closed system as well as the truth that the Gibbs free energy is a state function which means it does not depend on the path of the process.

ii. Direct total Gibbs free energy minimization: This can be done by any normal optimization method. Here, the objective function that should be minimized is the total Gibbs free energy. And since it depends on each chemical species' number of moles, the number of moles must be taken as decision variables. Although the number of moles is not constant, atomic balance can be applied.

$$\sum_i n_i a_{ik} = A_k \tag{5.1}$$

General format of this method is:

Minimize $G^{total}\left(n_1, n_2, n_3, ..., n_N\right)$

Subjected to:

$$\sum_i n_i a_{ik} = A_k \quad \left(k = 1, 2, 3, ..., \mathrm{w}\right)$$
$$n_1, n_2, n_3, ..., n_N \geq 0$$

So, the optimum (minimum) point can be got 1) analytically by using Lagrangian multipliers [65][66] since all the constraints are of type of equality ones, or 2) numerically by using any suitable algorithm.

In case of using Lagrangian multipliers, the equations to be solved are:

$$\sum_i n_i a_{ik} = A_k \quad \left(k = 1, 2, ..., \mathrm{w}\right) \tag{5.2}$$

$$G_i^o + RT \ln\left(\frac{y_i \hat{\phi}_i P}{P^o}\right) + \sum_k \lambda_k a_{ik} = 0 \quad \left(i = 1, 2, ..., N\right) \tag{5.3}$$

Where λ_k are lagrangian multipliers. If one compound is an element and G^o for elements is set equal to zero, then for other compounds, $G^o = \Delta G_f^o$. Note that there is a need of

iterative method (due to fugacity coefficients/number of moles dependency)also; in case of using Lagrangian multipliers. Moreover, this method gives all of the critical points (maxima, minima and saddle points), which adds another step of determining the global minimum to the calculations. As a result of that, using one of the numerical minimization algorithms of those designed to converge to the minimum point directly is preferred. Regarding numerical algorithms, any interior or exterior point algorithm can be applied. However, in case of using interior point algorithm, there is a must of ensuring that the initial guess is feasible, to overcome so, it is suitable to use exterior point algorithm. Notice that the initial amounts of moles is not applicable when one of the species is absent at the beginning of the reaction ($y_i = 0$). That is resulted from the natural logarithm calculations ($\ln(0) = -\infty$).

Generally, direct Gibbs free energy minimization is preferred over equilibrium constants-reaction coordinates method (especially in the case of multiple reactions) because it does not require chemical reactions set and there is no need to calculate equilibrium constants. The only thing that is needed is knowing all the chemical species involved in the system. Note that the two methods are equivalent to each other since they use the same mathematical property to get the equilibrium point. So, the same answer will be found if both of them are performed correctly.

The method used in this study is numerical minimization algorithm called sequential quadratic programming (SQP) because of its quadratic rate of convergence and affiliation to exterior point algorithms.

5.1. Assumptions and Justifications

1. The system follows Peng-Robinson Equation of State because this EOS is suitable for hydrocarbon compounds.
2. Total fuel conversion: However, the equilibrium amount of the combusted fuel depends on the process conditions (temperature and the pressure) and fuel composition. The assumption of total conversion is made due to un-provided exact composition of some hydrocarbon fuels (especially those cuts resulted from oil refinery such as Kerosene and naphtha) as well as the lack of important thermodynamic properties of such fuels (like acentric factor, critical temperature and critical pressure). In addition, the oxygen provided by the oxygen carrier and gasification agent (water) is sufficient to convert approximately all of the fuel to products ($H_2O, H_2, CO_2, CO, CH_4, C$)under selected conditions. Besides, the water with hydrocarbons reactions has very high equilibrium constants under those conditions. Furthermore, high temperature cracks long hydrocarbon series into other smaller hydrocarbon compounds.
3. The support material in catalyst has no interaction with the active agent/ fuel/air.
4. Iron oxide follows this reduction sequence: $Fe_2O_3 \rightarrow Fe_3O_4 \rightarrow FeO \rightarrow Fe$, and nickel oxide reduced as: $NiO \rightarrow Ni$.
5. All hydrocarbons lighter than fuel (except methane)have negligible amount in the system(due to the same reason mentioned in the first assumption of behavior of water and oxygen carrier with the hydrocarbons

under high temperature as well as temperature effect).So, they can be ignored in calculations (this assumption insured by K values calculations and experimental data found).

6. There is no free oxygen in the system because of its high reactivity with other compounds and elements (mainly Nickel, Hydrogen, Hydrocarbons, Carbon monoxide, and even free carbon may deposit on oxygen carrier surface).
7. Constant temperature and pressure throughout the reactor.
8. All binary interaction parameters are set equal to zero due to the lack of data, and at high temperature and low pressure, the system behaves like ideal gas since attractive forces among molecules have small magnitude and only remarkable inter-molecular forces are repulsive ones. So, the differences between attractive forces among different molecules are negligible.

So, according to these assumptions, equation (5.2) becomes (in matrix form) as follows:

$$\begin{bmatrix} 2 & 2 & 0 & 0 & 4 & 0 & 0 & 0 & 0 & 0 & 0 & 0 \\ 1 & 0 & 2 & 1 & 0 & 0 & 1 & 0 & 3 & 4 & 1 & 0 \\ 0 & 0 & 1 & 1 & 1 & 1 & 0 & 0 & 0 & 0 & 0 & 0 \\ 0 & 0 & 0 & 0 & 0 & 0 & 1 & 1 & 0 & 0 & 0 & 0 \\ 0 & 0 & 0 & 0 & 0 & 0 & 0 & 0 & 2 & 3 & 1 & 1 \end{bmatrix} \begin{bmatrix} n_{H_2O} \\ n_{H_2} \\ n_{CO_2} \\ n_{CO} \\ n_{CH_4} \\ n_{C} \\ n_{NiO} \\ n_{Ni} \\ n_{Fe_2O_3} \\ n_{Fe_3O_4} \\ n_{FeO} \\ n_{Fe} \end{bmatrix} = \begin{bmatrix} A_H \\ A_O \\ A_C \\ A_{Ni} \\ A_{Fe} \end{bmatrix}$$

Total system Gibbs free energy is the sum of all Gibbs free energies of different phases existing in the system. Since both liquid and gas phases' Gibbs free energies can be determined similarly [67] (by changing volume root choice to be that assigned for liquid phase in EOS), the system phases can be classified into fluid and solid ones. Even though, the fluid phase should be treated as sum of gas and liquid ones.

5.2. Gas phase mixture Gibbs free energy

By using residual property relation [68]:

$$G_{gas,mix} = G_{mix}^{ig} + G_{mix}^{R} \tag{5.4}$$

But the ideal gas mixture Gibbs free energy given by:

$$G_{mix}^{ig} = \sum_{i=1}^{n} y_i G_i^{ig} + RT \sum_{i=1}^{n} y_i \ln y_i \tag{5.5}$$

Where the ideal gas Gibbs free energy of pure substance is:

$$G_i^{ig} = \int_{298.15}^{T} C_{P_i} dT - T \int_{298.15}^{T} \frac{C_{P_i}}{T} dT + RT \ln \frac{P}{P_1} - S_{i_{298.15}} \left(T - 298.15\right) + G_{i_{298.15}} \tag{5.6}$$

(Note that 298.15 K here is the reference temperature, and P_1 is the reference pressure)

Regarding residual Gibbs free energy, the formula of pure substances is used with some modifications in the EOS constants by using mixing and combining rules as follows:

For pure components and by using Peng-Robinson [69] EOS:

$$\frac{G^R}{RT} = Z - 1 - \ln\left(Z - \frac{Pb}{RT}\right) - \frac{a}{2\sqrt{2}bRT} \ln\left(\frac{V + \left(1+\sqrt{2}\right)b}{V + \left(1-\sqrt{2}\right)b}\right) \tag{5.7}$$

So for mixture:

$$\frac{G_{mix}^R}{RT} = Z_{mix} - 1 - \ln\left(Z_{mix} - \frac{Pb_{mix}}{RT}\right) - \frac{a_{mix}}{2\sqrt{2}b_{mix}RT} \ln\left(\frac{V_{mix} + \left(1+\sqrt{2}\right)b_{mix}}{V_{mix} + \left(1-\sqrt{2}\right)b_{mix}}\right) \tag{5.8}$$

Where $Z_{mix} = \frac{PV_{mix}}{RT}$ and V_{mix} can be estimated from EOS as follow:

$$P = \frac{RT}{V_{mix} - b_{mix}} - \frac{a_{mix}}{V_{mix}\left(V_{mix} - b_{mix}\right) + b_{mix}\left(V_{mix} - b_{mix}\right)} \tag{5.9}$$

a_{mix} And b_{mix} are related to individual components' thermodynamic properties by:

$$a_{mix} = \sum_{i=1}^{n}\sum_{j=1}^{n} y_i y_j \sqrt{a_i a_j}\left(1 - k_{ij}\right), \quad b_{mix} = \sum_{i=1}^{n} y_i b_i \tag{5.10}$$

Where:

$$a_i = \frac{0.45724\alpha_i(T)R^2T_{c_i}^2}{P_{c_i}^2}\ ,\ b_i = \frac{0.0778RT_{c_i}}{P_{c_i}} \tag{5.11}$$

And:

$$\alpha_i(T) = \left[1 + k_i\left(1 - \sqrt{T_{r_i}}\right)\right]^2\ ,\ k_i = 0.37464 + 1.54226\omega_i - 0.2699\omega_i^2$$
$$T_{r_i} = \frac{T}{T_{c_i}} \tag{5.12}$$

5.3. Solid Phase Gibbs free energy

Here, total Gibbs free energy of solid phase can be set equal to the sum of each total Gibbs free energies for all components existing in such phase.

$$n_{total,solid}G_{solid,mix} = \sum n_{solid}G_{i,solid} \tag{5.13}$$

In this respect, Gibbs free energies of oxidized active agent in the oxygen carrier, reduced active agent and solid carbon deposit are calculated and modeled as a function of temperature (since solid phase is not affected by pressure remarkably)

Thus the total Gibbs free energy of the system is:

$$G^{total} = n_{total,gas}G_{gas,mix} + n_{total,solid}G_{solid,mix} \tag{5.14}$$

5.4. Heat Capacity vs. Temperature

Constant pressure heat capacities for gaseous chemical compounds (H_2O, H_2, CO_2, CO and CH_4)are considered as a function in temperature as follows:

$$C_{P_i} = a_i + b_i T + c_i T^2 + d_i T^3 + e_i T^4 + f_i T^5 + g_i T^6 + h_i T^7 \qquad (5.15)$$

Experimental data are taken from [70]. The coefficients for each species are found to be:

Table5.1: Constant pressure heat capacities' coefficients estimated at 1 bar

Component	a_i	b_i	$c_i \times 10^{-4}$	$d_i \times 10^{-9}$	$e_i \times 10^{-12}$	$f_i \times 10^{-15}$	$g_i \times 10^{-19}$	$h_i \times 10^{-24}$
H_2O	33.8	-0.83	0.32	-22.4	7.9	-1.5	1.6	-7
H_2	28.55	0.2	0.05	8.4	-4.94	1.4	-1.9	10
CO_2	18.24	8.6	-0.93	68.5	-33.9	10.7	-19	144
CO	32.84	-3	0.78	83.2	48	-15.75	27.7	-202.55
CH_4	45.47	-15.6	6.4	-971.6	824.58	-407.6	109.2	-12227.7

The same idea used for solid materials Gibbs free energy:

$$G_i = a_1 + a_2 T + a_3 T^2 + a_4 T^3 + a_5 T^4 + a_6 T^5 + a_7 T^6 + a_8 T^7 \qquad (5.16)$$

Table5.2: Solid Gibbs free energy (as function in temperature) coefficients

Solid	a_1	$a_2 \times 10^{-2}$	$a_3 \times 10^{-4}$	$a_4 \times 10^{-9}$	$a_5 \times 10^{-13}$	$a_6 \times 10^{-16}$	$a_7 \times 10^{-20}$	$a_8 \times 10^{-24}$
C	-1.66	0.533	-0.2	3.13	1.43	-2.17	4.4	-3
NiO	-250.1	3.87	-1.74	132.5	-708	227.8	-395.7	281
Ni	-2.8	-1.4	-0.02	-100	1435.4	-980.8	3366.24	-4643.7
Fe_2O_3	-850.61	13.13	-6.43	943.4	-10226	6585	-22492.2	31402
Fe_3O_4	-1141.5	3.041	-4.2	409.4	-4820.6	3550	-13213.7	19253.2
FeO	-281.5	1.26	-1.81	175	-1353.5	682.7	-1967.7	2446
Fe	-8.78	4.7	-2.26	334.6	-3125.3	1620.27	-4256.8	4347.07

The Figures below show how the model fits to experimental (or reported) data. The thick dots are the data while the solid line is the model.

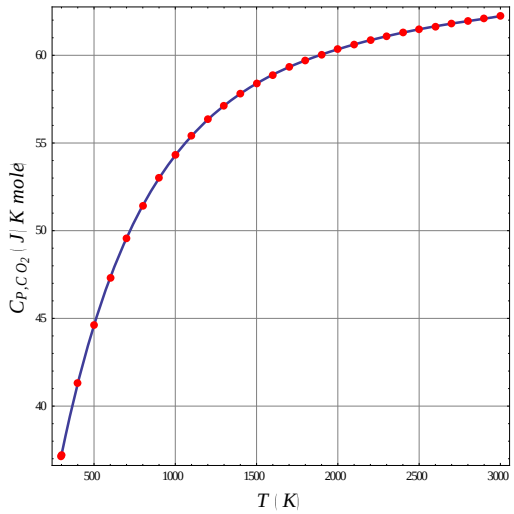

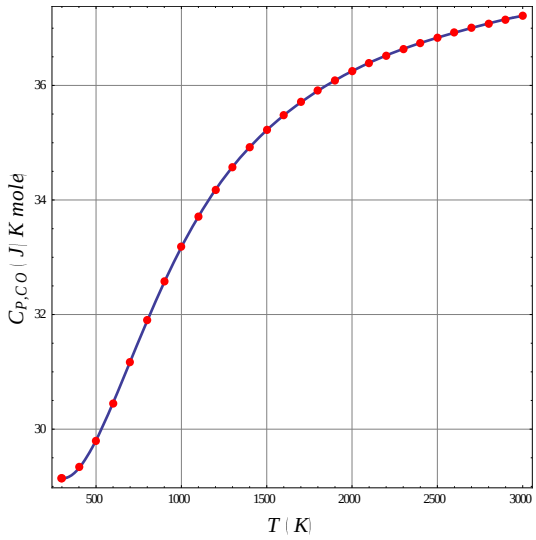

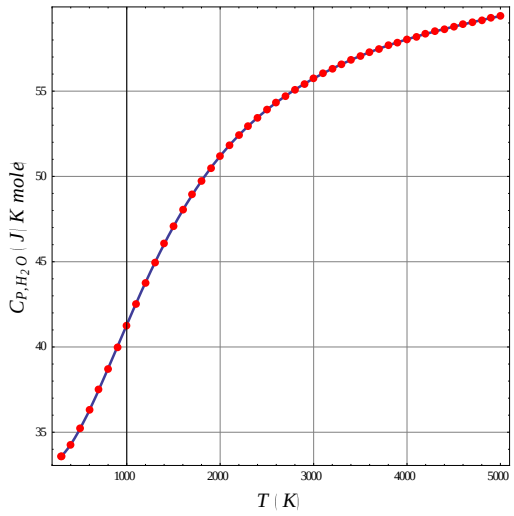

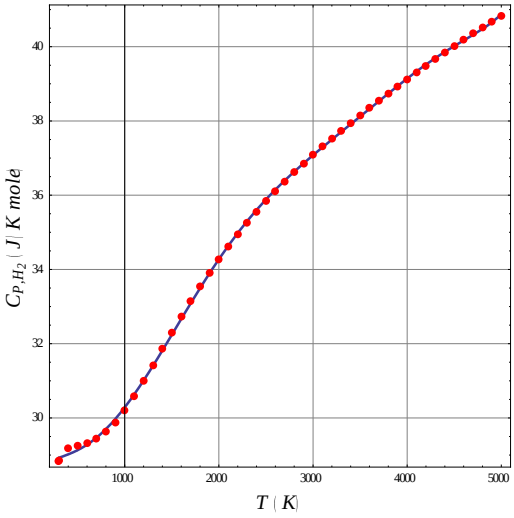

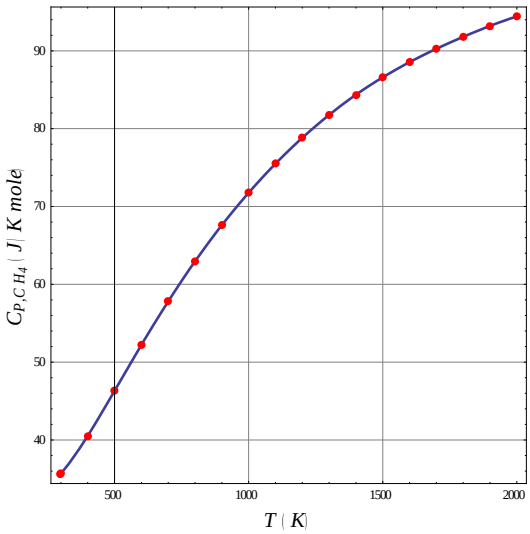

Figure 5.1: Heat capacitites of gaseous compounds

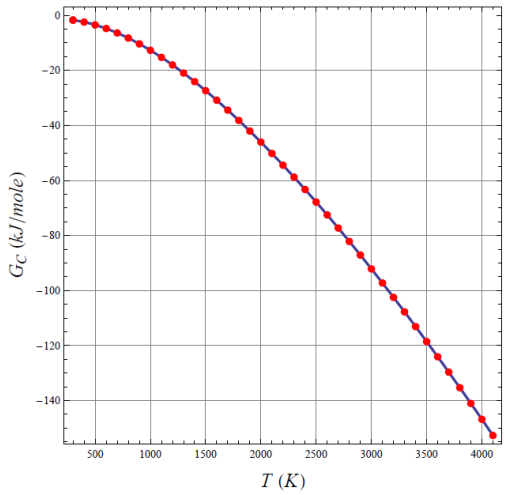
$G_C\ (kJ/mole)$
$T\ (K)$

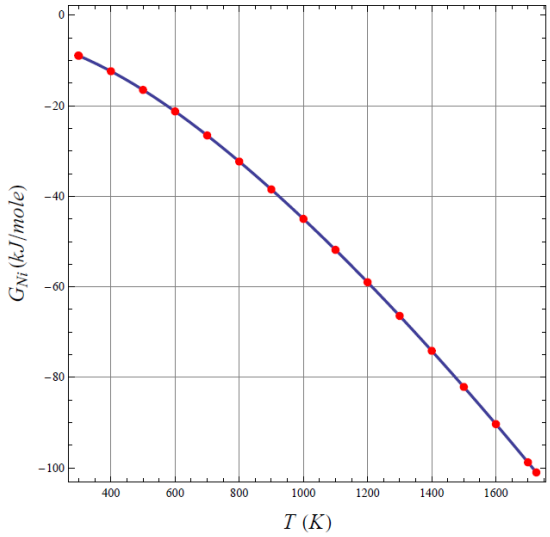
$G_{Ni}\ (kJ/mole)$
$T\ (K)$

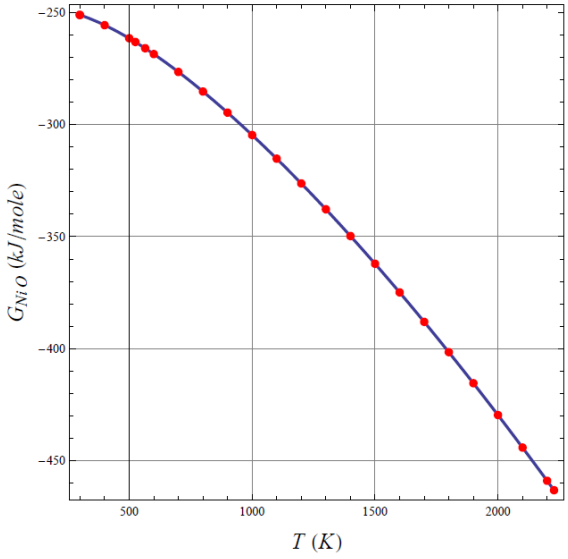
$G_{Ni\,O}\ (kJ/mole)$
$T\ (K)$

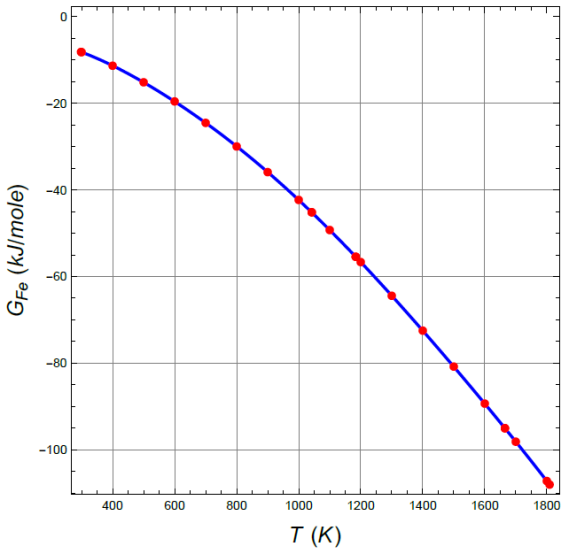
$G_{Fe}\ (kJ/mole)$
$T\ (K)$

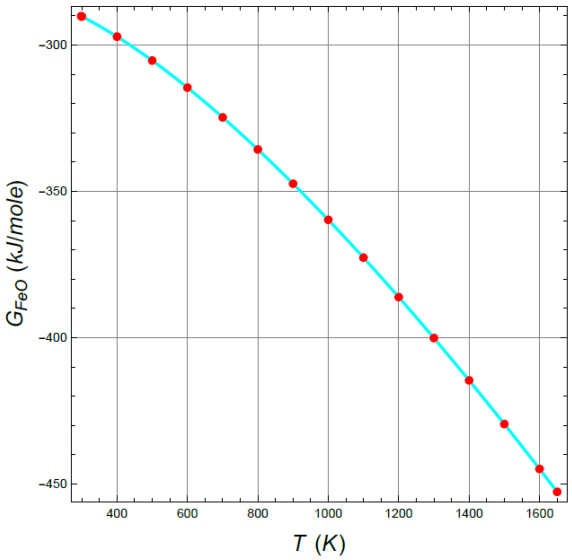
$G_{FeO}\ (kJ/mole)$
$T\ (K)$

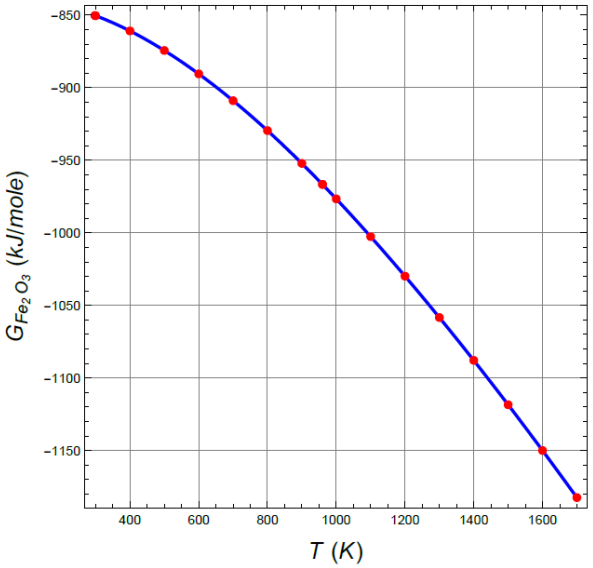
$G_{Fe_2O_3}\ (kJ/mole)$
$T\ (K)$

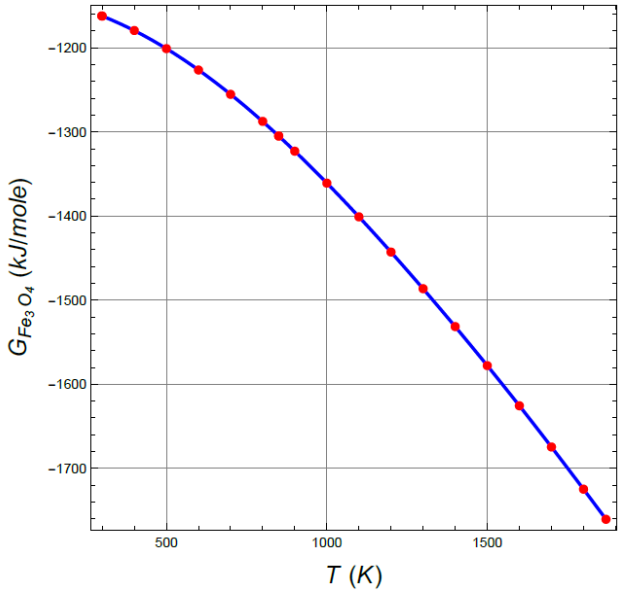

Figure 5.2: Gibbs free energies of solid materials

One of the advantages of this model is that it takes carbon deposition in account; so, the conditions that lead to its formation can be avoided accordingly. One of the ways to overcome carbon deposition is providing enough amount of steam. Actually, the more steam is provided, the more cracking and reforming is occurred. But, cracking process has a maximum limit at which all the hydrocarbons will be converted to hydrogen and CO. After that limit, the rest of the water will just keep being circulated over and over without doing anything. So, hypothetically, the optimum amount of water is the amount that is needed to convert all of the fuel to H_2 and CO, as:

$$C_nH_mO_f + (n-f)H_2O \rightarrow nCO + \left(n - f + \frac{m}{2}\right)H_2 \qquad (5.17)$$

So, each mole of $C_nH_mO_f$ needs (n-f) moles of steam so as to be completely converted to carbon monoxide and hydrogen. It is clear from reaction (5.17) that the needed amount of steam depends on the existing carbon and oxygen in the fuel and in some cases, this

reaction becomes impossible if the quantity (n-f) becomes negative. Fortunately, this study is dealing with n-Hexane (C_6H_{14}) as a model for heavy hydrocarbon fuel and it does not have oxygen in its molar composition (f=0).

5.5. Thermodynamic Model Testing and Validation

In order to check the validity of the created thermodynamic model, more than one process data found in literature was used.

Overall, general steam reforming/gasification of hydrocarbons can be considered as follows:

$$C_xH_yO_z + aH_2O \rightarrow bH_2 + dCO + eCO_2 + fCH_4 + gC_2H_4 + iC_2H_6 + jH_2O + kC + \ldots \quad (5.18)$$

5.5.1. Application of Steam/Biomass (Glucose) Gasification

Feed effect (Steam/Biomass ratio)

Steam/Biomass effect was studied under pressure of P=1atm and temperature of T=650℃.

Suppose that, the initial feed consists of n_S moles of steam (H_2O) and n_B moles of glucose (biomass) ($C_6H_{12}O_6$) only, so the atomic balance matrix will be as:

$$\begin{pmatrix} 2 & 2 & 0 & 0 & 4 & 0 & 0 & 0 \\ 1 & 0 & 2 & 1 & 0 & 0 & 1 & 0 \\ 0 & 0 & 1 & 1 & 1 & 1 & 0 & 0 \\ 0 & 0 & 0 & 0 & 0 & 0 & 1 & 1 \end{pmatrix} \begin{pmatrix} n_{H_2O} \\ n_{H_2} \\ n_{CO_2} \\ n_{CO} \\ n_{CH_4} \\ n_C \\ n_{NiO} \\ n_{Ni} \end{pmatrix} = \begin{pmatrix} 2n_S + 12n_B \\ n_S + 6n_B \\ 6n_B \\ 0 \end{pmatrix} \quad (5.19)$$

Equilibrium mole fraction of different species in the gas phase was calculated by using MATLAB program and the results are:

Table5.3: Equilibrium mole fractions' distribution resulted from glucose gasification at 650℃ and 1 atm

S/B (g/g)	y_{H2O}	y_{H2}	y_{CO2}	y_{CO}	y_{CH4}
0.4	0.1589	0.4349	0.1535	0.2111	0.0416
0.5	0.1868	0.4378	0.1578	0.1858	0.0318
0.6	0.2137	0.4367	0.1604	0.1647	0.0245
0.7	0.2395	0.4328	0.1619	0.1469	0.019
0.8	0.2643	0.4269	0.1623	0.1317	0.0148
0.9	0.288	0.4196	0.1621	0.1186	0.0116
1.0	0.3108	0.4115	0.1613	0.1073	0.0092
1.1	0.3325	0.4028	0.16	0.0974	0.0073
1.2	0.3533	0.3938	0.1584	0.0887	0.0058

Experimental data [7] are taken for two different catalysts (in terms of active agent loading and promoter addition [La_2O_3]), 20 sec reaction time.

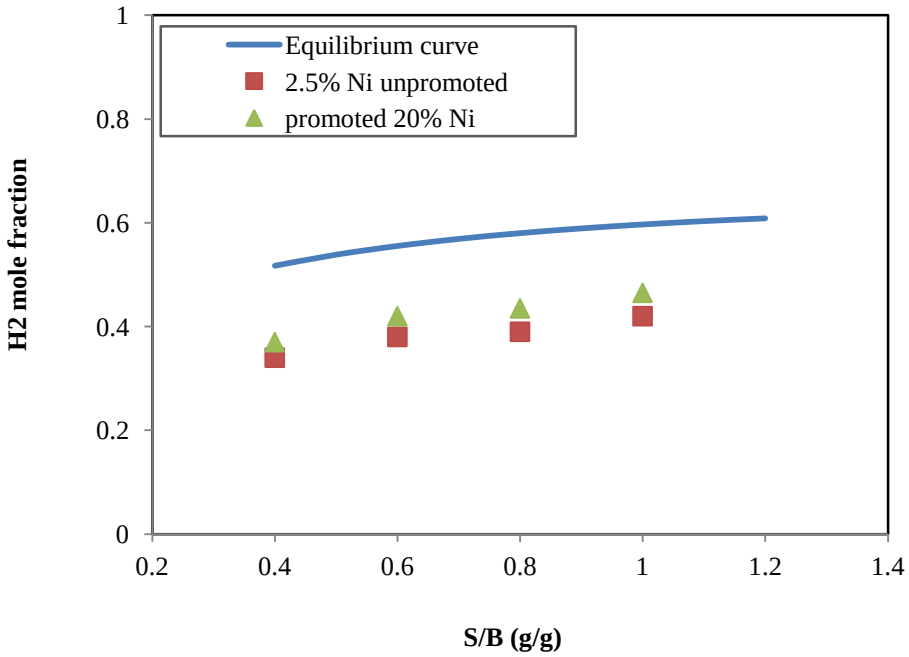

Figure 5.3: Hydrogen composition (dry basis) at different steam to glucose ratios (T: 650 °C and P: 1 atm)

Figure 5.3 shows, as the steam/glucose feed ratio increases, the equilibrium amount of produced hydrogen will also increase. This is mainly due to the fact that all hydrocarbons (lighter than glucose) resulted from gasification process will interact with water and produce CO and H_2. However, CO further reacts with steam according to water-gas shift reaction to produce H_2 also. Besides, solid carbon (coke) also reacts with steam (heterogeneous water-gas shift reaction) to produce H_2 and CO. So, as steam amount increases, all these reactions proceed. Regarding experimental data, it is clear that nickel amount affects the overall yield significantly as well as lanthanum oxide.

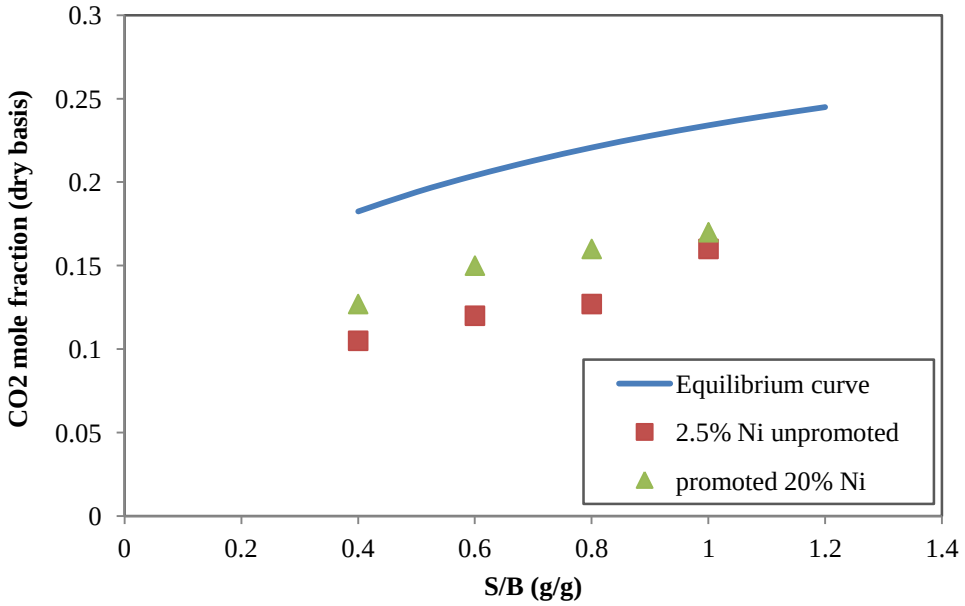

Figure 5.4: Carbon dioxide mole fraction (dry basis) from glucose gasification at 650°C and 1 atm

Carbon dioxide amount depends on the amount of oxygen provided in the system (due to combustion process).So, added steam (more oxygen) is expected to enhance CO_2 fraction.

In contrast, CO presence means incomplete combustion and therefore becomes much less as the provided amount of oxygen increased. Such behavior can be seen from the following Figure (Figure 5.5)

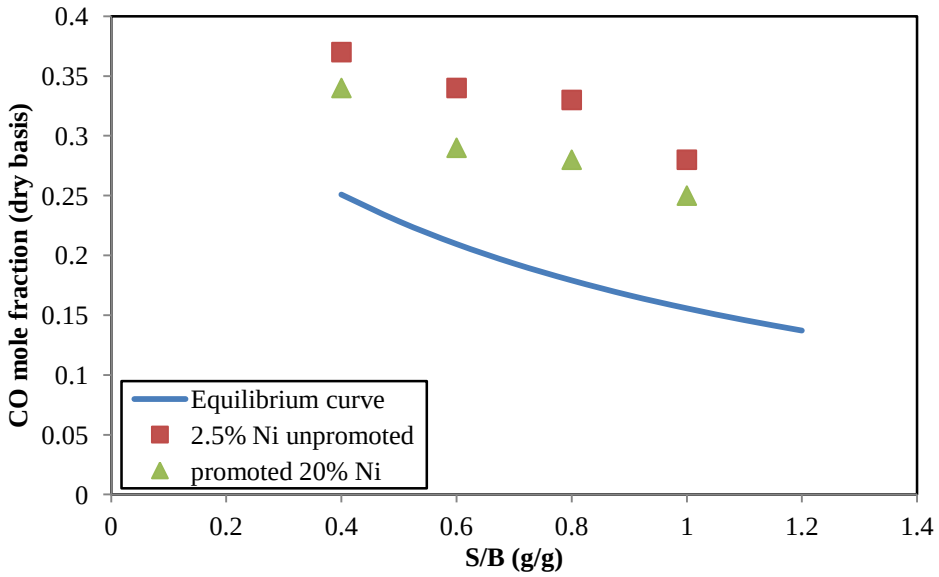

Figure 5.5: Carbon monoxide mole fraction (dry basis) from glucose gasification at 650°C and 1 atm

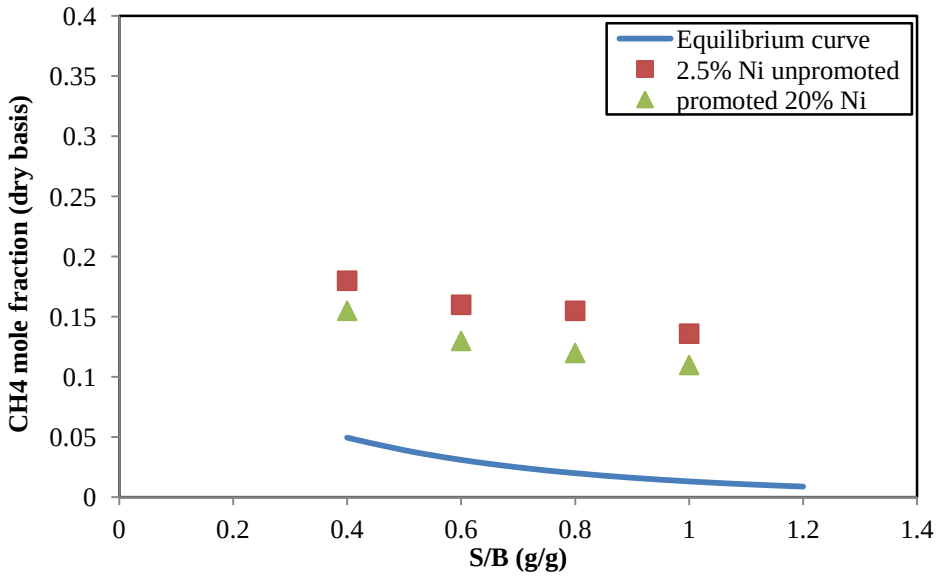

Figure 5.6: Methane mole fraction (dry basis) from glucose gasification at 650°C and 1 atm

The main reaction affecting methane content is steam reforming of methane. In addition, any free oxygen presence in the system will lead to direct combustion of hydrocarbons including methane.

Temperature effect

It is known that if the temperature is increased, molecules become more energetic and their motion becomes faster and faster. This offers huge possibility of them to collide with each other (according to collision theory) to break molecular bonds and to form other ones. Thermodynamically, molecules tend to form stable bonds and compounds. Practically, if temperature is changed, the reaction equilibrium will be shifted to another point so as to minimize this change effect on the system as stated by “Le Chatelier's principle". So, the reaction will proceed either forward or backward depending on its nature (whether it is exothermic or endothermic). Mathematically, change in temperature causes change in the equilibrium constants (K values) directly, and thus change in equilibrium distribution "equilibrium point". In the respect of exothermic and endothermic behavior of the reaction, temperature can be dealt with as a reactant. For example, if the reaction is endothermic, it means that the reaction will proceed forward if more heat is added, and it will move backward if it is cooled down (opposite is true for exothermic reaction).

The following Table shows equilibrium distribution for glucose gasification:

Table5.4: Equilibrium mole fractions' distribution for glucose gasification at feed ratio (S/B)=1(g/g) and 1 atm

T (℃)	y_{H2O}	y_{H2}	y_{CO2}	y_{CO}	y_{CH4}
500	0.4273	0.2488	0.2061	0.024	0.0937
550	0.3707	0.3242	0.1969	0.0489	0.0593
600	0.3286	0.3833	0.1795	0.0805	0.028
650	0.3108	0.4115	0.1613	0.1073	0.0092
700	0.3119	0.4141	0.1472	0.1244	0.0024
750	0.3196	0.4074	0.1362	0.1363	0.0006
800	0.3282	0.399	0.1267	0.1459	0.0002
850	0.3363	0.391	0.1184	0.1543	0.0001
900	0.3436	0.3837	0.111	0.1617	0
950	0.3502	0.3771	0.1044	0.1683	0
1000	0.3561	0.3712	0.0985	0.1742	0

Figure 5.7 represents that equilibrium mole fraction of hydrogen in glucose gasification process starts increasing in temperature range (500℃ 650℃), and then decrease asymptotically to a value of about 0.55. This can be referred to the exothermic/endothermic nature of hydrogen reactions with different species in gasification process. In details, dry reforming of methane, steam reforming of methane and heterogeneous water-gas shift reaction - all these are endothermic reactions (forward direction) and lead to hydrogen formation. So, any increase in temperature according to these reactions will lead to producing more amount of hydrogen. Besides that, other hydrocarbons' (higher than methane) steam gasification reactions and hydrogenating gasification of solid carbon are also endothermic hydrogen producer ones. But on the other hand, water-gas shift reaction is an exothermic reaction. Thus the resulted trend of equilibrium mole fraction of hydrogen is expected because of that conflicting nature of reactions involved in such systems. Note that not all mentioned endothermic reactions are important in this process (due to their K values) and can be ignored. But this is not the case with exothermic reactions.

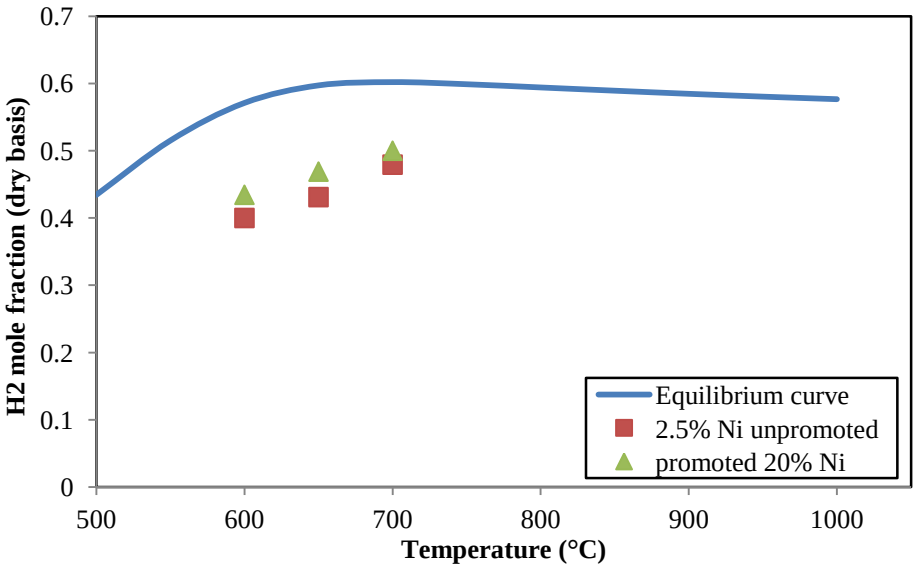

Figure 5.7: Hydrogen mole fraction (dry basis) resulted from glucose gasification at S/B=1(g/g)and 1 atm

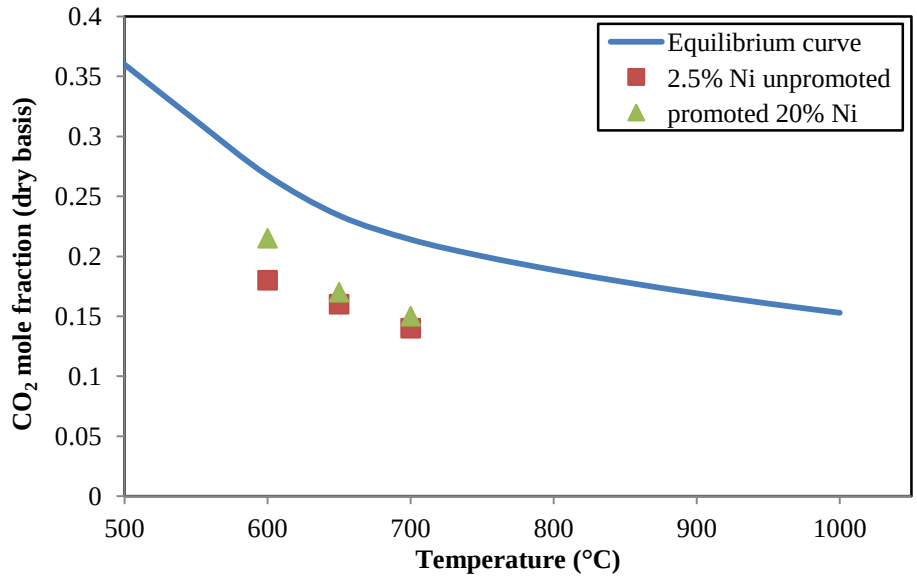

Figure 5.8: Carbon dioxide mole fraction (dry basis) resulted from glucose gasification at S/B=1(g/g)and 1 atm

Since all reactions including carbon monoxide as a product are endothermic (dry reforming of methane, hydrocarbons steam reforming, water-gas and heterogeneous water-gas shift reactions, boudouard reaction and hydrogenating gasification), carbon

monoxide equilibrium mole fraction increases as temperature increases. This is what is shown exactly in Figure 5.9.

Since some of the previously mentioned reactions include carbon monoxide on one side and carbon dioxide on the other, it is normally expected that as the portion of carbon dioxide increases, carbon monoxide fraction will decrease and vice versa .

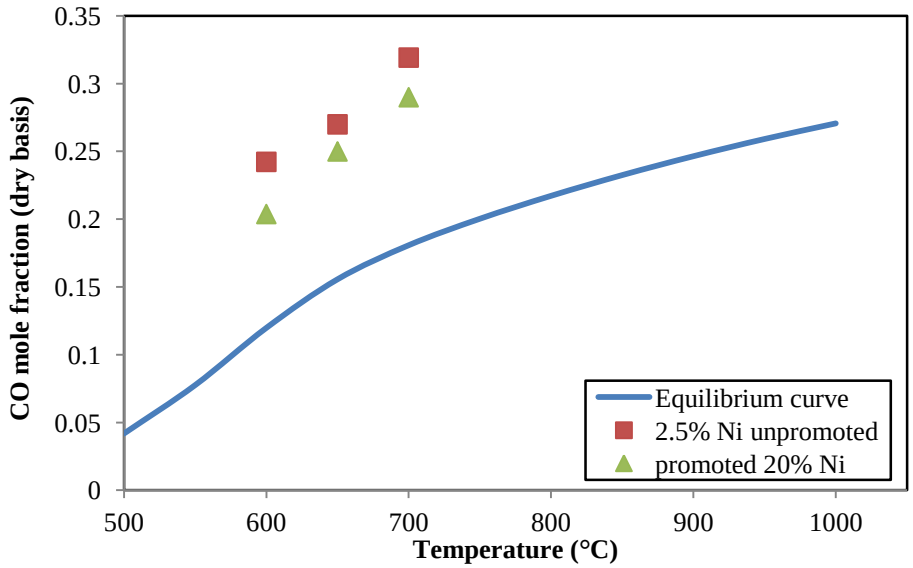

Figure 5.9: Carbon monoxide mole fraction (dry basis) resulted from glucose gasification at S/B=1(g/g)and 1 atm

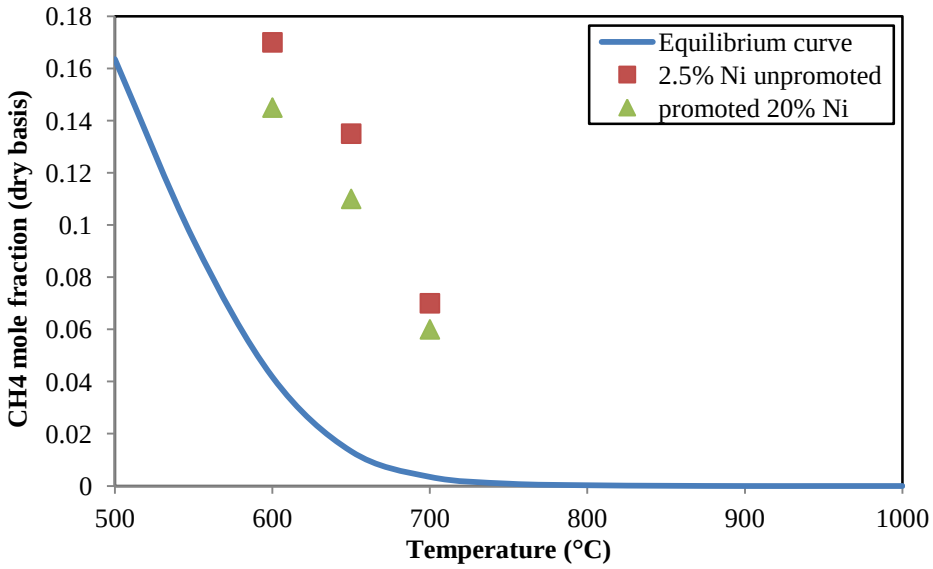

Figure 5.10: Methane mole fraction (dry basis) resulted from glucose gasification at S/B=1(g/g)and 1 atm

It is expected that (as mentioned in assumptions) as temperature increases, all steam gasification and reforming reactions(of all hydrocarbons) become faster and proceed forward rapidly. This can be concluded from their huge K values and endothermic nature. Thus all hydrocarbons' (even methane) equilibrium mole fractions become less as a result of that.

Nickel Loading (Active Agent) effect

Nickel plays a role of active catalyst in glucose gasification process. When more nickel is added, the total provided active area for reactants to react in presence of catalyst becomes larger. This allows reaction to proceed forward and facilitates reaching the equilibrium state.

Three catalysts with different nickel loading are compared with each other by letting the equilibrium point as reference. Results show that as nickel percentage increases, the catalyst performance becomes better and it approaches equilibrium distribution which is expected.

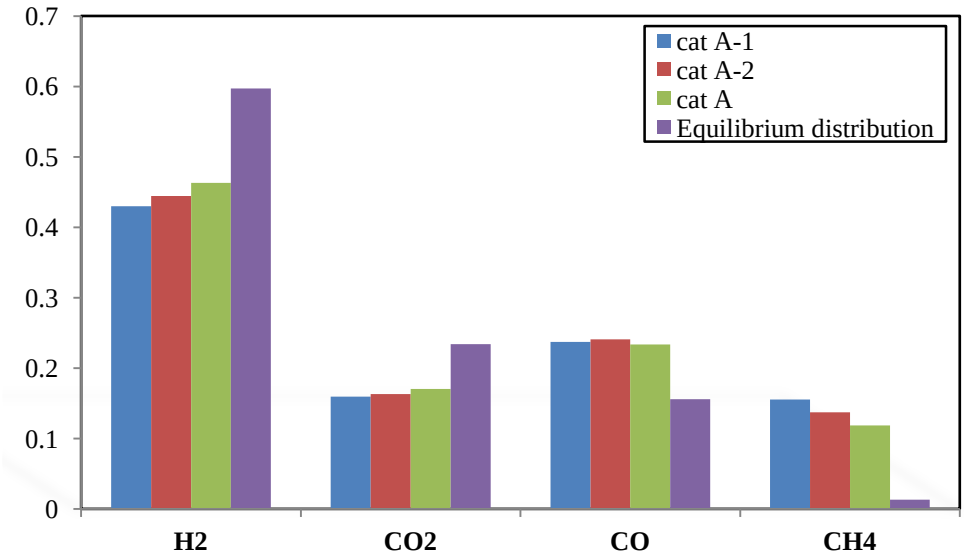

Figure 5.11: Nickel loading effect on gas phase composition

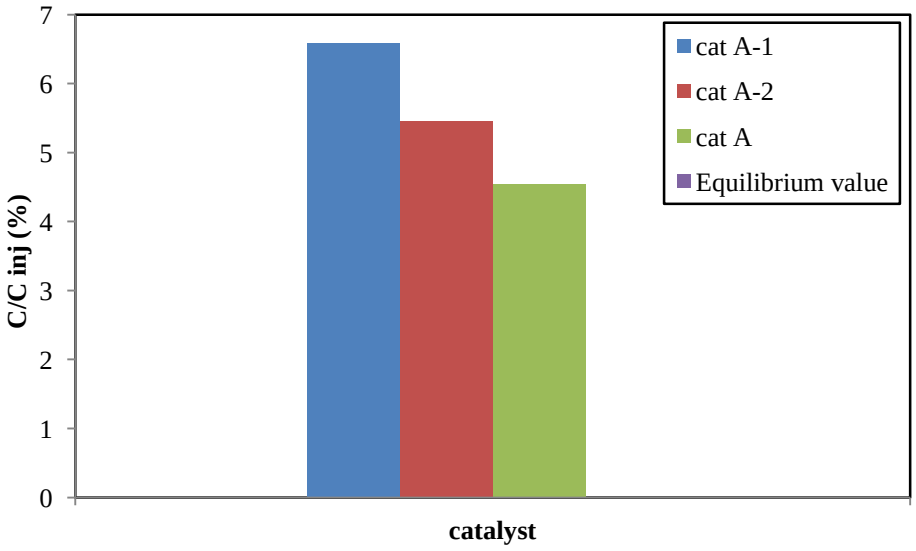

Figure 5.12: Nickel loading effect on solid carbon deposition

Thermodynamic calculations show that at S/B=1(g/g), 650℃ and 1 atm, there is no solid carbon existence in the system at equilibrium state. So, since nickel presence facilitates reaching the equilibrium state, more of it will prevent solid carbon from deposition. Although in real cases no reaction can reach equilibrium state exactly, approaching it asymptotically is possible but reaching it exactly it is not because it needs an infinite duration of time. Solid carbon deposition can be avoided completely by providing more than calculated needed amount of steam. Note that catalyst will not react with other species.

Promoter Addition effect

The idea of promoter addition is to enhance active agent effectiveness. If there is a lot of active agent but with little effectiveness, it only means that there is a part of such active agent not fully working. To overcome this common problem, suitable promoters are usually added to the active agent. So, promoter addition increases the catalyst's overall efficiency. On the other hand, this addition has an upper limit after which the opposite effect will occur because of the agglomeration.

Figures 5.13 and 5.14 show how promoter presence affects the catalyst performance on approaching equilibrium state.

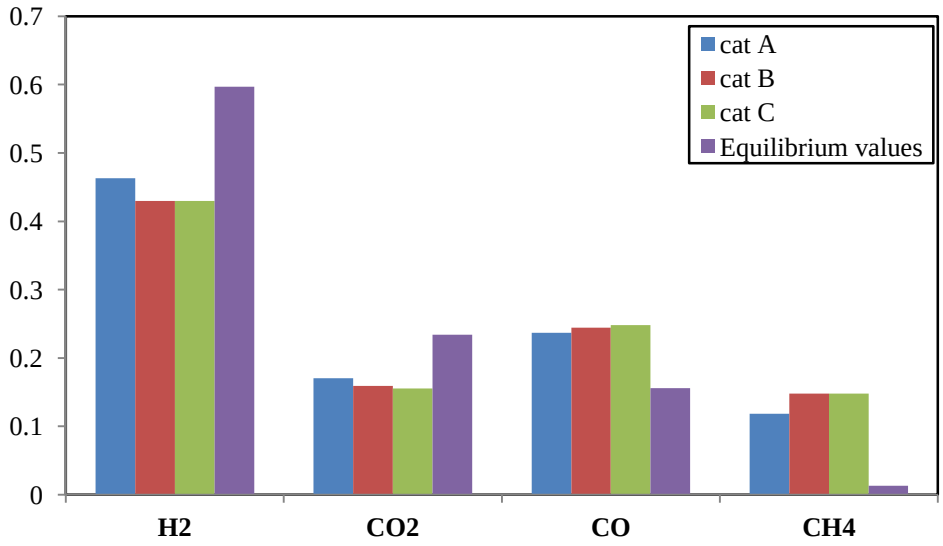

Figure 5.13: Effect of preparation method and promoter addition on gas phase composition

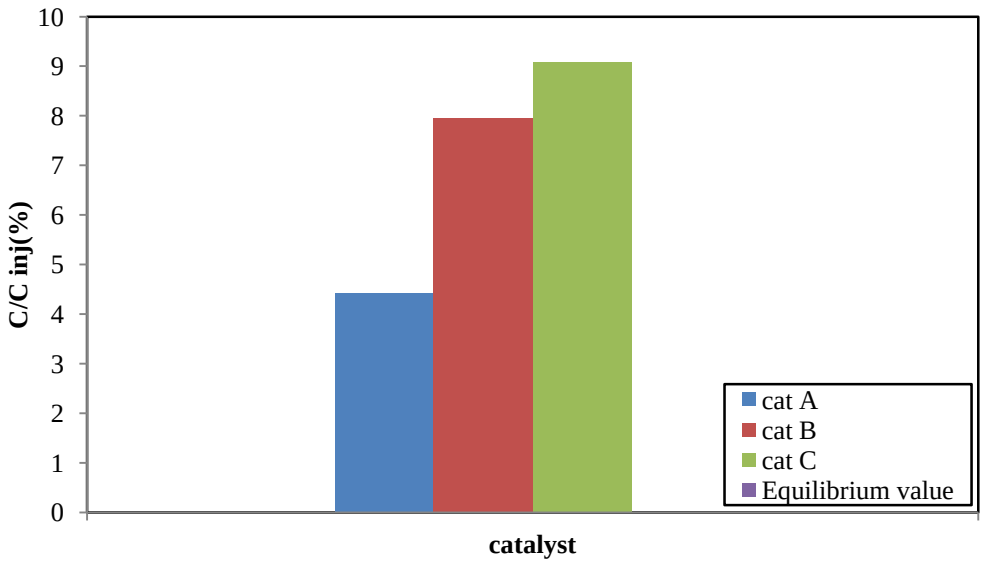

Figure 5.14: Effect of preparation method and promoter addition on solid carbon deposition

Figure 5.14 displays three columns although it includes four categories because the equilibrium amount of solid carbon under those conditions is zero.

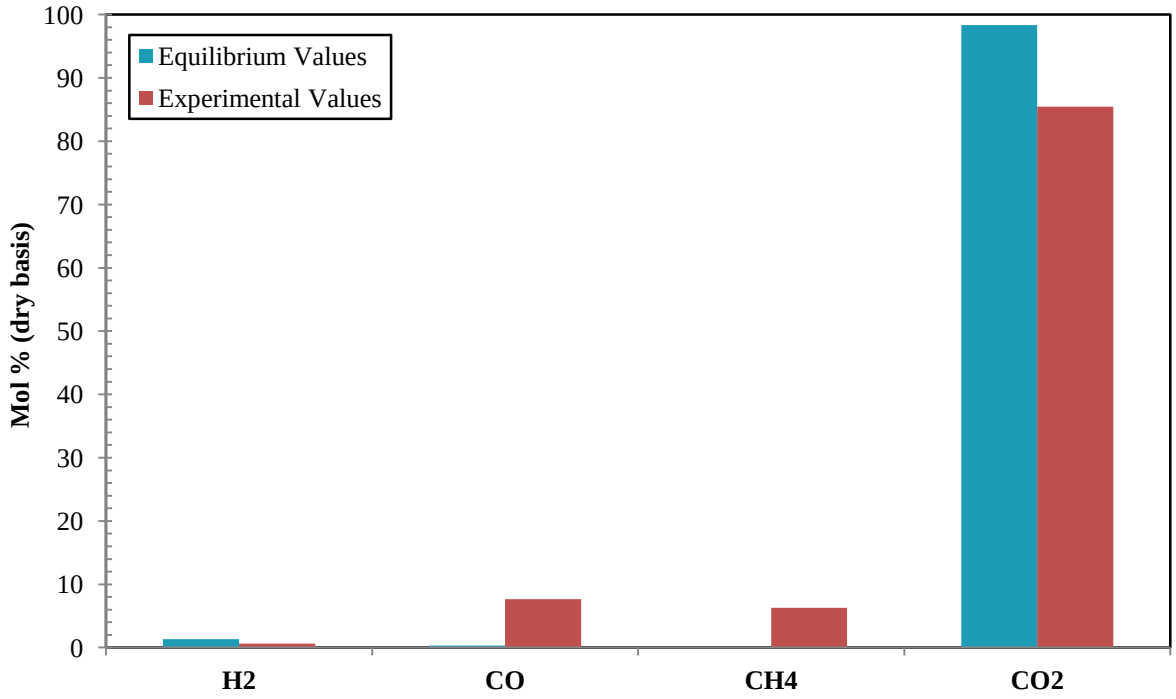

Figure 5.15: Glucose CLC with NiO(700℃ , S/G/NiO=1g/1g/5g and 20 sec.)

5.5.2. Application to Kerosene Fuel-based CLC with NiO

The procedure followed in kerosene gasification is quite different than that used in glucose gasification. This difference comes from the unfixed composition of Kerosene since it is a cut of a lot of hydrocarbons and its composition (those hydrocarbons' distribution) differs according to the crude oil it comes from and oil processing it has undergone. In many cases, lab analysis gives general physical properties (normal boiling point, density, heating value and hydrogen to carbon ratio H/C) of kerosene sample rather than its actual composition. In such cases, an approximate chemical formula is needed to perform thermodynamic analysis and calculations. So, the kerosene [6] analyzed in this study has an approximate chemical formula of$C_{12}H_{22.56}$. Moreover, the aim of kerosene gasification is not to produce hydrogen and carbon monoxide (desired products from any

reforming process) but to facilitate combustion of kerosene with oxygen carrier (OC "NiO").So, solid material remains no longer the catalyst, but becomes important reactant. Thus the provided amount of solid OC affects the equilibrium distribution directly.

To estimate the performance of OC, the equilibrium percentage of carbon converted or emitted as carbon dioxide ($\gamma_{CO_2} = \frac{C_{emitted\ as\ CO_2}}{C_{fed\ (in\ fuel)}}$) is used instead of equilibrium distribution.

The following Figures represent γ CO_2values for four different Kerosene/ steam/ Nickel oxide ratios:

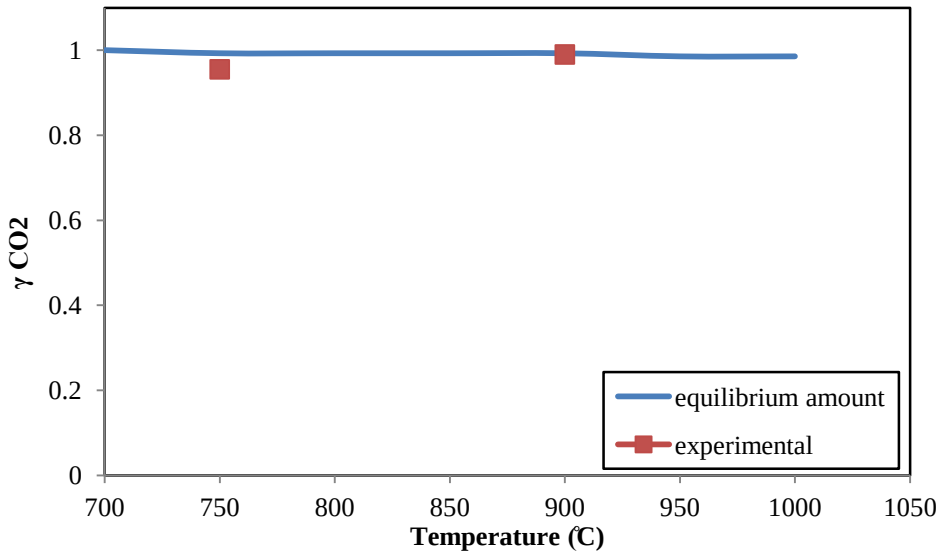

Figure 5.16: Kerosene Chemical-Looping Combustion with NiO (0.25 ml liq. Kerosene/min, 0.75 ml liq. Water/min and 250 g of N4MZ-1400 [40 wt% NiO])

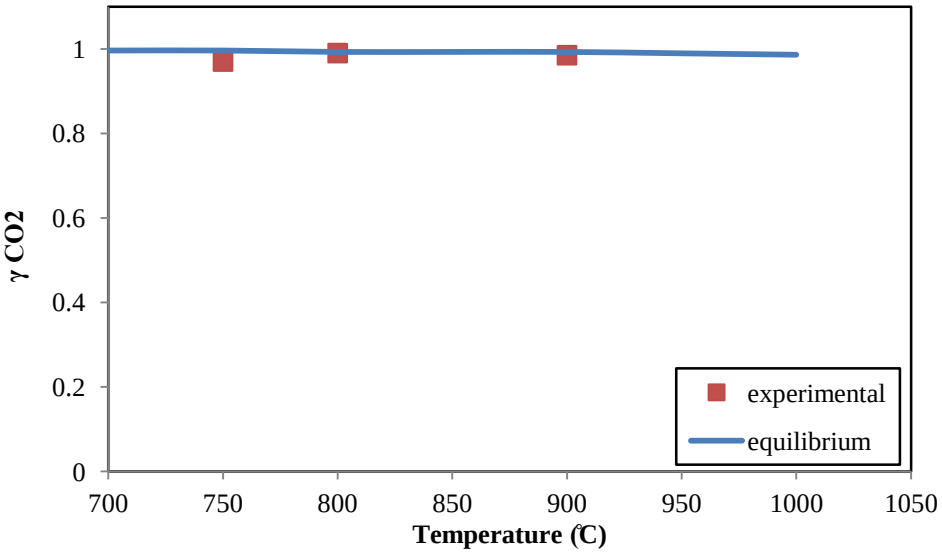

Figure 5.17: Kerosene Chemical-Looping Combustion with NiO (0.5 ml liq. Kerosene/min, 0.75 ml liq. Water/min and 250 g of N4MZ-1400 [40 wt% NiO])

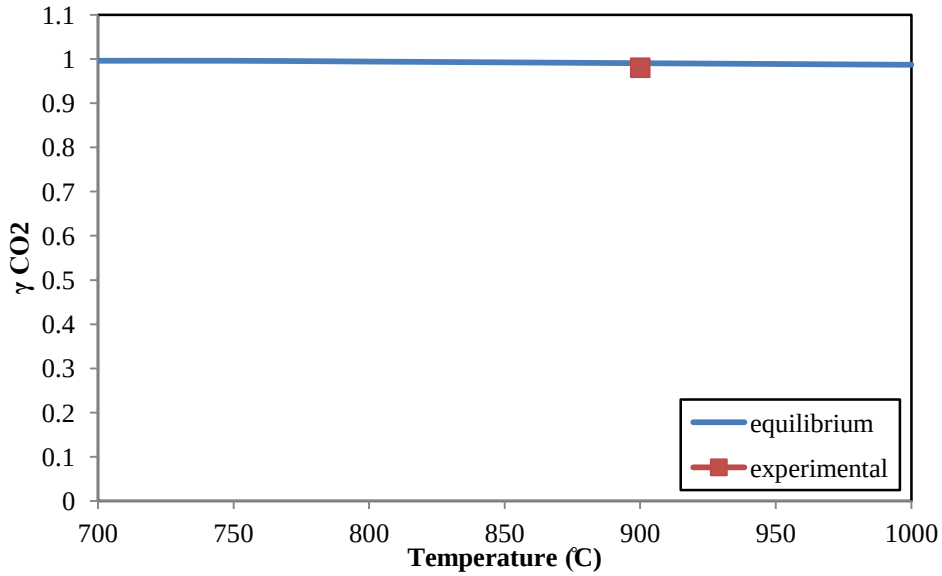

Figure 5.18: Kerosene Chemical-Looping Combustion with NiO (0.99483 ml liq. Kerosene/min, 0.75 ml liq. Water/min and 250 g of N4MZ-1400 [40 wt% NiO])

CHAPTER 6

REACTIVE CHARACTERIZATION OF OXYGEN CARRIER

The four samples underwent different characterizations and analyses in order to determine their physiochemical properties. In this respect, physical and chemical characteristics as well as functionality of each of them were investigated using different concepts and approaches.

6.1. X-Ray fluorescence (XRF) spectrometer results

First of all, XRF is performed so as to check the accuracy in preparation steps (to see how much real metal loadings get close to the targeted ones).The results are shown below:

Table 6.1: Nickel oxide content in four prepared OCs

Sample type	Targeted Ni%	Found Ni%	Error %
1	2.5	2.22	-11.2
2	5	4.55	-9
3	7.5	7.08	-5.6
4	10	9.99	-0.1

Table 6.2: Iron oxide content in four prepared OCs

Sample type	Targeted Fe%	Found Fe%	Error %
1	15	13.33	-11.13
2	15	13.28	-11.46

3	15	14	-6.67
4	15	14.5	-3.33

Table 6.3: Lanthanum oxide content in four prepared OCs

Sample type	Targeted La_2O_3%	Found La_2O_3%	Error %
1	2	1.93	-3.5
2	2	1.82	-9
3	2	2.13	6.5
4	2	2.27	13.5

So, all errors, as shown above, are within the range.

After that, XRD (X ray diffraction)analysis is carried out to know the crystallinity and crystals' size existing in the particles.

6.2. X-Ray diffraction analysis (XRD)

XRD showed overlapped peaks (and also shifted as a consequence of overlapping), even though the picture of crystallinity and corresponding compounds is so far clear. In general, XRD confirmed the existence of desired crystals (NiO and Fe_2O_3) and some unavoidable undesired ones ($NiAl_2O_4$). However, the goal of minimizing the content of those undesired ones was achieved to some extent as a result of systematic and careful synthesis.

Regarding the first and second OCs (2.5 Ni and 5 Ni), it shows peaks pointing to NiO, $NiAl_2O_4$ and Fe_2O_3.However, for the other two OCs (7.5 Ni and 10 Ni), beside that, an alloy formation of $FeNi_{0.5}AlO_4$ coming together with phase change of support (from γ-

Al_2O_3 to θ- Al_2O_3)is detected. Since this phase change does not appear in the first two carriers, it can be attributed to the interaction among NiO, Fe_2O_3, Alumina and oxygen.

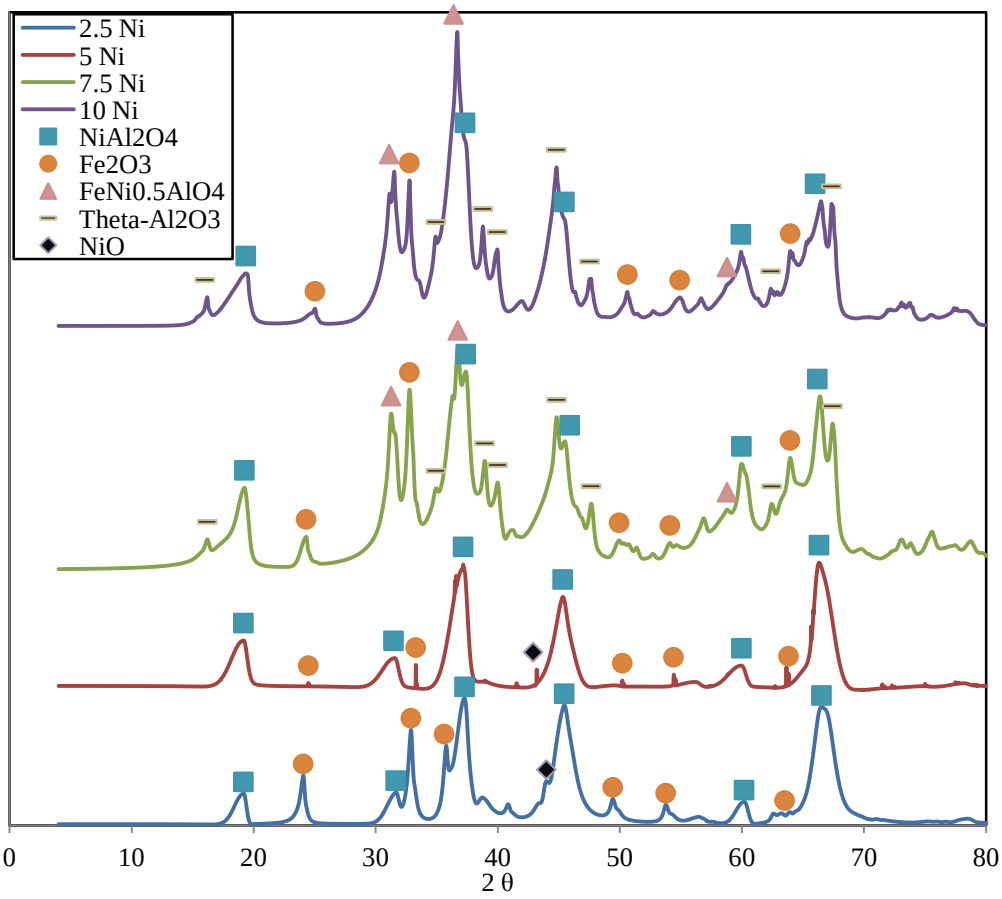

Figure 6.1: XRD Pattern for Four different Nickel content loaded OCs

Crystal size of each species is calculated using Scherer's equation according to:

$$\tau = \frac{\kappa \times \lambda}{\beta \times Cos\theta} \tag{6.1}$$

The results are shown in the Table below:

Table 6.4: Crystal size of XRD detected materials

OC	$NiAl_2O_4$ Crystal Size (nm)	NiO Crystal Size (nm)	Fe_2O_3 Crystal Size (nm)	$FeNi_{0.5}AlO_4$ Crystal Size (nm)	θ-Al_2O_3 Crystal Size (nm)
1	16.26	16.6	16.06	-	-
2	16.25	16.57	16.08	-	-
3	16.26	-	16.06	16.23	16.66
4	16.26	-	16.06	16.23	16.66

6.3. Temperature Programmed Reduction analysis (TPR):

Temperature programmed reduction is performed in order to test the reactivity of prepared OCs with the reducing agents (mainly hydrogen). Besides that, this analysis can also reveal the performance behavior and stability under repeated oxidation/ reduction cycles by means of determining oxygen carrying and releasing capacity and extent (how much fraction is oxidized and reduced). Moreover, it shows the temperature at which the OC displays higher reactivity and thus the operating temperature must be greater than or equal to get maximum possible utilization of that OC.

The TPR profiles for the four OCs are shown in Figure(6.2) below. It is clear that all the profiles indicate peak overlapping which needs to be de-convoluted in order to get exactly the right peaks associated with each chemical species existing in the OC. The Figure below shows that there are two main overlapping peaks. The smaller one (left shoulder) represents NiO reduction with the Hydrogen and the other one is for Fe_2O_3. Since the amount of ferrite is quite larger than that of NiO, it is reasonable for ferrite to take much more oxygen than NiO presents in the OC; in order to be reduced. Furthermore, as Ni load increases, the hydrogen consumption also increases as a result of more active agent (Ni) presence in the OC. However, with further increase in Ni load,

hydrogen consumption falls down pointing to less reducibility of the prepared or formed OC. This is due to the formation of $FeNi_{0.5}AlO_4$ crystals which are detected by XRD. Table 6.5 shows oxygen transferability for each prepared OC.

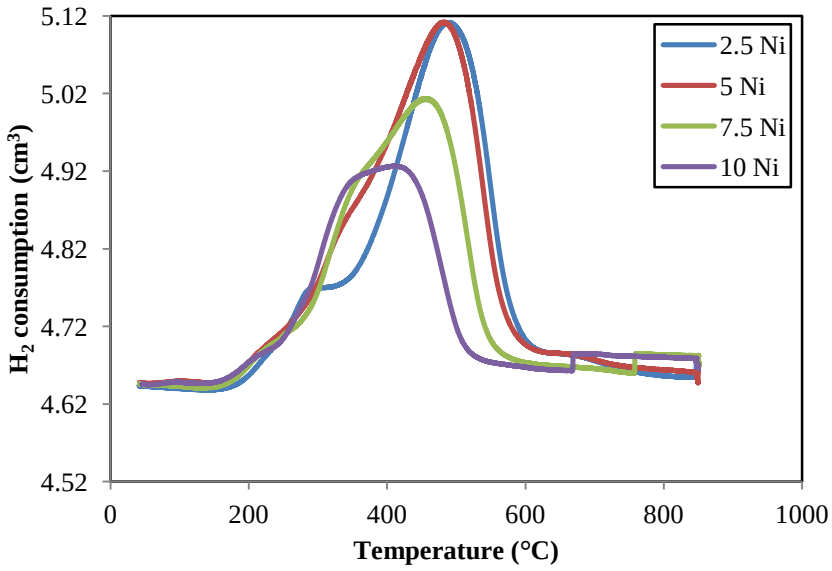

Figure 6.2: TPR profiles for four different Ni loaded OCs

Table 6.5: Oxygen Transferability

Oxygen Carrier	Oxygen Transferability (g O/g Oc)
2.5 Ni	0.052
5 Ni	0.055
7.5 Ni	0.053
10 Ni	0.048

Stability in performance is tested by measuring the fractional reduction of the four prepared OCs for four successive oxidation/ reduction cycles as shown in Figure (6.3) below. Regarding the first two OC, as shown in Figure 6.3, they have reduction percentages greater than the unity that can be attributed to non-stoichiometric reduction

reaction of $NiAl_2O_4$ with Hydrogen [71]. Non-stoichiometric reaction means the real amount of hydrogen taken by nickel aluminate is higher than that is stoichiometrically needed to get it reduced. Stoichiometric reduction of $NiAl_2O_4$ follows:

$$NiAl_2O_4 + H_2 \rightarrow H_2O + Ni + Al_2O_3 \qquad (6.2)$$

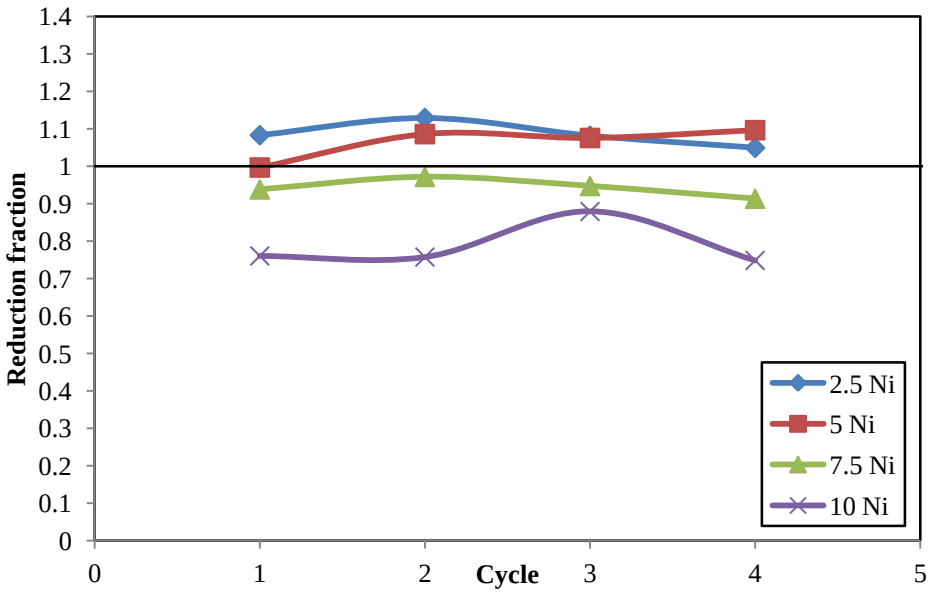

Figure 6.3: Stability testing using successive TPR/TPO cycles

All four prepared OC showed stable behavior and Figure (6.4) shows the average reduction percentage of four of them.

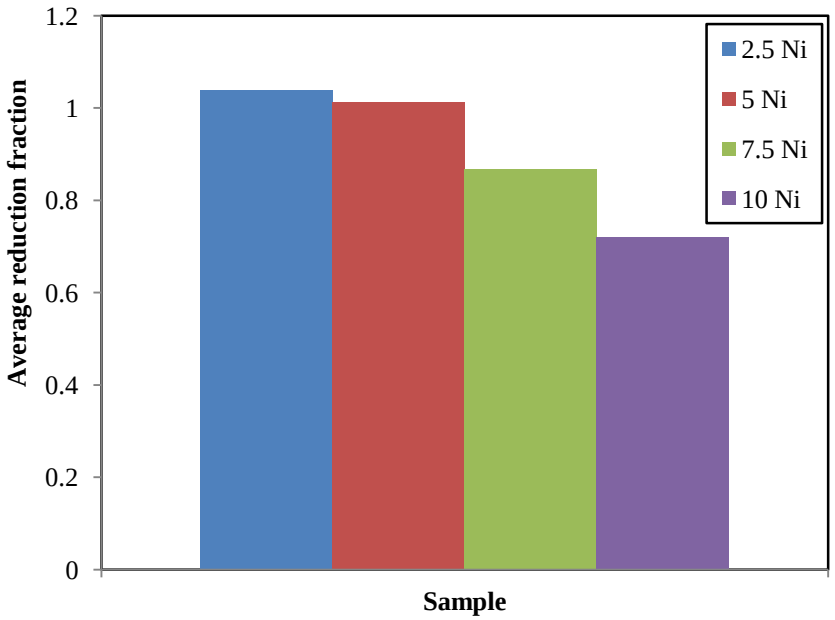

Figure 6.4: Average reduction fraction for four different Ni loaded OCs with H2

6.4. Scanning Electron Microscope analysis (SEM):

Due to high metal loading (especially Fe which is reported to have a strong tendency to agglomerate), seeing the morphology of the surface of the four OCs is highly important to check agglomeration. Furthermore, this enables confirming crystallinity state and crystal shape (somehow). In addition, as claimed, lanthanum presence will enhance metal dispersion on the support surface; this also has to be checked. To do so, SEM analysis has been performed and the results are as follow:

6.4.1. Morphology

SEM shows that the crystals are in sphere shape, with no sign of agglomeration. Figure 6.5 represents this fact.

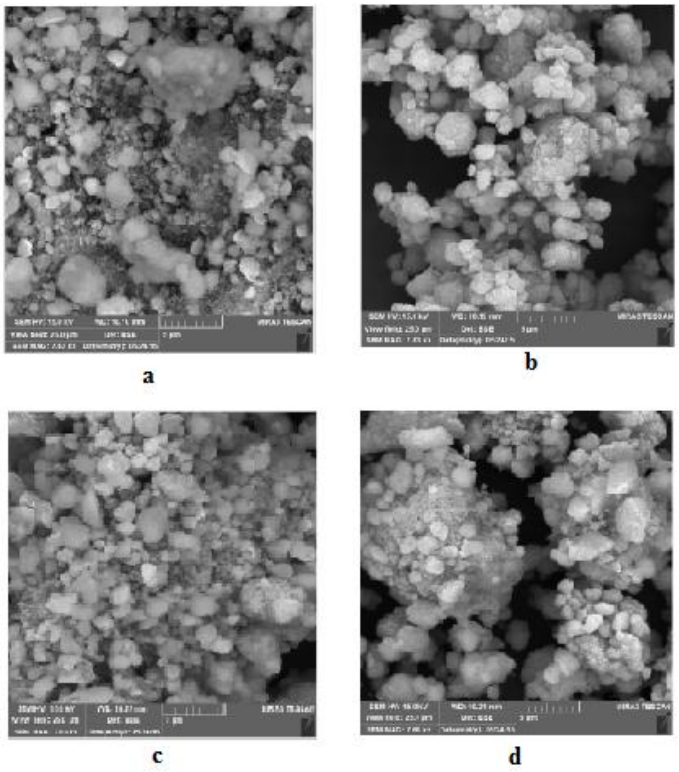

Figure 6.5: SEM Images for a)2.5 Ni, b)5 Ni, c)7.5 Ni and d)10 Ni

6.4.2. Dispersion:

All four prepared oxygen carriers show excellent dispersion for both nickel and iron which is intuitive as a result of lanthanum presence. As shown in Figure (6.6), iron dispersion approximately remains the same for all prepared carriers. This on other hand, can also help in well nickel dispersion when iron nickel interaction takes place (in other words, iron, nickel and alumina alloying increases the dispersion of one metal if the other is dispersed well).

Figure (6.6) shows that nickel particles' or crystals' concentration on the surface is increasing more and more which is what should be as a consequence of adding more nickel to prepare the next carrier from the present one (successive preparation).

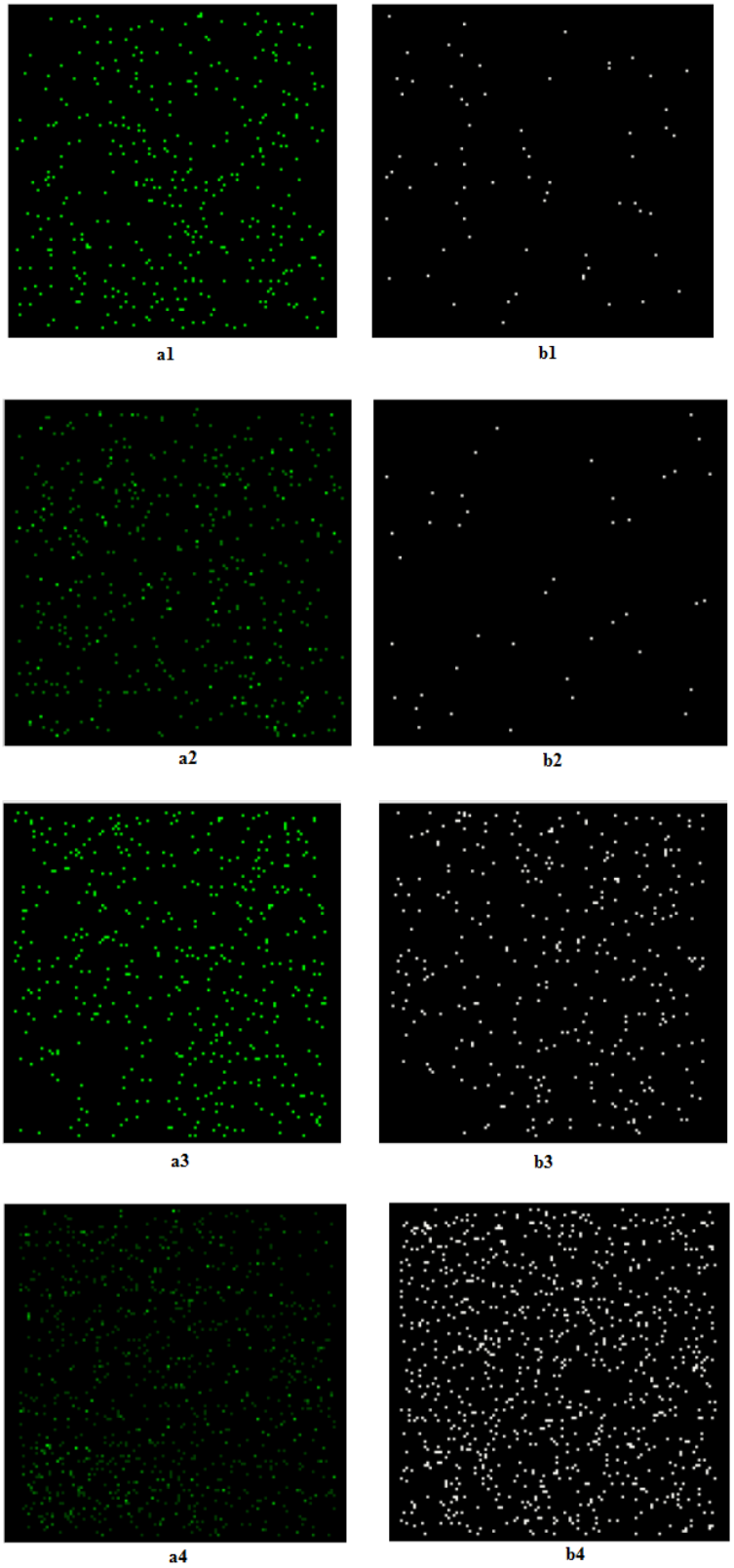

Figure 6.6: a) Ni dispersion and b) Fe dispersion in: 1) 2.5 Ni, 2) 5 Ni, 3) 7.5 Ni and 4) 10 Ni respectively

6.5. Surface Area Estimation (BET):

BET surface area results confirm the findings of SEM regarding agglomeration. As can be noticed from Table 6.6, all prepared OCs have almost the same surface area (keep in mind that the equipment has an error of about 10 m^2/g).So, all of them are within the range.

Table 6.6: Oxygen carrier surface area

Oxygen Carrier	Surface Area (m^2/g)
2.5 Ni	54.11
5 Ni	46.101
7.5 Ni	50.845
10 Ni	46.132

6.6. Temperature Programmed Desorption (TPD):

Combusting of heavy hydrocarbon and concomitant carbon deposition on a catalyst or oxygen carrier surface depends on many factors. For example, diffusivity of fuel inside catalyst pores, absorption, surface chemical reaction and desorption of products - all these factors affect the combustion process severely. It has been reported that carbon deposition on the catalyst surface hinders the combustion process by means of covering some active area and prohibiting the reactants from reaching it (decreasing the active available area for reaction). Furthermore, it decreases the overall efficiency of CLC of carbon dioxide capturing because when oxygen carrier, with carbon deposition, enters the oxidizer, that carbon will react with the air and form CO_2 which willthen be released in the atmosphere.

So, to avoid carbon deposition (or to minimize it), there are two approaches, either by applying heat (in presence of oxidizing agent), or by applying more oxidizing agent. Both of these two approaches have a certain lower thermodynamic limit (depends on the conditions) under which carbon deposition cannot be avoided totally. However, one of the practical ways for minimizing carbon deposition is to decrease the acidity of the oxygen carrier (which is one of the lanthanum roles).Figure (6.7) shows the acidity of different oxygen carriers measured in terms of consumption of ammonia gas that is basic one. So, as ammonia consumption increases, that indicates more acidity. Figure (6.8) represents that as nickel loading increases, the total acidity decreases. This can be attributed to the coverage of acidic sites of alumina by Ni as well as less nickel alumina interaction. However, when the interaction becomes dominant (in case of alloying " $FeNi_{0.5}AlO_4$"), acidity returns again, pointing to the interaction with alumina and its concomitant alumina phase change (as can be reported from [7]). This finding is clear in Figure 6.8.

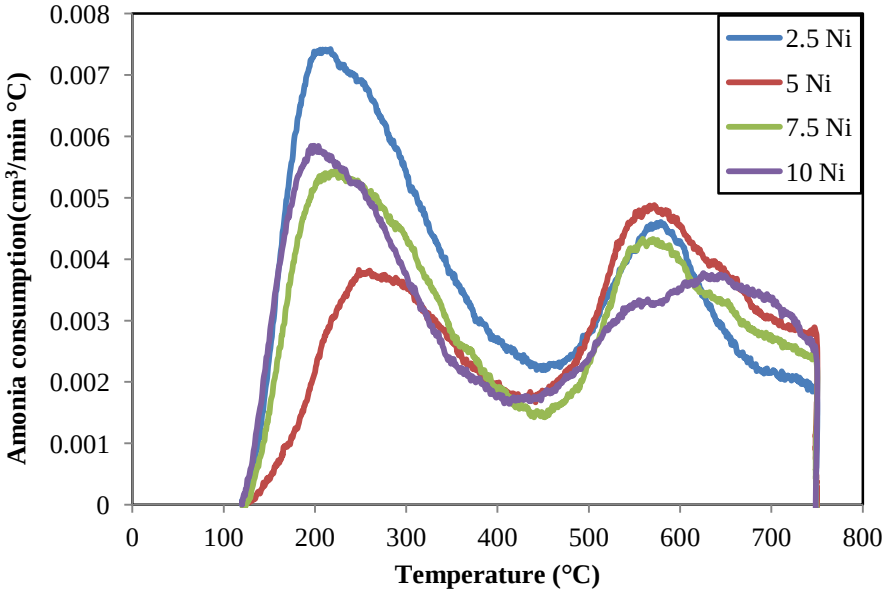

Figure 6.7: TPD Profiles for four different Ni loaded OCs

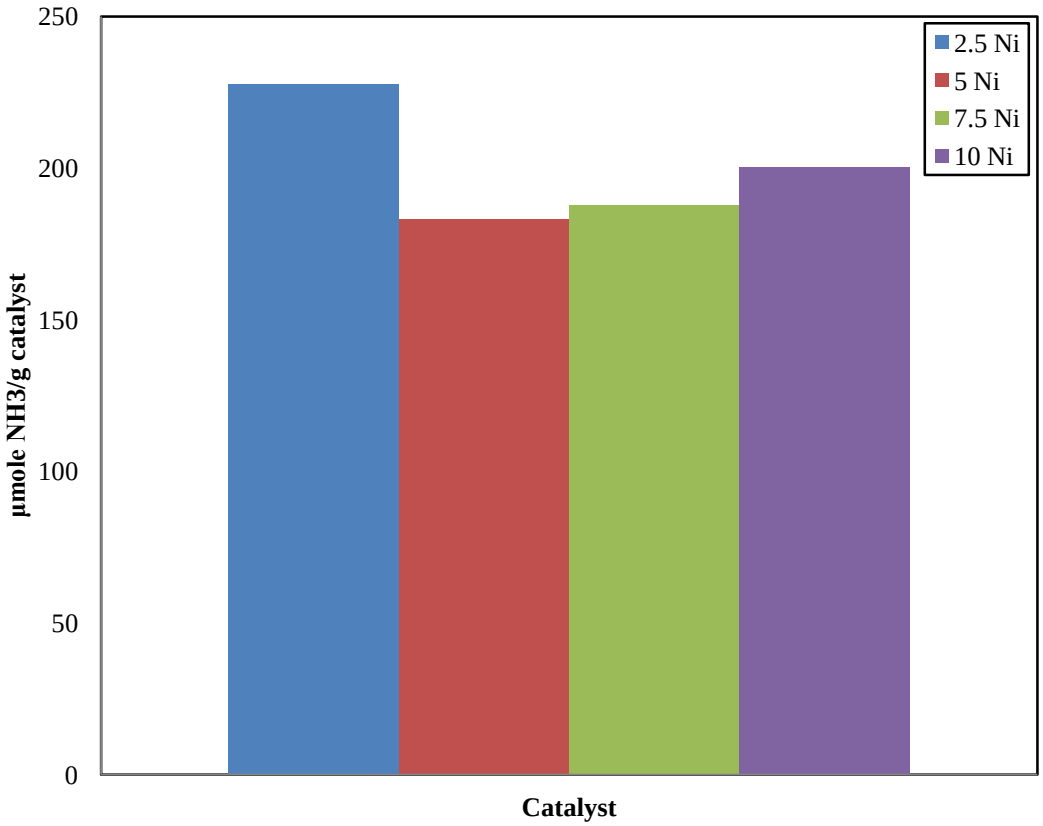

Figure 6.8: Acidity of four different Ni loaded OCs

CHAPTER 7

OXYGEN CARRIER EVALUATION

Based on the characterization results and findings, the second OC (5 Ni)is selected to be evaluated (because it shows the best characteristics in terms of the highest oxygen transferability, lowest acidity and remarkable NiO crystals detected by XRD).

Hexane is used as a model fuel. In order to achieve complete combustion, stoichiometric amount of OC is used as follows:

$$C_6H_{14} + \frac{19k}{k+1} NiO + \frac{19}{k+1} Fe_2O_3 \rightarrow 6CO_2 + 7H_2O + \frac{19k}{k+1} Ni + \frac{38}{k+1} FeO \qquad (7.1)$$

where k is the molar ratio of NiO to Fe_2O_3 in prepared OC.

Calculations of needed amount of OC to achieve full combustion are performed based on the assumption that the ultimate reduction of $Fe_2O_3$is to FeO due to its practicality and easiness, while the reduction of FeO to Fe is unlikely or difficult due to the presence of water vapor in the system. The oxygen carrier performance was evaluated under simulated real CLC conditions using RECAT-CREC Riser Simulator as shown in Figure (7.1) below:

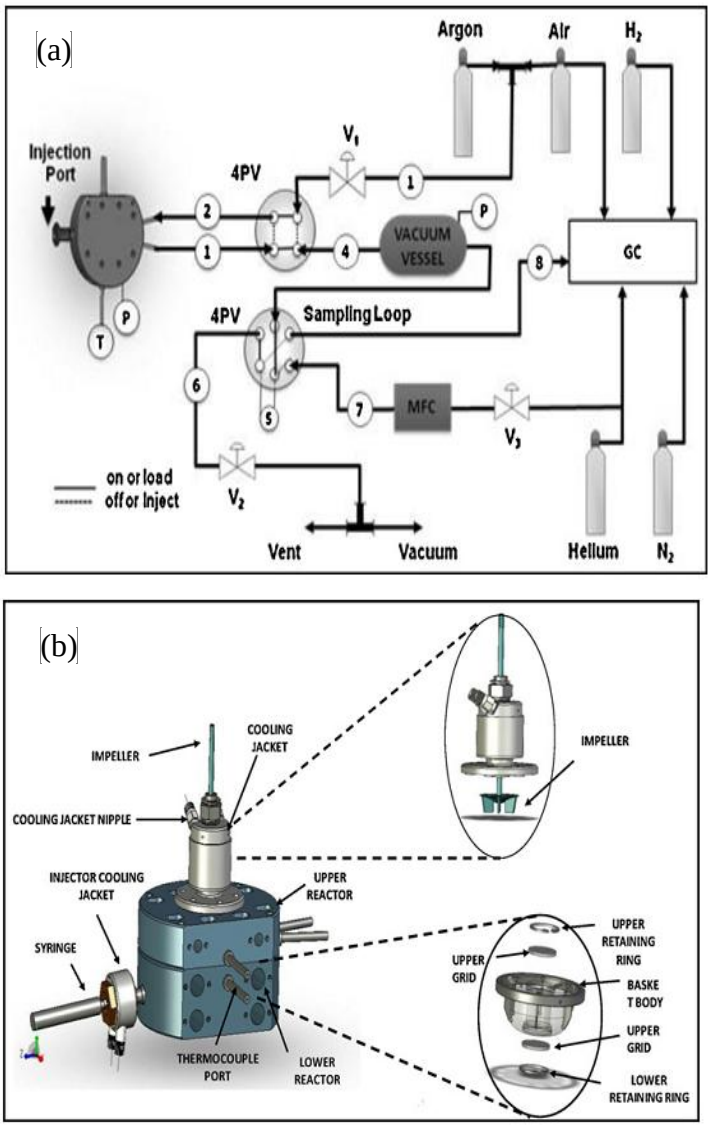

Figure 7.1: RECAT-CREC Riser Simulator Schematic diagram

First, temperature was set to the value of 600 C° while the contact or reaction time was varying among5, 10, 15 and 20 seconds. The main idea behind that is to see the time effect on the combustion process which helps in kinetic modeling. Furthermore, as reaction time increases, all hydrocarbon materials'(those are resulted by means of reforming/cracking and the fuel itself) combustion extent will also increase. In addition,

the undesired carbon monoxide, produced as a result of incomplete combustion and successive reforming of light hydrocarbons, needs time to react with OC.

Performance of the OC is determined by how much carbon is fed when fuel is being converted to carbon dioxide (γ CO_2). This value includes the effect of conversion as well as selectivity at the same time; it is related to them by:

$$\gamma_{CO_2} = \frac{n_{CO_2}}{6n_{0,C_6H_{14}}} = \frac{x\Theta}{1+\Theta} \tag{7.2}$$

So, as can be seen from equation (7.2), γ is zero if the conversion or the selectivity is zero. It reaches its maximum value when the conversion is 1 and the selectivity is ∞, which basically means that all injected fuel was combusted completely and converted to water vapor and carbon dioxide, nothing else.

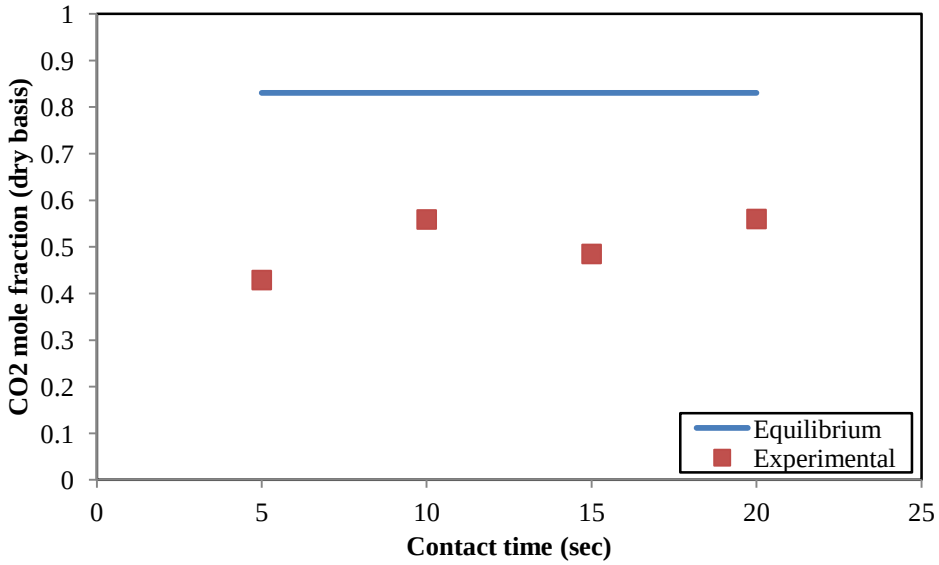

Figure 7.2: OC Performance at 600 °C

It is clear from above Figure that the optimum time is 10 seconds (among the four times). In fact, if larger reaction times are allowed, the value will continue to increase until it reaches the equilibrium. The drop in fuel conversion to CO_2 after 10 seconds indicates that after this period of time, the water produced by combustion of some of the fuel with OC starts to reform the remaining uncombusted fuel. As soon as it gets reformed/cracked, the reaction rate will be higher than it was (at the beginning).

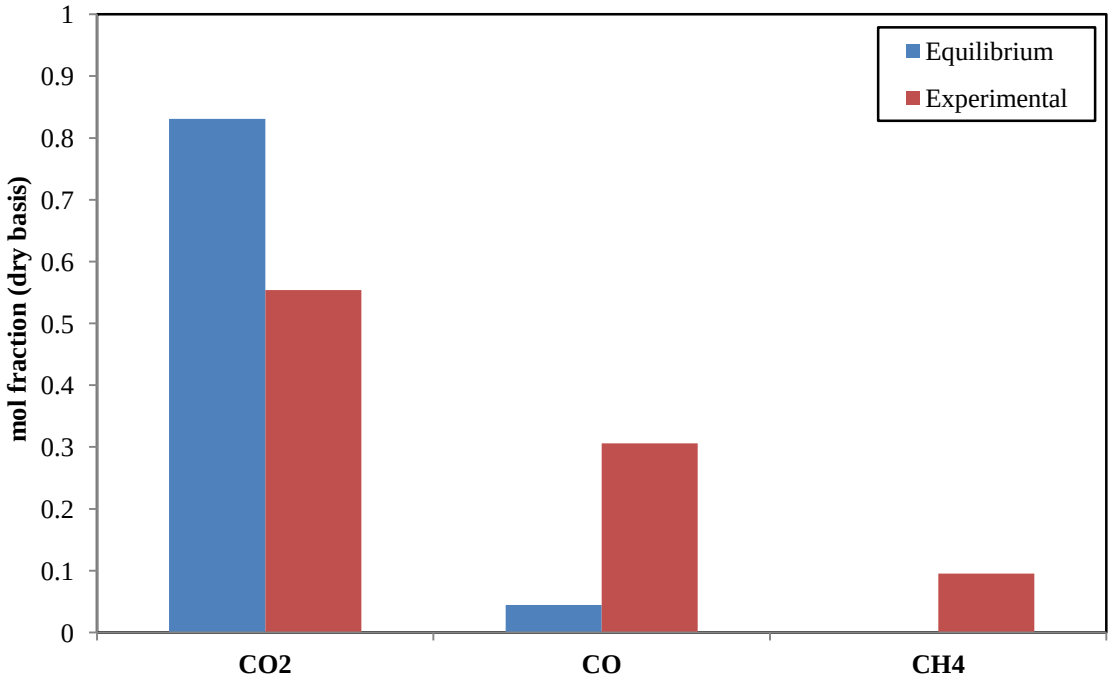

Figure 7.3: Hexane/OC combustion product distribution(600°C,10 sec., H/OC=1g/79.3g)

After that, temperature was changed systematically as 500 C°, 550 C°, 600 C° and 650 C° while the contact time for all these temperatures was kept as 10 seconds (which was found to be the best one).

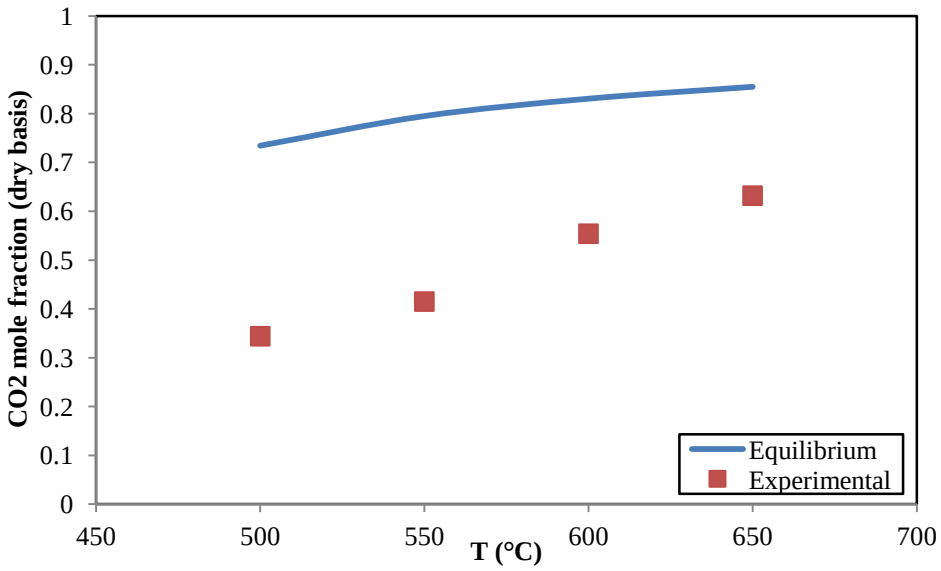

Figure 7.4: OC Performance for contact time of 10 seconds

As shown in above Figure, combustion reaction at higher temperatures is faster than that at lower ones. This is due to the fact that higher temperature is favored by cracking/reforming process as well as reaction with OC. In fact, the thermodynamic optimum temperature for this process is found to be 700°C and the corresponding γ_{CO2} is 0.95.However, that temperature exceeds the maximum allowed temperature for Riser (650 C°).

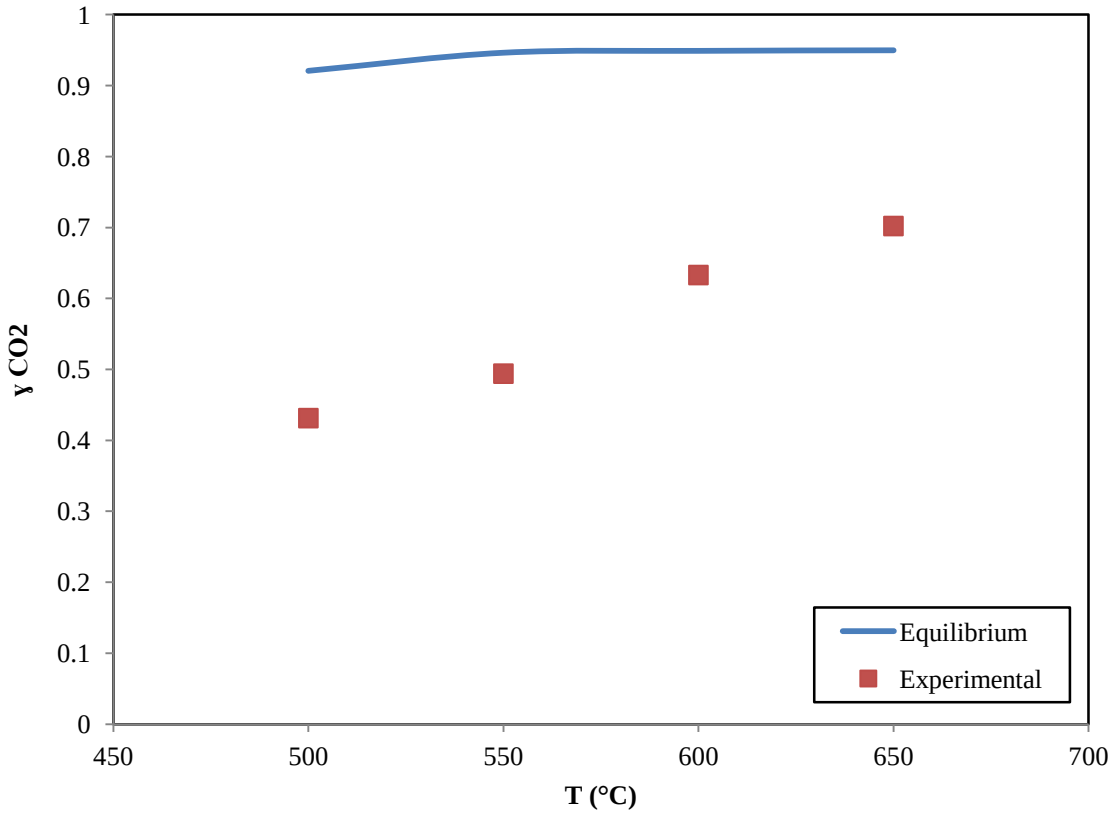

Figure 7.5: Hexane/OC combustion, Carbon conversion into CO2(10 sec, H/OC=1g/79.3g)

Regarding carbon deposition, thermodynamic calculations show that it can be totally avoided when the reduction temperature is equal to or greater than 480 C° under those operating conditions.

However, the optimum temperature among all tested ones was found to be 650°C.The stability of the OC was studied under 600°C (to prevent the reactor from being damaged), and 10 seconds as reaction time by conducting 6 successive oxidation/reduction runs, and the results are:

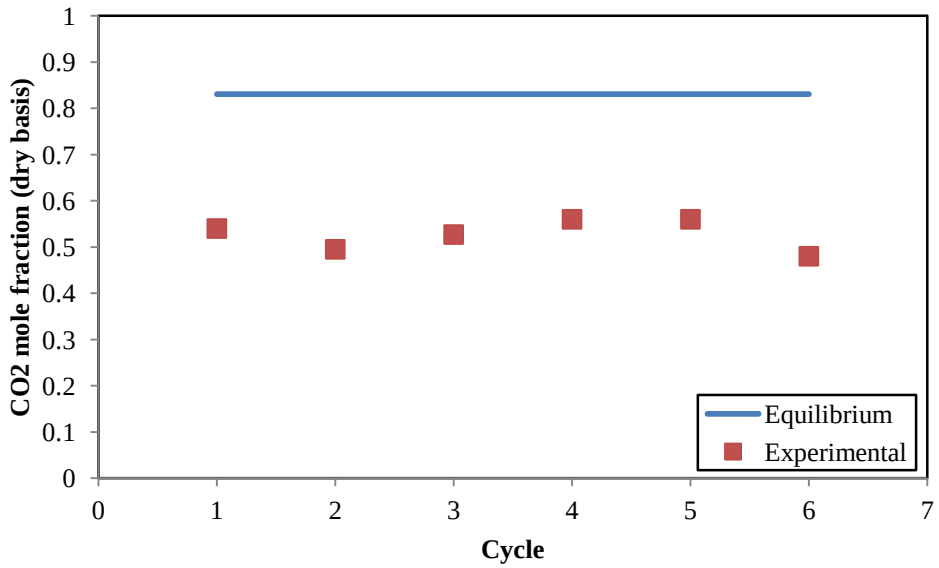

Figure 7.6: Stability Runs

By joining this stability test results with those got from TPR, it is clear that this OC (5 Ni) is stable in performance with both Hydrogen and Hexane (model fuel).

CHAPTER 8

CONCLUSION AND RECOMMENDATIONS

8.1. Conclusion

This study deals with the development of a Ni-Fe bimetallic OC that is highly reactive, cheap and less toxic to be used in liquid fuel based chemical looping combustion which is a promising proposed process for carbon capturing. For this purpose, four different nickel loaded (2.5, 5, 7.5 and 10%), lanthanum modified (2%), iron based (15%) and gamma alumina supported oxygen carriers are synthesized by using the incipient wetness technique. Then all prepared oxygen carriers have undergone several types of characterization tests (TPR/TPO, TPD, BET surface area, XRD, XRF and SEM-EDX) to investigate their properties and to select the best one among them based on those characterizations to be evaluated in a batch fluidized bed reactor with liquid fuel. After that, the best prepared OC (which is found to be 5 Ni one) is evaluated further with hexane as a fuel in RECAT-CREC Riser reactor at four different reaction times and under four different temperatures. On the other hand, thermodynamic model for equilibrium distribution of all chemical involved species is made using Gibbs free energy minimization technique. Accordingly, favored thermodynamic conditions to have ultimate conversion of fuel carbon to carbon dioxide are set. Findings are concluded as:

1. The best thermodynamic temperature for achieving the climax of carbon capture was found to be 700 C°.
2. The best prepared OC found, based on characterizations results, is the one that contains 5% Ni (second OC).
3. The best condition for hexane combustion with 5 Ni OC is 650 C° (among 500, 550, 600, and 650 C°) for contact time of 10 seconds (among 5, 10, 15 and 20 seconds).
4. Ferrite interacts with nickel oxide and gamma alumina in presence of oxygen to form a stable alloy ($FeNi_{0.5}AlO_4$).
5. Lanthanum presence helps in lowering Fe_2O_3 reduction temperatures as well as for NiO.

8.2. Recommendations

1. Introduce stoichiometric amount of water (for complete conversion to syngas) as:

$$C_6H_{14} + 6H_2O \rightarrow 13H_2 + 6CO$$

2. Use heavier hydrocarbon liquid fuel.
3. Prepare another Ni-Fe based OC with a little increase in lanthanum sandwich (between Fe layer and Ni layer).
4. Perform kinetic modeling for OC oxidation and reduction (with H_2 and the liquid fuel which is hexane in this case).

References

[1] B. Nordell, "Thermal pollution causes global warming," *Glob. Planet. Change*, vol. 38, no. 3–4, pp. 305–312, Sep. 2003.

[2] J. Adanez, A. Abad, F. Garcia-Labiano, P. Gayan, and L. F. de Diego, "Progress in Chemical-Looping Combustion and Reforming technologies," *Prog. Energy Combust. Sci.*, vol. 38, no. 2, pp. 215–282, Apr. 2012.

[3] M. R. Quddus, "Anovel mixed metallic oxygen carrierr for chemical looping combstion: Preparation, Characterization & Kinetics modeling, PhD Dissertation, The University of Western Ontario, London, ON, Canada" 2013.

[4] M. M. Hossain and H. I. de Lasa, "Chemical-looping combustion (CLC) for inherent CO2 separations—a review," *Chem. Eng. Sci.*, vol. 63, no. 18, pp. 4433–4451, Sep. 2008.

[5] J. Adánez, L. F. De Diego, F. García-Labiano, P. Gayán, a. Abad, and J. M. Palacios, "Selection of oxygen carriers for chemical-looping combustion," *Energy and Fuels*, vol. 18, no. 2, pp. 371–377, 2004.

[6] a. Hoteit, a. Forret, W. Pelletant, J. Roesler, and T. Gauthier, "Chemical Looping Combustion with Different Types of Liquid Fuels," *Oil Gas Sci. Technol. – Rev. d'IFP Energies Nouv.*, vol. 66, no. 2, pp. 193–199, Feb. 2011.

[7] J. Mazumder and H. de Lasa, "Fluidizable Ni/La2O3-γAl2O3 catalyst for steam gasification of a cellulosic biomass surrogate," *Appl. Catal. B Environ.*, vol. 160–161, pp. 67–79, Nov. 2014.

[8] Y. H. Tseng, J. L. Ma, C. P. Chin, Y. L. Kuo, and Y. Ku, "Preparation of composite nickel-iron oxide as highly reactive oxygen carrier for chemical-looping combustion process," *J. Taiwan Inst. Chem. Eng.*, vol. 45, no. 1, pp. 174–179, 2014.

[9] M. Ishida, D. Zheng, and T. Akehata, "Evaluation of a chemical-looping-combustion power-generation system by graphic exergy analysis," *Energy*, vol. 12, no. 2, pp. 147–154, 1987.

[10] T. Mattisson, A. Lyngfelt, and H. Leion, "Chemical-looping with oxygen uncoupling for combustion of solid fuels," *Int. J. Greenh. Gas Control*, vol. 3, no. 1, pp. 11–19, 2009.

[11] I. M. Dahl, E. Bakken, Y. Larring, A. I. Spjelkavik, S. F. Håkonsen, and R. Blom, "On the development of novel reactor concepts for chemical looping combustion," *Energy Procedia*, vol. 1, no. 1, pp. 1513–1519, 2009.

[12] A. Lyngfelt, B. Leckner, and T. Mattisson, "A fluidized-bed combustion process with inherent CO2 separation; Application of chemical-looping combustion," *Chem. Eng. Sci.*, vol. 56, no. 10, pp. 3101–3113, 2001.

[13] B. Kronberger, E. Johansson, G. Löffler, T. Mattisson, a Lyngfelt, and H. Hofbauer, "A Two-Compartment Fluidized Bed Reactor for CO2 Capture by Chemical-Looping Combustion," *Chem. Eng. Technol.*, vol. 27, no. 12, pp. 1318–1326, 2004.

[14] B. Kronberger, A. Lyngfelt, G. Lo, and H. Hofbauer, "Design and Fluid Dynamic Analysis of a Bench-Scale Combustion System with CO 2 Separation - Chemical-Looping Combustion," *Ind. Eng. Chemsitry Res.*, vol. 44, no. 3, pp. 546–556, 2005.

[15] P. Kolbitsch, T. Pröll, J. Bolhar-Nordenkampf, and H. Hofbauer, "Design of a Chemical Looping Combustor using a Dual Circulating Fluidized Bed (DCFB) Reactor System," *Chem. Eng. Technol.*, vol. 32, no. 3, pp. 398–403, 2009.

[16] E. Johansson, a. Lyngfelt, T. Mattisson, and F. Johnsson, "Gas leakage measurements in a cold model of an interconnected fluidized bed for chemical-looping combustion," *Powder Technol.*, vol. 134, no. 3, pp. 210–217, 2003.

[17] D. C. Thomas, A. Lyngfelt, and H. Thunman, "Construction and operational experience of a 10-KW Chemical-looping combustior" *Carbon Dioxide Capture Storage Deep Geol. Form.*, vol. 1, no. 2, pp. 625–645, 2005.

[18] H.-J. Ryu, G.-T. Jin, and C.-K. Yi, "Demonstration of inherent CO2 seperation and no NOx emission in a 50 kW Chemical-looping combustor: Continuous reduction and oxidation experiments" *Greenh. Gas Control Technol. 7*, vol. II, pp. 1907–1910, 2005.

[19] J. Adánez, P. Gayán, J. Celaya, L. F. de Diego, F. García-Labiano, and A. Abad, "Chemical Looping Combustion in a 10 kW th Prototype Using a CuO/Al2O3 Oxygen Carrier: Effect of Operating Conditions on Methane Combustion," *Ind. Eng. Chem. Res.*, vol. 45, no. 17, pp. 6075–6080, 2006.

[20] H.-J. Ryu, S.-H. Jo, Y.-C. Park, D.-H. Bae, and S. D. Kim, "Long term operation experience in a 50 kWth chemical looping combustor using natural gas and syngas as fuels," in *1st International Conference in chemical looping*, 2010.

[21] S. R. Son and S. D. Kim, “Chemical-looping combustion with NiO and Fe2O3 in a thermobalance and circulating fluidized bed reactor with double loops,” *Ind. Eng. Chem. Res.*, vol. 45, no. 8, pp. 2689–2696, 2006.

[22] L. Shen, J. Wu, J. Xiao, Q. Song, and R. Xiao, “Chemical-Looping Combustion of Biomass in a 10 kW th Reactor with Iron Oxide As an Oxygen Carrier,” *Energy & Fuels*, vol. 23, no. 5, pp. 2498–2505, 2009.

[23] L. F. De Diego, F. García-Labiano, J. Adánez, P. Gayán, A. Abad, B. M. Corbella, and J. M. Palacios, “Development of Cu-based oxygen carriers for chemical-looping combustion,” *Fuel*, vol. 83, no. 13, pp. 1749–1757, 2004.

[24] M. Ishida and H. Jin, “A Novel Chemical-Looping Combustor without NOx Formation,” *Ind. Eng. Chem. Res.*, vol. 5885, no. 95, pp. 2469–2472, 1996.

[25] M. Ishida and Hongguang Jin, “A novel combustor based on chemical-looping reactions and its reaction kinetics,” *Journal of Chemical Engineering of Japan*, vol. 27, no. 3. pp. 296–301, 1994.

[26] A. Abad, J. Adánez, F. García-Labiano, L. F. de Diego, P. Gayán, and J. Celaya, “Mapping of the range of operational conditions for Cu-, Fe-, and Ni-based oxygen carriers in chemical-looping combustion,” *Chem. Eng. Sci.*, vol. 62, no. 1–2, pp. 533–549, 2007.

[27] N. Ding, Y. Zheng, C. Luo, Q. L. Wu, P. F. Fu, and C. G. Zheng, “Development and performance of binder-supported CaSO4 oxygen carriers for chemical looping combustion,” *Chem. Eng. J.*, vol. 171, no. 3, pp. 1018–1026, 2011.

[28] M. Zheng, L. Shen, and J. Xiao, “Reduction of CaSO4 oxygen carrier with coal in chemical-looping combustion: Effects of temperature and gasification intermediate,” *Int. J. Greenh. Gas Control*, vol. 4, no. 5, pp. 716–728, 2010.

[29] T. Mattisson and A. Lyngfelt, “Capture of CO2 using chemical-looping combustion,” *... -Nordic Sect. Combust. Inst.*, no. 2, 2001.

[30] M. M. Hossain and H. I. de Lasa, “Reduction and oxidation kinetics of Co-Ni/Al2O3 oxygen carrier involved in a chemical-looping combustion cycles,” *Chem. Eng. Sci.*, vol. 65, no. 1, pp. 98–106, 2010.

[31] O. Levenspiel, *Chemical Reaction Engineering*, Third Edit., vol. 19. John Wiley & Sons, 1999.

[32] H.-J. Ryu, D.-H. Bae, K.-H. Han, S.-Y. Lee, G.-T. Jin, and J.-H. Choi, “Oxidation and reduction characteristics of oxygen carrier particles and reaction kinetics by unreacted core model,” *Korean J. Chem. Eng.*, vol. 18, no. 6, pp. 831–837, 2001.

[33] J. E. Readman, A. Olafsen, J. B. Smith, and R. Blom, "Chemical Looping Combustion Using NiO/NiAl 2 O 4 : Mechanisms and Kinetics of Reduction−Oxidation (Red-Ox) Reactions from In Situ Powder X-ray Diffraction and Thermogravimetry Experiments," *Energy & Fuels*, vol. 20, no. 4, pp. 1382–1387, 2006.

[34] A. Abad, F. García-Labiano, L. F. de Diego, P. Gayán, and J. Adánez, "Reduction kinetics of Cu- , Ni- , and Fe-based oxygen carriers using syngas ($CO+H_2$) for chemical-looping combustion," *Energy Fuels*, vol. 21, no. 6, pp. 1843–1853, 2007.

[35] Q. Zafar, A. Abad, T. Mattisson, and B. Gevert, "Reaction kinetics of freeze-granulated NiO/MgAl2O4 oxygen carrier particles for chemical-looping combustion," *Energy and Fuels*, vol. 21, no. 2, pp. 610–618, 2007.

[36] M. M. Hossain and H. I. de Lasa, "Reactivity and Stability of Co-Ni/Al2O3 Oxygen Carrier in Multicycle CLC," *AIChE J.*, vol. 53, no. 7, pp. 1817–1829, 2007.

[37] K. E. Sedor, M. M. Hossain, and H. I. De Lasa, "Reduction kinetics of a fluidizable nickel-alumina oxygen carrier for chemical-looping combustion," *Can. J. Chem. Eng.*, vol. 86, no. 3, pp. 323–334, 2008.

[38] M. M. Hossain, M. R. Quddus, and H. I. de Lasa, "Reduction Kinetics of La Modified NiO/La- γAl2O3 Oxygen Carrier for Chemical-Looping Combustion," *Ind. Eng. Chem. Res.*, vol. 49, no. 1, pp. 11009–11017, 2010.

[39] P. Erri and A. Varma, "Diffusional Effects in Nickel Oxide Reduction Kinetics," *Ind. Eng. Chem. Res.*, vol. 48, no. 2, pp. 4–6, 2009.

[40] B. Moghtaderi and H. Song, "Reduction properties of physically mixed metallic oxide oxygen carriers in chemical looping combustion," *Energy and Fuels*, vol. 24, no. 10, pp. 5359–5368, 2010.

[41] I. Iliuta, R. Tahoces, and G. S. Patience, "Chemical-Looping Combustion Process: Kinetics and Mathematical Modeling," *AIChE J.*, vol. 56, no. 4, pp. 1063–1079, 2010.

[42] A. Abad, J. Adánez, F. García-labiano, L. F. De Diego, P. Gayán, P. Kolbitsch, and T. Pröll, "CLC Modeling : the fuel-reactor at fast fluidization – Conversion of CH 4 using a NiO-based oxygen-carrier in a 120 kW th unit," *Int. Conf. Chem. Looping*, no. March, pp. 2009–2011, 2010.

[43] F. Garcia-Labiano and L. De Diego, "Reduction and oxidation kinetics of a copper-based oxygen carrier prepared by impregnation for chemical-looping combustion," *Ind. Eng. Chem. Res.*, no. 2, pp. 8168–8177, 2004.

[44] S. Y. Chuang, J. S. Dennis, a. N. Hayhurst, and S. a. Scott, “Kinetics of the chemical looping oxidation of CO by a co-precipitated mixture of CuO and Al2O3,” *Chem. Eng. Res. Des.*, vol. 32, no. 9, pp. 2633–2640, 2009.

[45] S. Y. Chuang, J. S. Dennis, a N. Hayhurst, and S. a Scott, “Kinetics of the Oxidation of a Co-precipitated Mixture of Cu and Al 2 O 3 by O 2 for Chemical-Looping Combustion,” no. 4, pp. 3917–3927, 2010.

[46] S. Y. Chuang, J. S. Dennis, a. N. Hayhurst, and S. a. Scott, “Kinetics of the chemical looping oxidation of H2 by a co-precipitated mixture of CuO and Al2O3,” *Chem. Eng. Res. Des.*, vol. 89, no. 9, pp. 1511–1523, 2011.

[47] A. Abad, J. Adánez, F. García-Labiano, L. F. de Diego, and P. Gayán, “Modeling of the chemical-looping combustion of methane using a Cu-based oxygen-carrier,” *Combust. Flame*, vol. 157, no. 3, pp. 602–615, 2010.

[48] C. D. Bohn, J. P. Cleeton, C. M. Müller, S. a Scott, and J. S. Dennis, “Measuring the kinetics of the reduction of iron oxide with carbon monoxide in a fluidized bed,” *Proc. 20th Int. Conf. Fluid. Bed Combust.*, vol. 203, no. i, pp. 555–561, 2009.

[49] A. Abad, J. Adánez, A. Cuadrat, F. García-Labiano, P. Gayán, and L. F. de Diego, “Kinetics of redox reactions of ilmenite for chemical-looping combustion,” *Chem. Eng. Sci.*, vol. 66, no. 4, pp. 689–702, 2011.

[50] H. Tian and Q. Guo, “Investigation into the behavior of reductive decomposition of calcium sulfate by carbon monoxide in chemical-looping combustion,” *Ind. Eng. Chem. Res.*, vol. 48, no. 12, pp. 5624–5632, 2009.

[51] C. Combustion, R. Xiao, Q. L. Song, W. G. Zheng, Z. Y. Deng, L. H. Shen, and M. Y. Zhang, “Reduction kinetics of a CaSO4 based onxygen carrier for Chemical-looping combustion” 2008.

[52] D. Marcia K. McNutt, “Mineral Commodity Summaries 2010,” *U.S. Geol. Surv.*, no. ISBN 978–1–4113–2666–8, 2010.

[53] A. D. Suzette M. Kimball, “Mineral commondity surraries 2015,” *U.S. Geol. Surv.*, no. ISBN 978–1–4113–3877–7, 2015.

[54] C. Linderholm, A. Lyngfelt, C. Béal, A. Trikkel, R. Kuusik, E. Jerndal, and T. Mattisson, “Chemical looping combustion with natural gas using spray-dried NiO-based oxygen carriers” *Carbon Dioxide Capture Storage Deep Geol. Form.*, vol. 3, pp. 67–74, 2009.

[55] A. Shulman, C. Linderholm, T. Mattisson, and A. Lyngfelt, “High reactivity and mechanical durability of NiO/NiAl2O 4 and NiO/NiAl2O4/MgAl2O4 oxygen

carrier particles used for more than 1000 h in a 10 kW CLC reactor," *Ind. Eng. Chem. Res.*, vol. 48, no. 15, pp. 7400–7405, 2009.

[56] C. Linderholm, A. Abad, T. Mattisson, and A. Lyngfelt, "160 h of chemical-looping combustion in a 10 kW reactor system with a NiO-based oxygen carrier," *Int. J. Greenh. Gas Control*, vol. 2, no. 4, pp. 520–530, 2008.

[57] J. Adánez, C. Dueso, L. F. de Diego, F. García-Labiano, P. Gayán, a Abad, F. Garcia-Labiano, and P. Gayan, "Methane Combustion in a 500 W th Chemical-Looping Combustion System Using an Impregnated Ni-Based Oxygen Carrier," *Energy & Fuels*, vol. 23, no. 1, pp. 130–142, 2009.

[58] L. F. de Diego, F. García-Labiano, P. Gayán, J. Celaya, J. M. Palacios, and J. Adánez, "Operation of a 10 kWth chemical-looping combustor during 200 h with a CuO-Al2O3 oxygen carrier," *Fuel*, vol. 86, no. 7–8, pp. 1036–1045, 2007.

[59] C. R. Forero, P. Gayán, F. García-Labiano, L. F. de Diego, a. Abad, and J. Adánez, "High temperature behaviour of a CuO/γAl2O3 oxygen carrier for chemical-looping combustion," *Int. J. Greenh. Gas Control*, vol. 5, no. 4, pp. 659–667, 2011.

[60] P. Gayán, C. R. Forero, A. Abad, L. F. De Diego, F. García-Labiano, and J. Adánez, "Effect of support on the behavior of Cu-based oxygen carriers during long-term CLC operation at temperatures above 1073 K," *Energy and Fuels*, vol. 25, no. 3, pp. 1316–1326, 2011.

[61] H. Gu, L. Shen, J. Xiao, S. Zhang, and T. Song, "Chemical looping combustion of biomass/coal with natural iron ore as oxygen carrier in a continuous reactor," *Energy and Fuels*, vol. 25, no. 1, pp. 446–455, 2011.

[62] M. a. Pans, P. Gayán, A. Abad, F. García-Labiano, L. F. De Diego, and J. Adánez, "Use of chemically and physically mixed iron and nickel oxides as oxygen carriers for gas combustion in a CLC process," *Fuel Process. Technol.*, vol. 115, pp. 152–163, 2013.

[63] C. H. Bartholomew and R. J. Farrauto, *Fundamentals of indurtrial catalystic processes*, Second Edi. WILEY-INTERSCIENCE, 2006.

[64] M. R. Quddus, M. M. Hossain, and H. I. De Lasa, "Ni based oxygen carrier over γ-Al2O3 for chemical looping combustion: Effect of preparation method on metal support interaction," *Catal. Today*, vol. 210, pp. 124–134, 2013.

[65] M. S. Bazaraa, H. D. Sherali, and C. M. Shetty, *Nonlinear Programming Theory and Algorithms*, Third Edit. John Wiley & Sons, 2006.

[66] D. P. Bertsekas, *Nonlinear Programming*, Second Edi. Athena Scientific, 2008.

[67] H. Binous, “Applications of thePenrobinson Equation of state using Mathematica,” *ChE*, vol. 42, no. 1, pp. 47–51, 2008.

[68] J. M. Smith, H. C. Van Ness, and M. M. Abbot, *Introduction to chemical engineering thermodynamics*, Seventh ed. Mc Graw-Hill, 2005.

[69] D.-Y. Peng and D. B. Robinson, “A New Two-Constant Equation of State,” *Ind. Eng. Chem. Fundam.*, vol. 15, no. 1, pp. 59–64, 1976.

[70] I. Barin, *Thermochemical data of pure substances*, Third Edit., vol. 55, no. 4. VCH, 1995.

[71] K. E. Sedor, M. M. Hossain, and H. I. de Lasa, “Reactivity and stability of Ni/Al2O3 oxygen carrier for chemical-looping combustion (CLC),” *Chem. Eng. Sci.*, vol. 63, no. 11, pp. 2994–3007, 2008.

Vitae

Name :Ahmed Aheed Ali Mohammed

Nationality :Sudanese

Date of Birth :2/27/1989

Email :g201205440@kfupm.edu.sa

Address :Al-Amarat 47th street

Academic Background :Graduated from Chemical Engineering Department, University of Khartoum in October 2010